UNIVERSIDADE DA BEIRA INTERIOR
Engenharia

Numerical analysis of flow around a fan blade of a CFM56-3

Bernardo Correia Pereira

Dissertação para obtenção do Grau de Mestre em
Engenharia Aeronáutica
(Ciclo de estudos Integrado)

Orientador: Prof. Doutor Francisco Brójo
Co-orientador: Eng. António Ferreira

Covilhã, junho 2015

Acknowledgments

This section will be written in Portuguese.

A realização deste trabalho assinala o fim de um ciclo bastante árduo mas igualmente gratificante. Mas toda esta caminhada não foi efetuada sozinho, e como tal tenho aqui a oportunidade de agradecer a quem me tem acompanhado.

Em primeiro queria agradecer aos meus pais e ao meu irmão por todo o apoio que sempre me prestaram, por acreditarem que seria sempre capaz de alcançar os meus objetivos, e por terem sempre feito tudo para que pudesse ter todas as condições para esta caminhada, por tudo isto e muito mais este êxito é também deles. Um agradecimento especial também aos meus avós que sempre me apoiaram e incentivaram para ultrapassar as dificuldades.

Queria agradecer ao meu orientador, Prof. Dr. Francisco Brójo que desde a primeira hora sempre me prestou todo o apoio e acompanhamento na elaboração deste projeto, é sem dúvida um grande e incansável profissional desta universidade. À instituição TAP mas em especial à equipa de engenharia da manutenção de motores quero agradecer pela forma exemplar como me acolheram, por todo o apoio e disponibilidade para me auxiliar nas tarefas deste trabalho. Um agradecimento especial ao Eng. António Ferreira por ter permitido e apoiado o estágio e acreditado em mim, e também á eng. Joana Palmeiro pelo incansável apoio ao longo do estágio.

Em seguida agradecer a todos os meus colegas de universidade, em especial ao Rui, Ruben, Alexey, Alexandre, Walter, Marc e João, que ao longo de 5 anos representaram uma segunda família e tornaram claramente esta viagem inesquecível, sem o apoio e camaradagem deles tudo teria sido mais difícil.

Finalmente, um agradecimento muito especial o qual quero desde á muito fazer por ser mais do que merecido e por ter sido indiscutivelmente crucial neste trabalho e na minha vida. Assim, quero agradecer-te Cláudia por me teres apoiado incondicionalmente ao longo deste trabalho, por teres cuidado sempre de mim e me teres dado o amor e carinho que me fez seguir em frente. Acreditaste em mim muitas vezes mais do que eu próprio e por isso quero dizer-te que este sucesso e também os que estão por vir são também teus.

To my Parents, Brother and Fiancée

"Whatever you are, be a good one."
Abraham Lincoln

Resumo

Este trabalho foi realizado em cooperação com a equipa de manutenção de motores da TAP Manutenção e Engenharia e surgiu com o intuito de analisar o escoamento em torno das pás da fan do motor CFM56-3. A análise do escoamento em torno da fan pretende essencialmente entender as relações entre a variação da corda e a alteração das propriedades, em particular duas propriedades essenciais, Mach number e Pressão total, procedendo posteriormente á validação dos resultados através das leituras dos testes efetuados no banco de ensaio da TAP-ME.

As equações de governo do problema são as equações de Navier-Stokes para escoamento compressível e adiabático. Foi então necessário adaptar as equações para um um moving reference frame de forma a serem ajustadas ao problema de uma pá em rotação. As equações de Navier Stokes em termos dos valores médios (RANS) são resolvidas, juntamente com o modelo de turbulência k-w sst. O volume de controlo do problema foi dividido em três domínios (inlet, blade, outlet), e foram criadas três pás com cordas diferentes (pequena, média, grande).

Após a construção do volume de controlo foram compostas no software Turbomesh malhas estruturadas em 2 domínios e não estruturada no terceiro e são então aplicadas as condições de fronteira adequadas. Procedeu-se á escolha do software comercial ANSYS CFX 15 como sendo o mais adequado á realização deste estudo, e são então realizadas 6 simulações, destas, três simulações foram executadas em regime de Take-off e as restantes três em Maximum continuous.

Após a realização das simulações e da obtenção de todos os resultados, são selecionados os mais relevantes para a investigação. As soluções numéricas foram então detalhadamente analisadas para a convergência e precisão para garantir a qualidade das mesmas. Os resultados são apresentados para todas as simulações em várias vistas e para duas propriedades essências, Mach number e Pressão total. É então efetuada uma análise comparativa destes dois parâmetros para permitir uma melhor compreensão das diferenças entre as diferentes cordas e diferentes regimes. Posteriormente existe uma análise para a validação do modelo numérico, em que as soluções numéricas são comparadas com os dados experimentais retirados de uma das bases de dados do banco de ensaio da TAP-ME. A comparação é efetuada para alguns parâmetros que podem ser medidos no banco de ensaio e é então concluída a validade do modelo uma vez que existe boa concordância entre valores.

Para finalizar são apresentadas as principais conclusões desta investigação e são também indicadas algumas propostas para trabalhos futuros assim como um trabalho que esta atualmente em desenvolvimento, que pretende aplicar os resultados deste trabalho.

Palavras-chave

Turbofan, CFM56-3, TAP-ME, DFC, FAN, Mach number, Pressão total

Abstract

This work was performed in cooperation with TAP maintenance and engineering, specifically the engine shop's engineering team. The main goal is to analyze the flow around a fan blade of a CFM56-3 engine. The flow analysis around a blade intends essentially to learn the relations between the chord variation and the consequent changes in the flow properties, particularly two, mach number and total pressure, and doing after a results validation process using the TAP-ME test bench readings as a reference.

The Navier-Stokes equations for compressible and adiabatic flow are the governing equations of this problem. However, it was necessary to adapt these equatios for a reference moving frame, so as to be adjusted to a rotating fan problem. The averaged Navier-Stokes equations are resolved along with the K-W SST turbulence model.

The control volume of this problem was divided in three domains (inlet, blade and outlet) and three different blade chords were created (small, medium and Large). After control volume construction the grids were created using the software Turbomesh, two domains use structured grids and the third uses an unstructured grid and the suitable boundary conditions are applied.

It was chosen the commercial software ANSYS CFX 15 as the most suitable for this study, then six simulations are performed, three of those simulations were executed in take-off regime and the other three in maximum continuous.

After the completion of the simulations and the results obtained, the most relevant for this investigation are selected. The numerical solutions were analyzed in detail for the convergence and accuracy in order to guarantee the quality of those solutions.

The results are then presented for all simulations in several views and for two essential properties, mach number and total pressure. Then a comparative analysis is performed for two parameters in order to learn the differences between variations in blade chord and different regimes.

Subsequently, there is an analysis to validate the numerical model, in which the numerical solutions are compared with experimental data taken from one of the databases of the TAP-ME test bench. The comparison is made for some parameters that can be measured on the test bench and is then completed and the validity of the model is proofed since there is good agreement between values. Finally, are present the main findings of this research and are also indicated some proposals for future works as well as work that is currently under development, which aims to apply the results of this work.

Keywords

Turbofan, CFM56-3, TAP-ME, CFD, Fan, Mach number, Total Pressure

x

Contents

List of Figures

List of Tables

Nomenclature

ATM   Automatic Topology and Meshing

Booster Low Pressure Compressor

CFD   Computational Fluid Dynamics

DOC   Direct Operating Cost

ECM   Engine Condition Monitoring

EGT   Exaust Gas Temperature

FPR   Fan Pressure Ratio

GTE   Gas Turbine Engine

HPC   High Pressure Compressor

HPT   High Pressure Turbine

IGB   Inlet Gearbox

ISA   International Standard Atmosphere

LPC   Low Pressure Compressor

LPT   Low Pressure Turbine

MC   Maximum Continuous

MRO   Maintenance Repair and Overhaul

N1   Fan revolutions per minute

OAT   Outside Air Temperature

OGV   Outlet Guide Vanes

RANS   Reynolds Averaged Navier-Stokes

SNECMA Société Nationale d'Etude et de Construction de Moteurs d'Aviation

SOR   Stable Operating Range

SST   Shear-stress transport

SV   Shop Visit

SVR   Shop Visit Rate

TAP   Transportes aéreos de Portugal

TAT   Turn Around Time

VBV   Variable Bleed Valves

VSV   Variable Stator Vanes

Chapter 1

Introduction

"First you guess. Don't laugh, this is the most important step. Then you compute the consequences. Compare the consequences to experience. If it disagrees with experience, the guess is wrong. In that simple statement is the key to science. It doesn't matter how beautiful your guess is or how smart you are or what your name is. If it disagrees with experience, it's wrong. That's all there is to it." **Richard Feynman**

In this first chapter, we will describe the general history and characteristics of the turbofan engines, regarding the general differences between these engines to others used at this time, and the characteristics that have made from this engine the most used in today's commercial aviation. After, we will have a brief explanation of the operation of the TAP accompanied by a set of data that allow us to understand the importance of the CFM56-3 (all versions) engine in the company, analyzing data on the annual interventions that are made in TAP maintenance engine shop.

1.1 Turbofan

The Gas Turbine Engine (GTE) is one of the most complex machines ever built, because of the dynamic behavior and the highly demanding engineering required for its operation. Due to its several advantages is used for various forms of transportation and ground based electric power generation [1]. Even being patented for the first time in 1791 by John Barbor, the gas turbine was used successfully for the first in 1939, and this, so called, whittle engine formed the basis of the modern gas turbine engine. The GTE is a practical application of physics 3rd law of motion, when the air is forced through the engine is generated a force in the opposite direction, producing the acceleration. Useful power is extracted from GTE by 3 different ways, from the momentum exchange resulting from the ejection of gas at high velocities through the nozzle, second from a direct mechanical connection of the engine shaft to accessories such as pumps or generators, and the third, the high pressure hot air extracted from the compressor that can be used in several areas of the aircraft [1]. The GTE represent, in a general way, a practical implementation of the Joule-Brayton thermodynamical cycle. The ideal Joule-Brayton cycle is shown in figure 1.1.

In this cycle the energy content of a working fluid increases along with pressure and temperature, through a mechanical compression and heat addition (combustion). The fluid is then allowed to expand and cool, while mechanical power is extracted by forcing the flow to impinge on a moving surface (turbine) [2]. In the general GTE, the efficiency of the ideal cycle is obtained by dividing the net useful work by the energy that is consumed in this process (see 1.1) [1]:
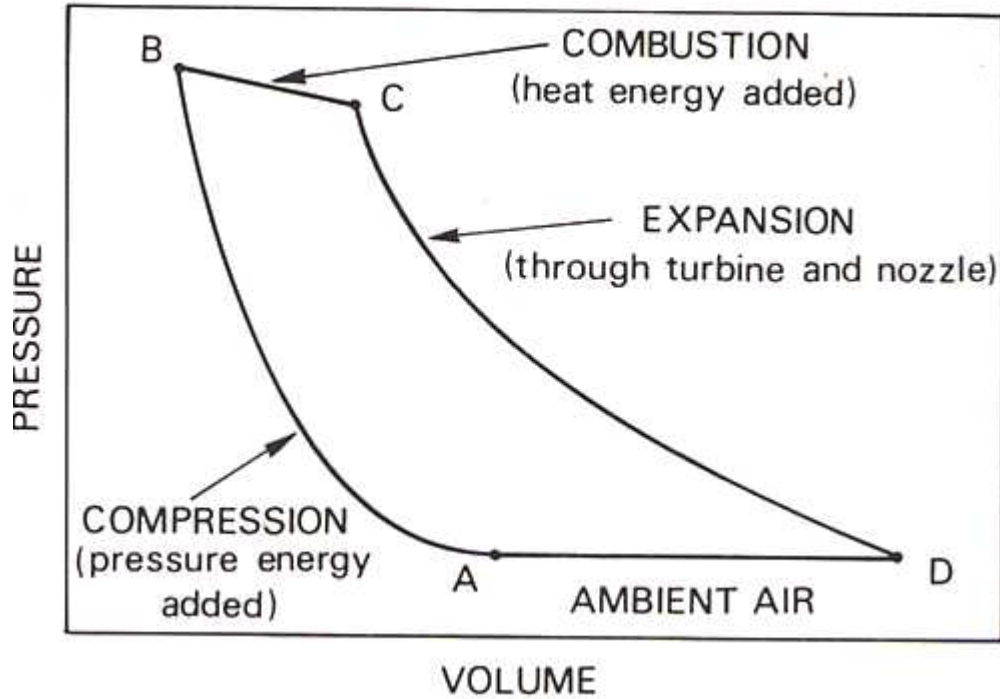
Figure 1.1: Joule-Brayton ideal Cycle diagram v-s [2]

$$\eta_i = \frac{W_{out} - W_{in}}{Q_{in}} \quad (1.1)$$

One of the most important aspects of the engine modeling and monitoring, is the Engine Pressure Ratio (EPR), that can be defined by dividing the exhaust Pressure by the Inlet Pressure [1].

$$EPR = \frac{P_{exhaust}}{P_{intake}} \quad (1.2)$$

The actual thrust (Fn) produced by the GTE can be defined as follows [1]:

$$F_n = \dot{m}(V_{eff} - V_0) \quad (1.3)$$

where V_0 is the velocity at the engine entering (relative to the aircraft), V_{eff} is the velocity at the engine exhaust and $\dot{m}$ is the mass flow that passes through the engine. Assuming that the expansion at the turbine happens until atmospheric pressure is reached and based on equation (Fn) its possible to conclude that there are two ways to achieve a specific engine thrust, using low mass flow with high flow speed or high mass flow with reduced flow speeds, combining this variables will give several efficiency solutions which will mean different engines [1]. For military purposes high thrust and small and compact dimensions are required and the specific fuel consumption or engine noise are not primary concerns, therefore the engines for this operations can have low mass flow and high flow speeds. In the other hand, for civil aircraft, the specific fuel consumption along with the engine noise are the most critical factors and that can be achieved by engines with high mass flows and reduced flow speeds. Following this,

the turbofan engine were created for civilian application in general. The turbofan design was conceived in order to improve the fuel efficiency, using the relationship stated before, high mass flows with low flow speeds. The turbofan engine has an additional component, the Fan, that is installed at the engine inlet in order to increase the amount of air admitted to the engine. However, the inlet airflow is divided and part is directed to the core of the engine, toward the compressor, combustion chamber and turbine, undergoing in the GTE process explained before, the other part is bypassed through a duct, which ends in a nozzle, this flow undergoes in a momentum exchange with the airframe and the resulting thrust does not require any burn of fuel, but some work is derived from the turbine to drive the fan [1]. Even with this extra power that is required to drive the fan, the total thrust (bypassed+core) achieved, requires less burned fuel than the necessary to obtain that thrust in a normal GTE (without bypass) [1]. The most common turbofan is the two-spool, in this design, the fan, LPC and LPT are connected by one shaft (1st Spool LP) and thus rotate synchronously. The HPC and HPT are divided by the combustion chamber and are connected by another shaft (2nd shaft HP) usually concentric with the LP shaft [2]. Turbofan engines are classified by their *bypass ratio* (BPR) that can be defined as the ratio of bypass to core mass flows. State of the art engines can have bypass ratio as high as 16,6 (Kuznetsov nk-93, Russian engine) in other hand some early turbofans used ratios as low as 0,3. Based on the relation discussed previously we can see that bypass ratio is chosen to prioritize either fuel efficiency or aircraft speed. The core exhaust has a higher velocity than the bypass exhaust, and when the bypass ratio is high a large and slow mass of air is passing through the bypass nozzle, in this design the thrust is created due to high mass flow movement rather than high exhaust velocity. To maintain the same thrust with a smaller bypass ratio its necessary to increase the velocity of the bypass ratio flow by same factor. In both designs the resulting thrust is the same, but there is a difference in terms of fuel efficiency, mainly because, in the low bypass ratio design more fuel has to be burned since the core flow increases and the fuel air ratio needs to be approximately the same [1].

1.1.1 Axial Fans

Turbofan engines are, in a simple way and as previously showed, a turbojet engine which is provided with a large fan. These design were developed to combine some of the best features of both engines, but the major advantage of turbofan engines is that it provides a better fuel efficiency. Considering this, it is important to study the fan and all is characteristics, although, there are several types of fans, those usually are distinguished based on a classification of the rotor flow exit direction, in this project the axial flow fans will be the ones to be discussed.

The operating principle of axial-flow fans is simply deflection of air, after flow passes the blades, the flow pattern has helical shape, and thus, flow can be decomposed into two component, an axial velocity and a tangential velocity. Axial velocity is the desired velocity in this type of fans, since it moves the gas from/to the desired spaces, in the other hand the tangential velocity is an energy loss.

In order to increase the efficiency of the airflow on the axial fan it is usually required an evenly distributed flow over the working face of the fan, this means that the axial velocity should be the same from root to tip on each blade, however, the blade velocity is a function of the radial distance, concerning this, the velocity gradients are then compensated by blade twisting, which results in a smaller blade angle toward the tip. If the same hub to tip blade angle is maintained this results in a loss of fan efficiency since thrust will take place mostly on the outer region of the blade. Similarly, an incorrect blade twist might cause stall in the exterior portion of the
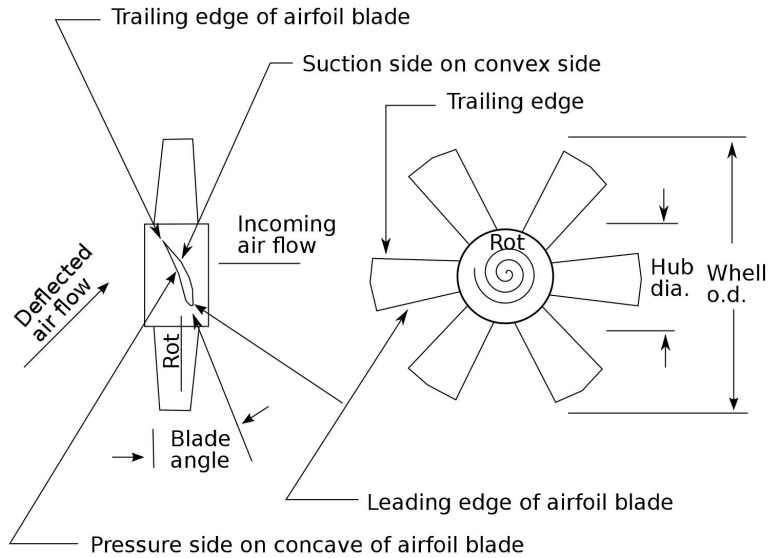
Figure 1.2: Airfoil shaped blade axial fan [3]

blade, decreasing significantly the efficiency when working with higher static pressures. [3]
The airfoil used in the fan blades are asymmetric, these airfoils usually have a blunt leading
edge which provides robustness to inlet flow perturbations and structural strength (1.2). These
airfoils are set up with a certain angle of attack in order to deliver the desired performance,
when the airfoil moves through the gas, produces a positive pressure on the lower surface of
the airfoil (high pressure side) and a negative pressure gradient in the upper side (low pressure
side). Both forces have approximately the same direction, but the upper side force is twice the
positive gradient force.[3]

The force can be decomposed in lift and drag forces, the first one is perpendicular to the
relative air velocity whereas the second is parallel. lift force is the desired component and the
drag force is the undesired since it causes power-consumption, however this two components
are connected to each other and the design must be made to obtain high lift forces but a good
lift-drag ratio. As an example, if the maximum section height of the airfoil profile increases,
lift usually increases but lift-drag ratio tends to worsen. All parameters of the airfoil are chosen
according to the desired application, the angle of attack and the overall range of operation has
to be considered when choosing the right airfoil shape.

The aspect ratio of the blade is an important feature, represents the ratio between the total
blade height and the chord length, with a bigger aspect ratio, the lift and the lift-drag ratio will
increase. The major contribution for that, comes from the vortexes that are created when the
fluid, flows from the lower surface to the upper surface, appearing especially on the blade tip.
Regarding a ducted fan the clearance between the blade tip and the engine case will sense this
phenomenon. The vortexes have a strongly negative influence in the lift force,but increasing
the aspect ratio will reduce the vortexes intensity, and consequently improve lift force.

There are some basic concepts of airfoil performance that apply even for blades in an axial fan,
as follows:

- A symmetric airfoil creates no lift when the angle of attack is 0°;

- Increasing the angle of attack the lift coefficient increases as well, this is valid until a
  certain angle (critical angle) from which the lift will decrease.

1.1.1.1 Influence of the Tip Clearance

Based on [3], where we can find a series of tests performed to evaluate the influence of the tip clearance on the performance of axial fans, we can state that when the tip clearances increase, the following performance changes can be sensed,

- The mass Flow decreases, but not significantly;

- The maximum static pressure in the operating range decreases considerably;

- The mechanical efficiencies decrease considerably ;

- The noise level at free delivery increases.

In a general way, it is possible to conclude about the fan performance in the operating range, that the smallest possible tip clearance will result in optimal performance in terms of pressure, efficiency and noise level [3].

In annex A.3 is possible to visualize the tip clearance in a CFM56-3 engine serviced in TAP engine shop.

1.1.2 CFM56-3 TAP

1.1.2.1 TAP

Throughout the years, TAP has created a solid company that is a reference in the airline business, not only nationally but also worldwide. The last few years proof that TAP has a fully implement, modern business model, and is now the 4th biggest company in Portugal. TAP Portugal similarly to other airliners is divided in several sectors, as *TAP Serviços* or *TAP Maintenance and Engineering*, etc. as we can see in figure 1.3.
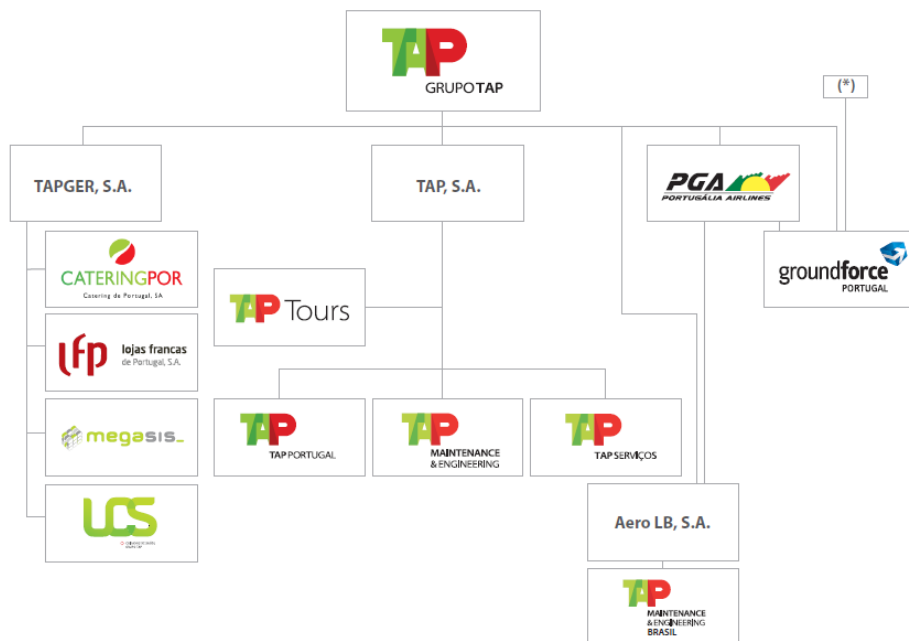
(*) Controlled by and external independent entity in accordance with the Competition Authority directives

Figure 1.3: Organizational chart[4]

TAP *Maintenance and Engineering* (TAP-ME) is the area responsible for the maintenance of all aircraft parts and is divided in several sectors where is included the engine shop (Manutenção de Motores). The engine shop is the sector responsible for the maintenance, repair and overhaul of both, TAP and customers engines. This engine shop has a particular organization [4] that permits an engine to enter the shop, be subdivided and separated in several areas, which one responsible and specialized in some specific engine parts.

The TAP engine shop is certified and has all the necessary equipment to perform maintenance work in a wide variety of engines, as we can see in figure 1.1, but the CFM engines are by far the most serviced engines. Analyzing the table 1.1, that presents the number of shop visits per engine from 2009 to 2013, is possible to notice that during this period the total number of shop visits changed significantly along this years [5].

The CFM56-3, in all his versions, is the engine that throughout the years has more shop visits performed at TAP-ME, based on this information is possible to conclude that this specific engine is a very significant part in the total work volume, therefore this study and their conclusions can be of great value for TAP-ME engine shop [5].

Table 1.1: Engine Shop Activities 2009-2013 [5]

	2009	2010	2011	2012	2013
Engines	TAP & Customers				
JT3D	6	2	0	0	0
JT8D	2	4	3	2	2
RB211	10	1	0	1	0
CFM56-3	28	43	25	31	19
CFM56-5A	11	9	4	3	7
CFM56-5B	21	18	17	18	27
CFM56-5C	7	8	3	8	10
CFM56-7B	7	6	9	9	6
CF6-80C2	1	3	2	1	2
CF6-80E1	1	0	2	1	0
PW4156A	1	0	0	0	0
PW4168A	7	4	3	9	4
Shop Visits Total	102	98	68	83	77

A better understanding of the aerodynamics involved in the operation of this engine will be very helpful to the engineering team in their work, probably making the maintenance process quicker and more accurate, which may result in significant financial savings.

As will be seen throughout this work the EGT is one of the most important parameters, because it permits to evaluate the engine's general performance. During the maintenance process an engine can be submitted to several different tests, the tests performed in the test bench are very important in the maintenance process and can be performed at many different stages. It is possible to visualize in table 1.2 that the CFM56-3 is the most tested engine with a maximum of 61 tests performed in 2010 and a minimum of 31 in 2013. From these assays performed in TAP-ME engine shop, there are several performance parameters that can be extracted for different operational regimes.

Table 1.2: Total engine tests per engine from 2009 to 2013[5]

Year	JT3D	JT8D	RB211	CFM56-3	CFM56-5A	CFM56-5B	CFM56-5C	CFM56-7B	CF6-80C2	Total
2009	13	3	13	44	13	25	9	8	0	128
2010	2	3	4	61	6	18	10	6	4	116
2011	1	5	1	40	6	19	6	10	2	94
2012	0	2	0	40	7	20	8	8	1	87
2013	0	1	0	31	7	19	18	6	4	88

In figure 1.4 we have a graph indicating the EGT margin for several versions of the CFM56-3. The red blocks represents the EGT margin actually measured in the test bench, the yellow and green lines on the top of the red blocks represents the EGT margin which is present in the contract. In other words, the first engine shows a measured EGT margin of 66 degrees but the target EGT margin displayed in the contract is 75 degrees. However, in some cases the information regarding the target contract EGT margin is not available or this information is not part of the contract at all.
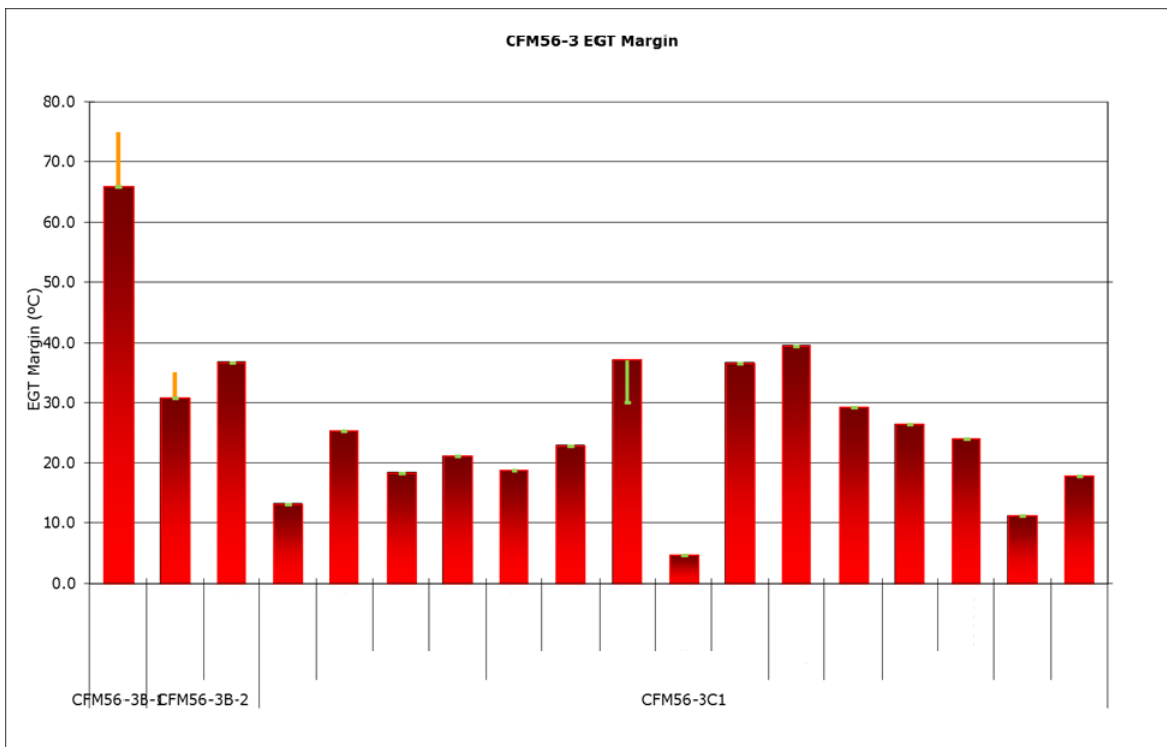
Figure 1.4: EGT margin comparison [5]

1.1.2.2 CFM56-3

The CFM56-3 can be operated at four different thrust ratings, and is operated in a variety of operating temperatures and conditions. The CFM56-3 is operated in large numbers, and will remain an important engine in the global repair and overhaul market in the next years. The engine is operated worldwide, and utilized in a wide variety of operations, so many factors influence the maintenance costs of this engine.

The first group of factors affecting the engine's operating parameters, outside air temperature (OAT), engine flight hour to engine flight cycle ratio, take-off thrust de-rate and the type of environment in which the engine is operated.

The second group of factors includes the engine's thrust rating, on-wing interval achieved prior

to each shop visit, the degree of deterioration, as well as the engine's life limited parts and their remaining life influence the timing of engine removals.

Finally, the third group of factors are the maintenance status of the engine at removal and the workscope of its previous shop visit. In these engine models, the EGT margin, which presents the difference between the maximum EGT and the actual EGT on the engine, is the best way to evaluate and measure the performance of a certain engine, especially because this parameter is used as a contractual target that is connected with financial compensations. The last CFM56-3s where manufactured in 1999, and so most of these engines have been through their first shop visit and have reached maturity. Most CFM56-3s recover about 70% of the original EGT margin after the first shop visit. The subsequent removals of the most engines will therefore be forced by erosion of EGT margin, if the remaining life cycles on life limited parts are not limiting. The first issue to consider is that EGT margins for the CFM56-3 are expressed for a standard OAT of 30 degrees centigrade and with the engine at maximum thrust and sea level [6]. Available EGT margin is higher when OAT's are lower than 30 degrees centigrade. EGT reduces by 3.2 degrees for every one degree reduction in OAT, and so EGT margin increases by the same amount. The implications of this are that a specific engine will have an available EGT margin of 62 degrees centigrade, fresh after a shop visit, when OAT is 20 degrees, instead of a lower EGT margin with the standard 30 degrees. In this conditions the engine with this additional 32 degrees will increase the engine's on wing time [6].

In operation, the blades in gas turbines, particularly in turbofan engines, are subject to wear resulting from particles (sand, dust) which causes erosion. In the forward section of the engine, in the fan and compressor section, erosion generally causes a flattening of the leading edge of the blades. Here, the fan blades are many times larger than any other blades of the propulsion unit.

When using new (unworn) fan blades, the profile will be aerodynamically optimized, which is adversely altered due to the wear. With this type of deterioration of the aerodynamic profile, the turbofan engine will become less efficient, resulting in a higher fuel consumption in order to achieve the same performance. From an economic point of view, the repair of deteriorated blades is worthwhile, particularly to regain an aerodynamically optimal blade. For this purpose several techniques and processes have been established towards providing deteriorated fan blades with a geometry that permits optimal efficiency [6].

The most recent device was created by *Lufthansa Technik AG* and is called "Device For re-contouring a Gas Turbine blade", this device for re-contouring a blade includes at least one support configured to rest on an edge of the blade during the process, one side is configured to rest on an intake side or an outlet side of the blade during the re-contouring and a machining unit is configured to fuse at least one partial area of the edge of the gas turbine blade using a beam of energy that is targeted such that material of the blade solidifies into a new contour, substantially without the addition of supplementary material. However it is also possible to perform this procedure with the addition of very small amounts of supplementary material [7].

Regarding the information that has been analyzed is important to understand how relevant is the issue of optimizing engine time on the wing for the airlines.

When airlines decide to discontinue the operation of one obsolete aircraft, engines may be sold to be used in other aircraft, as a less expensive alternative to the repair of replacement engines, or to be used for land power plants.

Based in [8] consider that three components of aircraft Direct Operating Cost (DOC) can be directly attributed to engine performance, design and reliability: the cost of fuel, engine acqui-

sition and engine maintenance. The authors state that for a typical wide body aircraft, those costs would be more than 40% of the DOC of the aircraft, split as follows: 55% for fuel, 30% for engine maintenance and 15% for engine acquisition. The values above represent a perspective in a certain calendar time and cannot be taken as an absolute truth. However, they provide a valid illustration of the importance of engines within aircraft operating cost. Actually a proportion of the cost depends on fuel price (i.e. crude oil price) and fuel consumption, and related cost depends not only on engine performance but is also highly dependent on the aerodynamic characteristics and structural efficiency of the aircraft.

The percentage of any cost component of the airline's DOC depends significantly on the unit cost of fuel, meaning on the cost of a barrel of crude oil, which in recent decades has presented high variations. When the fuel price increases, the percentage of the other costs components of DOC decreases, and vice versa. Modern aircraft are now built with more fiber reinforced plastics (composite materials) to reduce weight, advanced aerodynamic features (such as winglets/Boeing and sharklets/Airbus on the wing tips) to reduce drag, and in flight fuel transfer between tanks to optimize the aircraft's center of gravity and reduce drag. All these characteristics, together with engine performance, are relevant for aircraft fuel consumption and cost.

Despite the above considerations, the engine related costs are very important in the airline activity. Putting aside fuel consumption and other engine ownership costs that depend essentially on external factors with little controllability by the airline, engine maintenance cost is one of the most important parts of controllable DOC by management decision and has two main components [8]:

a)   On aircraft – includes inspection, servicing and defect correction tasks performed during line maintenance (between flights) and base maintenance (during periodic inspections) of the aircraft;

b)   Off aircraft or SVs – extensive and time consuming work that may be an engine repair, a performance restoration or an overhaul, all of which are performed in engine shops.

As indicative figures, an aircraft manufacturer considers that On Aircraft (Line) Maintenance is 5% of ownership costs (10% of engine direct maintenance cost), and SVs account for 40% of ownership costs (80% of engine direct maintenance cost). In general engine ownership costs can be split as follows [8]:

i)   Acquisition 35%;

ii)   Spares acquisition 15%;

iii)   Shop Visits 30%;

iv)   Life Limited Parts 10%;

v)   Line (and base maintenance) 5%;

vi)   Support 5%.

Actual proportions of On Aircraft and Off Aircraft vary significantly with engine models and airlines, but Off Aircraft (SV) maintenance is always much more expensive than On Aircraft maintenance. Another important difference is that engine On Aircraft maintenance expenses occur almost uniformly along time and shop maintenance occurs in periods of about two to five

years per operating engine. The expenses, for a wide body aircraft, may vary from US$1 to 10 million.

In [8] is considered that an engine SV cost depends on Shop Visit Rate (SVR), i.e. the number of SVs per 1,000 engine flight hours (EFHs), the workscope of each SV pattern (the sequence of different workscopes) and the man hours and material spent in each SV. Despite the fact that manufacturers design engines to achieve a long time on the wing, engine maintenance unit cost is not always a monotone function in relation to SVR or engine time on the wing. The engine SV maintenance unit cost is the cost of the engine SVs divided by the engine flight hours operated by the engine between SVs.

Due to wear and material degradation, the total cost of an SV increases with increasing engine time on the wing. This is an obvious fact, therefore it is not possible to assume a priori that engine maintenance unit cost (engine maintenance cost per flight hour) will always decrease when engine time on the wing increases (i.e. when SVR decreases). To decide when to remove an engine for an SV is not a deterministic problem. Since engines are maintained essentially under the concept "On Condition" and aircraft operators manage the engine to avoid the risk of unscheduled removal, the decision to remove the engine is done conservatively before engine condition monitoring parameters achieve allowed limits [8]. Engine time on the wing is not necessarily the most important factor in engine maintenance cost, but when an engine is installed on an aircraft, time on the wing is quasi the only factor that management may use to control engine maintenance cost, assuming that the airline is following the required and approved maintenance and operational practices.

Empirical research work done in [9] [10] presented evidence, using two different methodologies, that after the airline business deregulation in the USA, airline managers changed maintenance behavior towards optimizing engine time on the wing to reduce costs in order to face the climate of stiff increased competition. We may conclude that optimizing engine time on the wing is relevant in managing airlines because it has a strong influence on maintenance costs, an important part of controllable DOC, by preventing over maintenance, provided there is an adequate monitoring of the ECM parameters, proper inspections on the physical status of the critical components and the reliability of the engine is taken into consideration to avoid the risk of in-service failure.

1.2   CFD analysis

The use of numerical methods to solve complex engineering problems has increased in the last few years, especially because this process is strongly linked to the computer processing and storage capabilities, so since the world have been witnessing a great development in this area this has increased the applicability and accuracy of this methods. The CFD became a powerful tool in flow analysis, heat and mass transfer or any other flow associated processes.[11]. There is a wide range of advantages in the application of this CFD methods in engineering when compared with experimental methods, because a CFD analysis allows a substantial reduction in costs and time spend to obtain a solution and offers us an almost unlimited solution in terms of its detail. Along with this, is possible to have access to a powerful method that give the ability to solve complex problems, where an analytical approach does not exist and the experimental test is almost impossible.

However, is important to keep in mind the alert made by [12] , where the author states that the numerical methods should not be considered a substitute of the experimental tests but

as an additional tool with great value, because there are always associated errors and some simplifications that are assumed by the user, and this will divert the simulation results from the real process.

Currently, as have been stated before, the CFD is widely spread in the resolution of fluid flow related problems, as such, a variety of CFD codes are now more or less accessible/disseminated, and those are equipped with very robust algorithms capable of solving almost all kinds of flow. Those codes allow a very detailed and complete analysis, through 3 phases, preprocessing, solver ans post-processing.

However, it is important not start the creation of a numerical model without first, clearly identify the problem. In this phase it's necessary to set goals for the model and define the wanted results. [14]. The necessary physical-mathematical models to be implemented should be created, and the possible simplifications applied, as well the needed accuracy must be defined and the level of priority regarding the final results. Ultimately, calculation boundaries must be created in accordance with our boundary conditions.

A global perspective regarding the modeling process implemented in many commercial softwares, can be analyzed in figure 1.5.

Figure 1.5: Modeling Process [35]
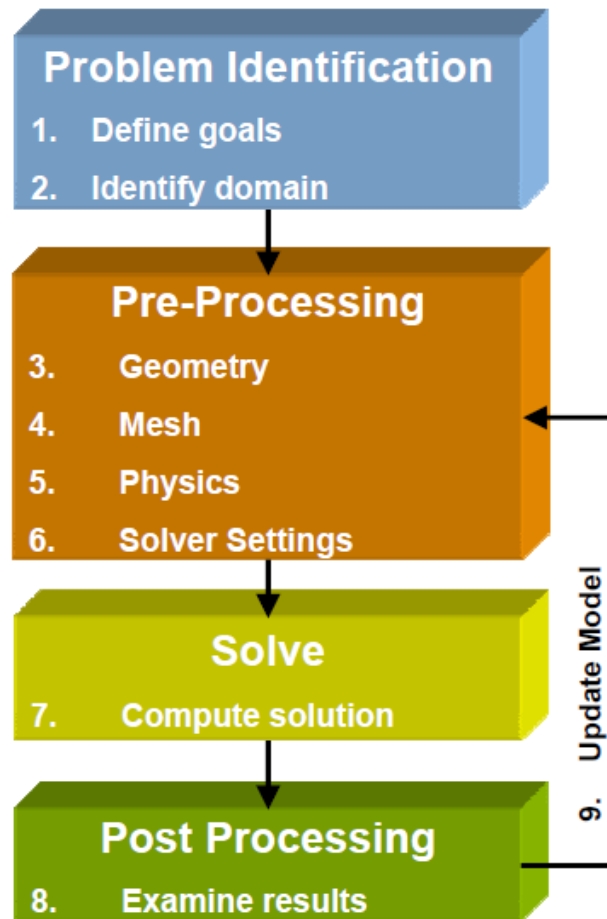
The next phase will be, the preprocessing, this phase works as an entry variable for the program, here is necessary to start defining the control volume geometry and the respective mesh. Also in this phase, the fluid properties and the physical properties of the flow are defined, and the adequate boundary conditions must be set. The mesh creation process is of major importance in

the general problem resolution, so is crucial to learn very clearly were the strongest gradients are more likely to happen, and design a more refined mesh in those regions, or even consider the flow properties that are needed to create a model. Therefore, with a higher Reynolds number will be needed a more refined mesh than when a smaller Reynolds number is verified.

The creation of a good quality mesh is of such a great importance than this will influence the necessary calculation time, because a good mesh is more likely to obtain good and fast convergence towards a solution [35]. The accuracy of the numerical solution will increase as the number of elements that comprise a mesh increases. In fact, the accuracy of a solution as well as its costs in terms of computational hardware, or calculation time will be, inevitably dependent on the mesh resolution.[35]. More than 50% of the time spent in a CFD project will likely be devoted to the definition of the domain geometry and mesh generation.[35]. After the conclusion of the pre-processing phase, all conditions should be ready to move on to the solution calculation, while monitoring the solution convergence.

As said before regarding the mesh creation process, will be of great advantages choosing a good set of initial conditions, in a way that if those conditions are close to the final solution, the iteration process will converge rapidly resulting in shorter calculation times. In the other hand, if the initial conditions have a very significant difference from the final solution, the computational calculation time will be much bigger to achieve the desired convergence. In some cases, unappropriated initial conditions will lead to a divergence and a consequent fail to achieve a numerical solution. After, is necessary to evaluate the accuracy of the results, to do this evaluation is necessary to compare the numerical results with some experimental results, sometimes this represents a very challenging process because normally experimental data are very difficult to obtain. Usually the accuracy of a solution is directly linked to the precision and adequacy of the physical models, the resolution and independence of the mesh and also the numerical errors [35]. The mesh independency is obtained when the increasing or decreasing of the mesh resolution does not influence the numerical results. Lastly, in the post-processing phase the results should be carefully analyzed in order to extract the relevant data. The majority of the CFD codes, at this time, are equipped with several tools to visualize and analyze the results by creating reports and graphics. If the user concluded, during this analysis, that the physical models or the boundary conditions or even the mesh are not adequate, the numerical model should be revised and updated, going back to the preprocessing phase.

A general numerical resolution process is represented in the flowchart displayed in figure 1.6.

1.2.1   Numerical Mesh

The discrete locations at which the variables are to be calculated are defined by the numerical grid which is essentially a discrete representation of the geometric domain on which the problem is to be solved. It divides the solution domain into a finite number of subdomains (elements, control volumes etc.). Most common options are as follows:

Structured Mesh: This is the simplest grid structure, since it is logically equivalent to a Cartesian grid. Each point has four nearest neighbors in two dimension and six in three dimensions. An example of the grid structure is given in Figure 1.7. The connectivity to the nearest points, simplifies programming and the matrix of the algebraic equation system has a regular structure. The disadvantage of structured grids is that, they can be used only for geometrically simple solution domains. Another disadvantage is that it may be difficult to control the distribution of the grid points: concentration of points in one region for reasons of accuracy produces unnecessarily small spacing in other parts of the solution domain and waste of resources. [24]
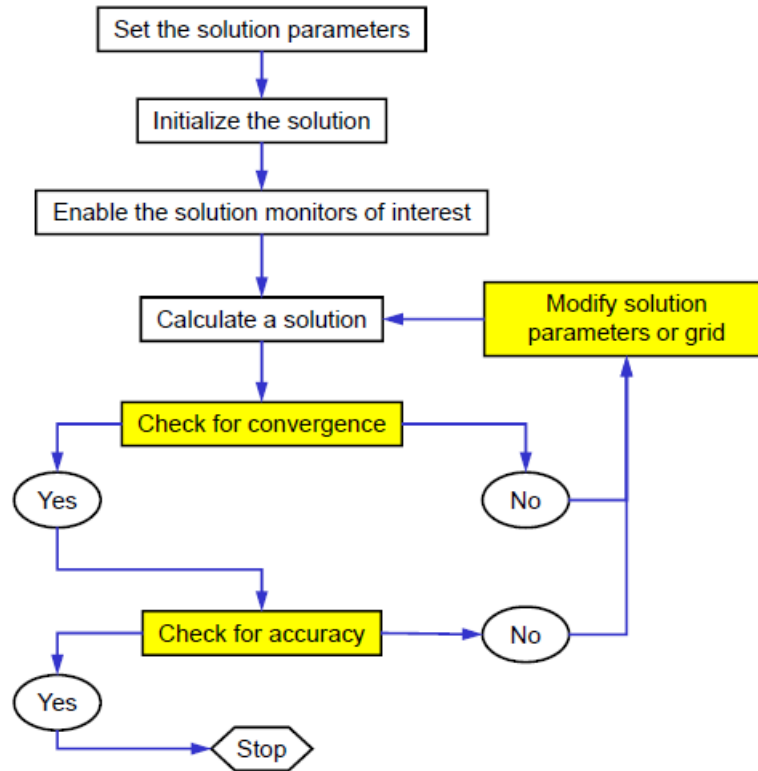
Figure 1.6: Computational Calculation Process[35]
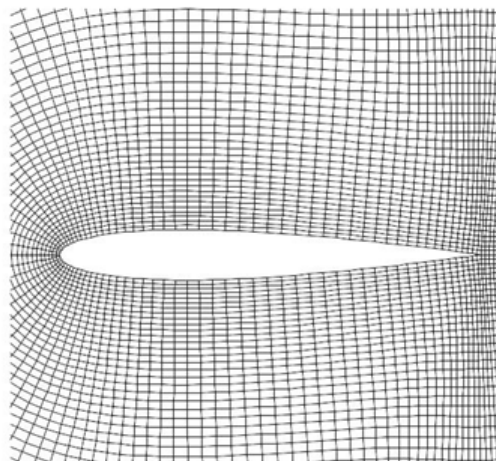
Figure 1.7: Structured Mesh [32]

Unstructured Grid: For very complex geometries, the most flexible type of grid is one that can fit arbitrary solution domain boundary. In principle, such grids are applicable to any discretization scheme, but they are best adapted to the finite volume and finite element approaches. The elements or control volumes may have any shape; nor is there a restriction on the number of neighbor elements or nodes. In practice, grids made of triangles or quadrilaterals in 2d, and tetrahedral or hexahedral in 3D are most often used. An example of unstructured grid is given in Figure 1.8. [24]
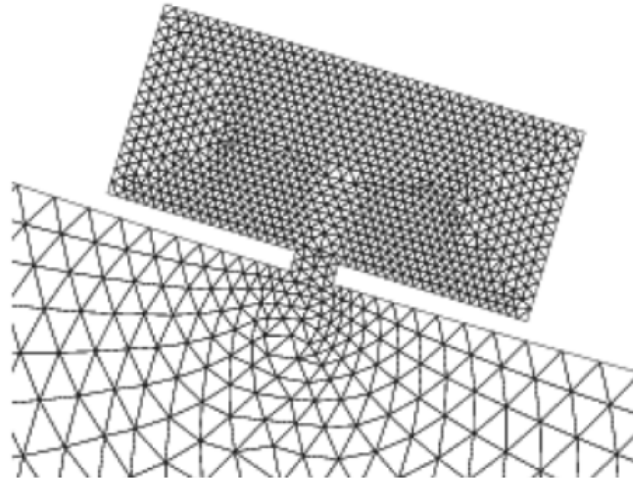
Figure 1.8: Unstructured Mesh[32]

1.3 Motivation and Objectives

This dissertation is a mandatory stage to acquire the Master's Degree, and finish the Aeronautical Engineering course that I have started 5 years ago . From the first moment, I have decided that this work had to be done with a real goal that can, not only help me to pass this stage, but also bring some knowledge to a real problem that can, by means of is application, help in some specific challenges, but of course not despising its scientific or theoretical component. The choice by the CFD area appeared naturally, was always the area where I had more interest, and knew from the first hour that doing a project like this will be challenging but very rewarding for self-development. Connecting this, to a native interest in exploring and understanding the Jet Engines, specially the Turbofan Engines, made very clear for me the specific area where a wanna develop my project.

After a few contacts with TAP Maintenance and Engineering department, specifically in the engine shop, we reached an agreement in order to carry out an internship, in the engine maintenance shop, with the goal of conduct a study in the engine CFM56-3.
The Engine Engineering group informed us about a problem that they are experiencing during the maintenance of the engine CFM56-3. As we have seen before, the EGT margin, in this type of engine, continues to be the main indicator of performance used by the airliners and by the MRO's organizations, so the maintenance contracts are usually signed, setting an target EGT margin. TAP ME being a MRO, has received, as we have seen before, several CFM56-3 (all versions), in some of those engines a performance restoration is required and the company will need to perform several maintenance works in the engine, but these procedures are usually tied to a restrictive budget that do not permit to change some parts to new ones. Having that in mind, some parts can be repaired or changed in order to achieve the required performance. From this problem, the engineering team decided to search for new solutions, and the best path to do so, is a deeper understanding of the air flow inside the engine, in order to know the characteristics and the relations between different parameters. Therefore, **this study emerged with the objective of better understand the flow around the fan blades and search for relations between a variation in the blades chords and changes in the flow characteristics, specially in terms of flow pressure. Find a direct relation between blade chord variations, and changes in EGT would be a very interesting breakthrough for the engine maintenance,**

yet we understand that with a CFD analysis performed only on the fan and with a limited number of experimental results to compare, find this sort of relation with a good accuracy it will be difficult.

The turbofan engine is a very reliable engine and the most used engine in aviation nowadays, one problem that is experienced in this engines, is the blade erosion due to particle ingestion, specially when the engine is mounted with a small ground clearance like the CFM56-3 is, this phenomena will change the blade geometry and decrease the blades chord. Despite not being the main goal, we think this work can also be helpful in concluding which changes will be caused in the fan performance as a result of the blade erosion in this type of engine.

1.3.1 Predictions

In the last few years, the engine shop at TAP has created a database where the results of several engine tests in the test bench have been recorded along with the blades chord length. Some engines have been tested several times with different blade sets (changing blade chord), which has permitted to evaluate the performance changes due to blade chord variations. The engineering team has been analyzing these data in order to understand the implications of blade chord changes.

So far, it was possible to conclude that when the blade chord is reduced also is the engine thrust ,which will result in EGT decrease (EGT margin increase). This tendency that was noticed with the statistical data from the test bench, has been very useful in the maintenance process, by using this relation to obtain a higher EGT margin even sacrificing some available engine thrust. The results in this work are expected to confirm this relation, in a certain way, so to change in the last few years, the engine shop at TAP has created a database where the results of several engine tests in the test bench have been recorded along with the blades chord length. Some engines have been tested several times with different blade sets (changing blade chord), which has permitted to evaluate the performance changes due to blade chord variations. The engineering team has been analyzing these data in order to understand the implications of blade chord changes. So far, it was possible to conclude that when the blade chord is reduced also is the engine thrust ,which will result in EGT decrease (EGT margin increase). This tendency that was noticed with the statistical data from the test bench, has been very useful in the maintenance process, by using this relation to obtain a higher EGT margin even sacrificing some available engine thrust. The results in this work are expected to confirm this relation, in a certain way, so it can be used in a beneficial way.

1.4 Thesis Structure

The present work is organized in 5 main chapters. In the first chapter, the Introduction, we begin with a general explanation of the turbofan engines describing the working principles and the main differences to other engines (turbojet), after we have a specific description of the Fan its aerodynamic characteristics specially in the axial fan type, due to its importance in this engine type and specifically in this work. Following, is a section dedicated to present (TAP) the company where this work was conducted, describing the general structure and the work that is performed in the engine shop showing statistical data from the past few years that permits a better understanding about the operation conducted in this facility. In connection with this a very important section is presented, that discusses the role of this engine in the

aeronautical world and some maintenance technical data which helps to understand the life and the work that is needed in this engine throughout is life, as well as the difficulties that this maintenance processes face in order to restore the engine's performance. This section ends with the necessary reflection regarding the optimization of the maintenance process in order to increase the engine's time on-wing, and understand the chain of costs in an airline.

The last part of this chapter, was dedicated to describe the methodology used in a CFD analysis, explaining all phases of a general process and the specificity's that each phase has, and finishing with an overview in one of the most important part of this process, the numerical mesh.

Chapter 2, the Literature survey, is were we pretend to gather a significant amount of information regarding previous researches in this area that allows us to identify the scientific advances throughout the years and the state of the art in the main fields related to this work. Continuing with the same goal, is created a description of the engine that will be analyzed in this work, first a general description of specification of the engine and after a more detailed analysis of the engine module where this work will take place. Finally, the chapter will be completed with a resume of the facilities and equipments that TAP has available to analyze and study the engines, so we can understand what kind of data is available for validation and how is being collected.

The chapter 3 will be dedicated to the problem formulation, the governing equation, for this problem are presented with the necessary simplifications for our case and an explanation of it's meaning in our flow analysis. After this, and since our analysis will be performed in a moving reference frame we will transfer those equations from a stationary to a rotating moving reference frame. Then, the turbulence model, that was chosen, the K-ε SST is presented by the demonstration of the equation that compose this model, and closing this chapter is the modeling of the turbulence in the near wall flow.

The Numerical Model implemented in this work is presented in chapter 4, where we can learn the model details in the present work that will simulate the flow passing first in the inlet domain and after through the fan blades. The chapter starts with the definition of the computational domain and the boundary conditions to be applied in our case, after the mesh strategy for our domain will be presented. In the end of this chapter is also possible to learn how the chosen solver does the simulation process as well as the parameters used to define the simulation and the evaluation of the convergence criteria.

Finally, chapter 5 will present the results obtained in our simulations. The chapter will start with analysis of the solutions convergence, presenting several parameters that can confirm the good convergence of our solution. The following section includes the simulations results with images obtained from CFX that shows the flow properties in different locations for all our simulations, and relevant comparisons will be made in order to easily find relationships between variables.

Following, will be an important section, where is intended to make a comparison between the experimental results from the test bench and the numerical results, that will allow the validation of those results. The last section of this chapter are dedicated to describe the final conclusions from the present project and to detail the work that is under development and the future work that can be realized from this investigation.

Chapter 2

Literature Survey

We can define the scope of this work in one main field, which is the search for a relationship between the flow characteristics around the fan and the blade chord. Taking this into consideration and after a careful research we were unable to find any similar analysis to this engine. Regarding, the fan blades as far as our research went, we didn't find any previous work done with this geometry, or even studies that analyze the same relationship as we are trying to do in this project. We learn that this occurs with this specific studies generally because the engine geometry as well as other engine data are classified, and some specific data, not even the operator of the engine has access.

In light of this information, we decide to create a literature survey that discusses the previous work done in three fields, the simulation of axial flow fan numerically using CFD code, the validation of the numerical predictions with experimental results and the fan blade erosion and its effects.

A number of previous projects have been done, using different simple CFD models to simulate an axial flow fan or propeller.

In Beiler [14] a numerical analysis of the flow in axial flow fans with skewed blades has been conducted to study the three-dimensional flow phenomena pertaining to this type of blade shape. The particular fans have a low pressure rise and are designed without stator. Initial studies focused on blades skewed in the circumferential direction, followed by investigations of blades swept in the direction of the blade chord. A Navier–Stokes code was used to investigate the flow. The simulation results of several fans were validated experimentally. The three-dimensional velocity field was measured in the fixed frame of reference with a triple sensor hot-film probe. Total pressure distribution measurements were performed with a fast response total pressure probe. The results were analyzed, leading to a design method for fans with swept blades. Forward swept fans designed accordingly exhibited good aerodynamic performance. The sound power level, measured on an acoustic fan test facility, improved.

Curnock et al. [15] investigated how the radial profiles can be used to make an estimation of turbofan performance, accurate gas turbine performance models based on thermodynamic principles can bring many benefits in these models it is a normal practice to represent the different components by means of its performance maps or component characteristics describing the relationships between the thermodynamic variables representing the component. It is well known that the fans of high-bypass engines have strong radial profiles of all thermodynamic variables and it is common to average these profiles so that one or two characteristic maps can represent the fan. Three different fan representations were compared in this work, and three models were created. Several relationships were tested for the 3 models, specially bypass ratio and power setting, the SFC and also changes in geometry.

Berbente [16] describes various kinds of options regarding the computational mesh generation that is required by the analysis of flow in axial turbomachinery (fan, compressor). Cases of both

rotating and fixed blade row profiles and axial stage are presented. This work can be considered a useful guide of the first steps in computational analysis of flow in turbomachinery, are presented the very best options of mesh generation that lead to a good level of computational accuracy. The steps for the computational mesh generation are described and fully details with regards the defining of the computational domain and the identification of the boundaries are given and detailed explanations regarding the boundary types and conditions are pointed out for several cases.

In Ahmed [17] are presented the computational study and first iteration of design refinement of a two-stage fan that has been designed for small turbofan engines. An analysis of the original configuration indicated that the fan is unable to meet the design point parameters. Systematic flow field analysis revealed certain problems with the 1st stage rotor blade that could be improved by making small adjustments to its geometric features; such as blade lean, sweep, chord and contour. After these changes incorporated in modified design, the performance maps were created. These maps indicated an overall gain of 6% and 8% in fan 1st stage rotor design point pressure ratio and isentropic efficiency, respectively. After the 1st stage rotor redesign, the whole fan (two-stage) design point efficiency and pressure ratio improved by 5-7% and 1.4%, respectively. With this predicted improvement in its performance, the redesigned fan meets the projected design point parameters.

Yang et al. [18] performed a flow mechanism analysis and experimental study of a forward-skewed impeller and a radial impeller in low pressure axial fan. The forward-skewed blade was obtained by the optimization design of the radial blade and CFD technique. Measurement of the two blades was carried out in aerodynamic and aeroacoustic performance. Compared to the radial blade, the forward-skewed blade has demonstrated the improvements in efficiency, total pressure ratio, Stable Operating Range (SOR) and less aerodynamic noise. Detailed flow measurement and computation were performed for outlet flow field for investigating the responsible flow mechanisms. The results show the forward-skewed blade can cause a spanwise redistribution of flow toward the blade mid-span and reduce tip loading. This results in reduced significantly total pressure loss near hub and shroud endwall region, despite the slight increase of total pressure loss at mid-span.

Jingjun et al. [19] investigated the tip leakage flow between a blade and a casing wall. This phenomenon has a strong impact on compressor pressure rise capability, efficiency, and stability. This work presents the potential of passive tip leakage flow control to increase the aerodynamic performance of highly loaded compressor blades. Experimental investigations on a linear compressor cascade equipped with blade winglets mounted to the blade tips have been carried out. Results for a variation of the tip clearance and the winglet geometry are presented. Current results indicate that the use of proper tip winglets in a compressor cascade can positively affect the local aerodynamic field by weakening the tip leakage vortex. Results also show that the suction-side winglets are aerodynamically superior to the pressure-side or combined winglets. The suction-side winglets are capable of reducing the exit total pressure loss associated with the tip leakage flow and the passage secondary flow to a significant degree.

In Amoo [20] the design and progress in the design and structural analysis of commercial jet engine fan blades is reviewed and presented motivated specially by the key role fan blades play in the performance of advanced turbofan engines. This work intends to present the recent

developments that have increased the fan structural durability, stability and reliability, is presented as a review of the fan blade environment and current state of structural design in order to aid in developing fan blade technologies.

In Sahili et al. [21] full-geometry Computational Fluid Dynamics (CFD) modeling of air flow distribution from an engine cooling fan is investigated. Different models were used, the Core model, the Extended-Hub model, and the Multiple Reference Frame (MRF) model. Results are in good agreement with data obtained from an experimental test facility and the different models were compared to understand the differences and the more suitable under specific circumstances.

In Dwivedi et al. [22] an axial flow fan of small dimensions that are used in industry applications has been evaluated. CFD investigation of this axial fan was conducted using forward and backward skewed blade profiles, the software FLUENT was used and the results were compared with experimental results from literature. The modeling of the axial fan was carried out in GAMBIT and the simulation uses standard K-ε model. The analysis was carried out with blade stagger angle of 25°, Skewed angle of 8.3°, at 1440 rpm and 1800 rpm. Good agreement was found between experimental results and results from literature.

In Gobran et al. [23] the prediction of the particle dynamic and erosion characteristics due to dust ingestion in an axial flow fan, installed in a high bypass-ratio turbofan engine that operates in a dusty environment is studied. Dynamic behavior comprises the particle trajectory and its impact velocity and location. While the erosion characteristics are resembled by the impact frequency, erosion rate, erosion parameter and the penetration rate. The study was carried out in two flight regimes, takeoff and cruise. The computational domain employed was a periodic sector through both the fan and its intake bounding an angle of 9,47° and where the number of fan blades was 38. The intake is a stationary domain while the fan is a rotating one and the FLUENT solver is used to solve this problem. During takeoff flight regime, the pressure side of fan blade experienced higher particle impact and erosion damage. The highest erosion rate was found at the corner formed by blade tip and trailing edge of pressure side. During cruise conditions, less erosion rates resulted. Maximum erosion rates are found at the leading edge of the pressure side.

The accuracy of the CFD model is verified with experimental results. To ensure confidence in a set of experimental data, the data set needs to conform to certain air performance test methods (standards), in this case for turbofan fans. These standards aim to provide a specified environment where the fans can be tested. When comparing different fan designs, the fan test results all need to adhere to similar conditions, standardized setup and testing procedures to eliminate any uncertainties in the comparison.

As previously mentioned is very difficult to find publicly available works in this area (using real geometry) regarding this was noticed the project of Gašparovič, P. (2008) working on CFD modelling of transonic flow in a fan of aircraft engine, specifically on the turbofan engine DV-2, since this work is only available in slovak language we establish contact with the author and we were informed that the main goal of this work was the comparison of CFD results with experimental results, the parameters to be compared was the total pressure ratio and the isentropic total efficiency. The author chose 3 cases to simulate, first, the geometry without tip clearance, simple unstructured mesh, with turbulence model Spalart-Allmaras, second, the geometry without

clearance, a structured mesh with detailed boundary layer and a turbulence model K-ω SST, and the last one, the geometry with tip clearance (0,63mm) structured mesh with detailed boundary layer and using turbulence model K-ω SST. The simulations were performed using the ANSYS CFX, using a rotation speed of 13100 rpm, a mass flow of 53 kg/s and a total pressure ratio of 2.3. Good agreement was found between numerical and experimental results and was possible to assess the validity of this CFD methods in the simulation of a fan of aircraft engines in transonic regime. CFD methods where able to successfully predict the performance of the fan, including the effect of losses in boundary layer.

This literature survey was finished with a rigorous analysis of Xisto,C. (2009) and Vinha, N. (2011) this two documents were created in UBI, however, these works had different scopes from each other, and also from this work, were considered relevant to be analyzed, mainly because are two very well documented and implemented examples of a CFD analysis of blades cascades, using the resources available at our university.

2.1 CFM56-3

Taking into account the objectives and even the origin of this project becomes crucial to include this section dedicated to understand and study the engine CFM56-3, specifically it's history and the role in the company. After, is important to analyze in more detail the Module in which this project will be focused (Nº1 Fan and Booster Module).

The engine CFM56-3 is not currently being used in TAP fleet, but as we can see in table 1.2 this type of engine is usually the most tested in the test bench and represents a very significant number of shop visits in the TAP engine shop.

This engine its a modern turbofan developed by CFM International in the late 70's and certified in 1984 to be part of the Boeing 737 project. CFM International it's a company owned equally, by the American, GE Aircraft Engines and by the French company SNECMA .The company (CFM), and product line (CFM56), got their names by a combination of the two parent companies commercial engine designations: GE's CF6 and Snecma's M56. CFM56-3 is a two spool axial engine with a bypass ratio of 5, and it's available in several thrust rates, as we can see in table 2.1.

Table 2.1: Engine Versions [25]

Version	Thrust	Aircraft Model
CFM56-3 B-1	20000	B737-300 & B737-500
CFM56-3 B-2	22000	B737-300 & B737-500
CFM56-3 C-1	23500	B737-400
CFM56-3 B-1 Derated	18500	B737-500

All versions available, share the same general characteristics since they originate from the 23500 lbs version, using successive thrust derating. As a first approach, the engine's composition can be generally described in order to understand the overall operation and get familiarized with some specific and important components for this work. The high pressure Turbine (HPT) has

a single stage which drives 9 stages from the high pressure compressor (HPC) both connected create the high pressure spool with a rotating speed of N2. In the other hand, the low Pressure Turbine (LPT) with 4 stages drives the single stage fan and the low pressure Compressor (LPC or booster) which is composed with 3 stages, creating the low pressure spool with a rotating speed of N1. Every rotor stage (indicated above) has the correspondent static stage [25].

The engine is equipped with an annular combustor chamber supplied by 20 fuel injectors, providing perfect conditions for the combustion process which will be responsible for driving both turbines by the combustion products action. The flow rate direction in the compressors is controlled by 12 bleed valves the Variables Bleed Valves – VBV, located between the Booster2 and the HPC, and also by 4 variable stators (Variable Stator Vanes –VSV), located in the first 4 stator stages of the HPC [25].
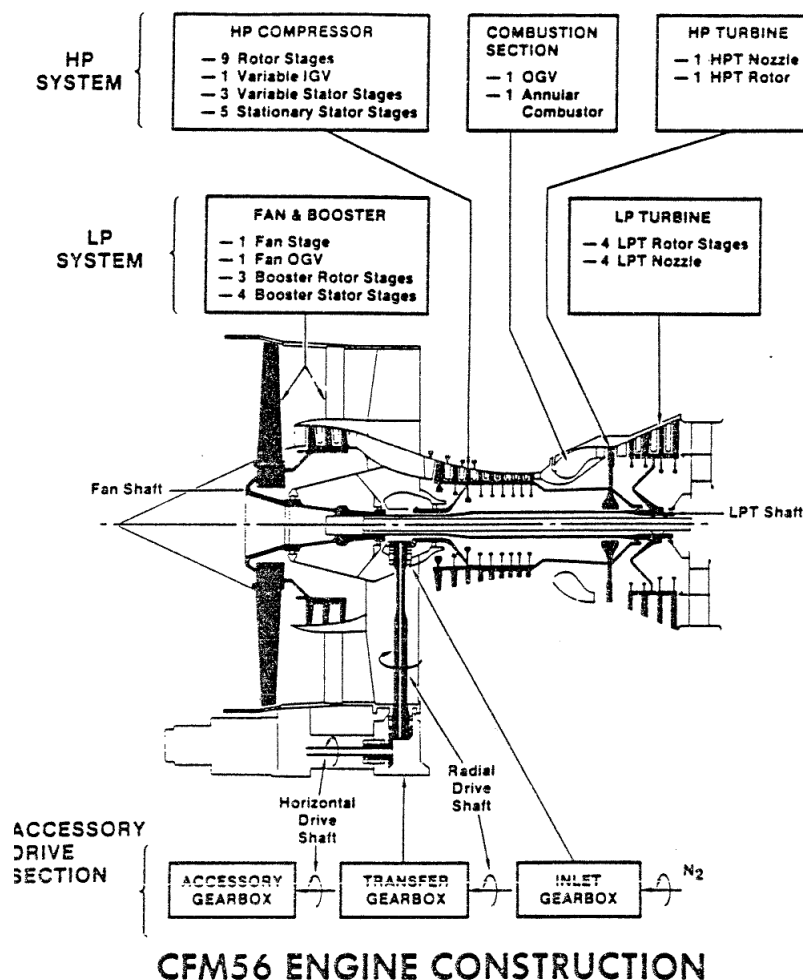

Figure 2.1: Engine Modules [25]

This engine in terms of shop maintenance benefits from its modular construction, the modular concept means that the CFM56-3 is composed by several independent modules, that are assembled to form the all engine. This concept presents several advantages, first of all, the possibility to divide the engine in several modules will decrease significantly the TAT since we have the possibility to substitute a faulty module by a good one and the engine will be operational while the faulty module is being repaired. Is also beneficial when is necessary to perform some work in some areas of the engine, it's just necessary to disassemble some modules to have access to a specific part, avoiding a full disassembling of the engine. Besides, having and transporting

modules is easier and cheaper than with complete engines. In the CFM56-3 the modular concept made possible for GE and SNECMA to manufacturer separately and after assemble it.

CFM56-3 is composed by 3 major modules and 1 Accessory Drive, which can be divided in 17 minor modules.

The 3 major modules are: Fan, Core and LPT. In annex A.1 is possible to consult in detail all the components in this 3 major modules [25].

2.1.1 Minor Module Nº1 Fan and *Booster*

Since our study will be conducted in the Fan major module in this section we will describe the main components that compose the module.

In figure 2.2 is described the Fan major module, and are presented the four minor modules that composed the fan major module.
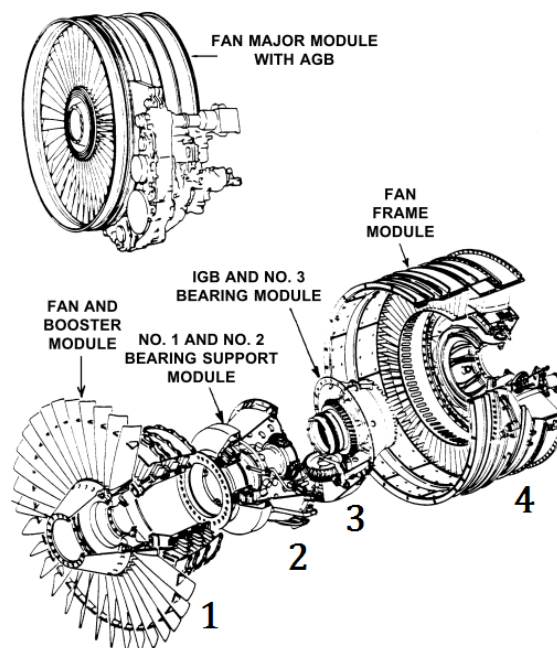

Figure 2.2: Fan Major Module [25]

Table 2.2: Legend Fan major module figure [25] 2.2

Fan Major Module
1- Fan and *Booster*
2 - Bearings support Nº1and Nº2
3- IGB Internal Box
4 - Fan Frame

More specifically, can be said that the majority of this work will take place in minor module Nº1 Fan and *Booster*.

This is the engine inlet minor module, so is located inside the Fan frame. Generally, we can divide this minor module in three main groups, the fan rotor, the *booster* rotor and the *booster* stator. The fan rotor and the booster rotor, as a matter of fact, form a single rotor because the booster is mounted behind the fan disc and both are mounted on the fan spool. One of the fan rotor, main duties is the production of about 80% of the global thrust, i.e. about 17500 lb, to

do that is necessary to drive a great amount of air which is the by-pass flow, after the fan the flow will pass through the fan OGV's. The ensemble, rotor and stator receives a small amount of the total air mass that drives the fan, and in this stage the flow is compressed before being admitted into the HPC. Both rotors of this minor module are connected to the same spool than the LPT [25].
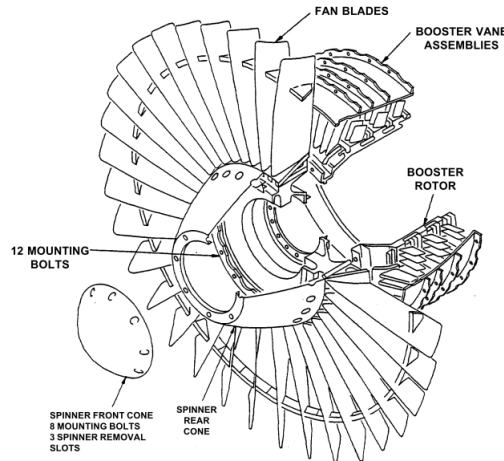

Figure 2.3: Minor Modeule Nº1 Fan and Booster [25]

2.2 Test Bench

A Turbofan engine like the CFM56-3 during is project phase is subject to several tests, throughout the development all the components individually and later all engine can be evaluated with this tests, being possible to make the necessary changes in order to approximate the output from the initial objective.

However, the tests performed in the engines will be necessary throughout an engine's life in order to ensure the safety of the engine and its components. When an engine arrives at TAP engine shop, being from a client or from the fleet, are subject to an acceptance test that evaluates the performance levels, and permits to guarantee the mechanical integrity of the engine and its components. The tests performed in an engine, enables the analysis in a quantitative way to the performance margins, that give a good estimation about performance or degradation of an engine. This thesis, will use data from this tests performed in the TAP test bench to validate the numerical results. TAP has a database build with results from the test bench that allow us to understand the engine's performance and make a comparison with our numerical results.

In the next few paragraphs it will be presented a brief description of the TAP test bench and the data acquisition process in order to understand the data that we have available to make the necessary validation.

There are several kinds of test bench's (interior,exteriors, sea-level or altitude), in this work we will be focusing only on TAP test bench which is interior and sea level test bench. This test bench has an entry channel and an exhaust channel, a control room and a preparation room. In figures 2.4 and 2.5 are presented pictures of the CFM56-3C engine in the TAP test bench [4].

Figure 2.4: Test Bench

Figure 2.5: CFM56-3C in Test bench

Since this work will be focused in analyzing the flow around the fan blades and validating this results with available data from the test bench is important to understand the limitations that we face during the data acquisition on TAP test bench.

In figure 2.6 are represented all the data collection stations in the CFM56-3 engine. The TT25 & PT25 and TS17 & PT17 stations, that are located between the LPC and HPC, and in the secundary flow after the fan, respectively, are only part of the assay when the engineering team request this data, therefore the readings for this two stations are only available for a small number of engines.

The TT49.5 & PT49.5 station is the EGT sensor and is located between the 1st and 2nd blade rows

of the LPT. This station is composed by 9 sensors located around the LPT case. This 9 sensors are used to deliver more accurate readings, for this the EGT indication displayed in the cockpit is the average value calculated from the 9 sensors indications. The use of all these sensors for one temperature indication, is necessary because the flow will have very high gradients that will make characteristics, such as temperature or pressure, vary in a significant way radially along the blades, so the use of several probes tries to minimize these errors [25].

For all other stations there are only one probe that gives the necessary indications, therefore the strong gradients present inside the engine will induce some error in the readings. Values indicated by this stations, are all local values (from a specific point)but they are used as the indication for an area.

In a CFD analysis the values obtained are from very specific locations (can be chosen by user), and the simulation, usually, are accurate enough to "feel" these gradients and all other flow associated phenomenons. Even with this information, is important to notice that TAP test bench is calibrated by responsible companies, in order to ensure the results reliability and ensures the compliance with all the legislations. The test bench delivers a results file with several parameters after each assay, the data is collected in some different engine regimes. These results are displayed as observed parameters, values for standard day, and values that have the *K3* symbol. The observed parameters are the values that are actually measured at the time of the assay, however to make a comparison possible between engine's performance, a correction to these values is necessary. Thereby, the observed parameters will be corrected in order to get the results corrected for a standard day conditions, which according to ISA is a temperature of 288,15K and a Pressure of 101,325 KPa. The mass flow and the rotational speed are also corrected for a standard day according to specific formulas. When the values are displayed with the *K3*, this means that corrections for humidity, condensation, and other installation errors have been made, these specific corrections are calculated using coefficients defined by CFM, and the test bench is prepared to automatically apply these corrections [4].
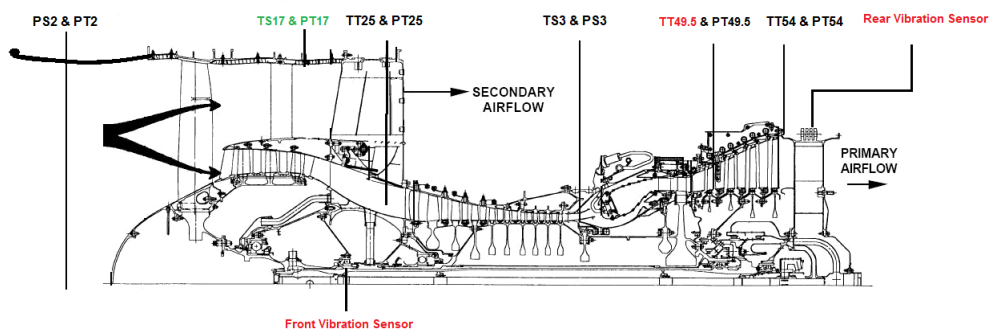

Figure 2.6: Principal Data Collection Stations [25]

When a certain assay is performed in an engine there is a specific procedure that needs to be followed in the test bench. In figure 2.7 is possible to analyze one profile used in the test bench, this profile sows the variation in N1 speed and N2 speed over the assay duration.
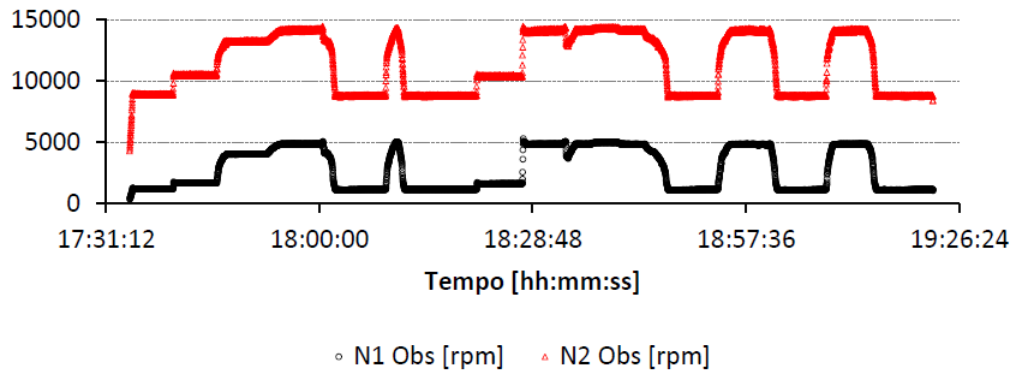
Figure 2.7: Test bench procedure [4]

Chapter 3

Problem Formulation

In this chapter we will be presenting the equations that represent the mathematical model used to characterize the flow through the fan of the CFM56-3 engine, using the ANSYS® solver, CFX® . For that we will describe the system of equations which is composed by three basic principles from physics, the Mass Conservation, the Momentum Conservation and the Energy Conservation, along with a brief explanation from each one of those principles, separately. Then will be highlighted the necessary differences to implement those equations using a rotating reference frame. Finally, tit will be described the equations that will characterize the turbulent flow and the model used to simulate that turbulent flow, and also the specific case of the near wall flow.

3.1 Governing Equations

The cornerstone of CFD is the fundamental governing equations of fluid dynamics, they are the mathematical statements of three fundamental physical principles, the continuity, momentum and energy equations. Applying the necessary simplifications to adapt the equations to our flow characteristics, we will have the system of equations that govern our case.

3.1.1 System of Equations

The set of equations solved by ANSYS CFX are the Navier-Stokes equations in their conservative form. The solver will calculate, for all flows, the mass conservation and the momentum conservation equations. An energy conservation equation will be added in compressible flows. The governing equations stated in the next sections will be described for a compressible and Newtonian fluid during an adiabatic and inviscid flow, and those equations will be solved in a stationary (or inertial) reference frame. We will perform an inviscid analysis of the flow, this generally is the best approach when we intend to simulate a high Mach number flow, because in this conditions the inertial forces are much higher than the viscous forces and this forces can be despised.

3.1.1.1 Mass Conservation

The equation for conservation of mass, or continuity equation, in the differential form, can be written as follows [26]:

$$\frac{\partial \rho}{\partial t} + \nabla \cdot (\rho \cdot \vec{v}) = S_m \quad (3.1)$$

Equation3.1 is the general form of the mass conservation equation and is valid for incompressible as well as compressible flows.The source S_m is the mass added to the continuous phase from the dispersed second phase (for example, due to vaporization of liquid droplets).

3.1.1.2 Momentum Conservation

The momentum conservation equation for the same conditions prior stated, can be written as follows [26]:

$$\frac{\partial}{\partial t}(\rho \vec{v}) + \nabla \cdot (\rho \vec{v} \vec{v}) = -\nabla p + \nabla \cdot (\overline{\overline{\tau}}) + \rho \vec{g} \quad (3.2)$$

where p represents the static pressure and $\vec{g}$ the acceleration of gravity. $\overline{\overline{\tau}}$ is the stress tensor

$$\overline{\overline{\tau}} = \mu \left[\left(\nabla \vec{v} + \nabla \vec{v}^T \right) - \frac{2}{3} \nabla \cdot \vec{v} I \right] \quad (3.3)$$

where μ is the dynamic viscosity and I is the unitary tensor.

Adapting 3.2 to our case (inviscid) in the Navier-Stokes equations for an inviscid flow the term regarding the viscosity will disappear and the so called Euler equation can be written as follows [26]:

$$\frac{\partial}{\partial t}(\rho \vec{v}) + \nabla \cdot (\rho \vec{v} \vec{v}) = -\nabla p + \rho \vec{g} \quad (3.4)$$

As we can see in Euler equation (3.4), the only forces that will be represented on the right term of the equation are the body and pressure related forces.

3.1.1.3 Energy Conservation

The Energy conservation equation for our flow (inviscid), in it's differential form can be written as follows [26]:

$$\frac{\partial}{\partial t}(\rho E) + \nabla \cdot (\vec{v}(\rho E + p)) = -\nabla \cdot \left(\sum_j h_j J_j \right) + S_h \quad (3.5)$$

where J_j is the diffusion flux of species j and S_h includes the heat of chemical reactions, and E can be defined as follows [26]:

$$E = h - \frac{p}{\rho} + \frac{v^2}{2} \quad (3.6)$$

and the sensible enthalpy h is defined for ideal gases as,

$$h = \sum Y_j h_j \quad (3.7)$$

Resuming all the equations previously defined, we can describe the system of equations for an adiabatic flow of a compressible, Newtonian and inviscid fluid written in a divergent form.

The last two equations presented in system 3.8, are the ideal gas equations that relates the pressure with ρ and the internal energy with the absolute temperature.

$$\begin{cases} \frac{\partial \rho}{\partial t} + \nabla \cdot (\rho \vec{\nu}) = 0 \\ \frac{\partial}{\partial t}(\rho \vec{\nu}) + \nabla \cdot (\rho \vec{\nu} \vec{\nu}) = -\nabla p + \rho \vec{g} \\ \frac{\partial}{\partial t}(\rho E) + \nabla \cdot (\vec{v}(\rho E + p)) = -\nabla \cdot \left(\sum_j h_j J_j \right) + S_h \qquad (3.8) \\ \rho = \frac{p}{RT} \\ E = C_\nu T \end{cases}$$

In an compressible case like ours the ideal gas equations make a connection between the energy equation and the mass and momentum conservation equations, this connection appears with the possible variation of ρ, resulting from the pressure and temperature variations throughout the flow [26].

3.1.2 Rotating Reference Frame Equations

Besides the system of equations defined above for a stationary reference frame, there are many problems where it is advantageous to solve the equations in a moving (or non-inertial) reference frame. These problems typically involve moving parts, such as rotating blades, impellers, and moving walls, and it is the flow around the moving parts that is of interest, being our case a rotating fan blade this rotating reference frame will be the best approach. With a moving reference frame, the flow around the moving part can (with certain restrictions) be modeled as a steady-state problem with respect to the moving frame.When a moving reference frame is activated, the equations of motion are modified to incorporate the additional acceleration terms which occur due to the transformation from the stationary to the moving reference frame [27].

If we consider a coordinate system that is translating with a linear velocity $\vec{v_t}$ and rotating with angular velocity $\vec{w}$ relative to a stationary (inertial) reference frame, as illustrated in figure 3.1. The origin of the moving system is located by a position vector $\vec{r_0}$.
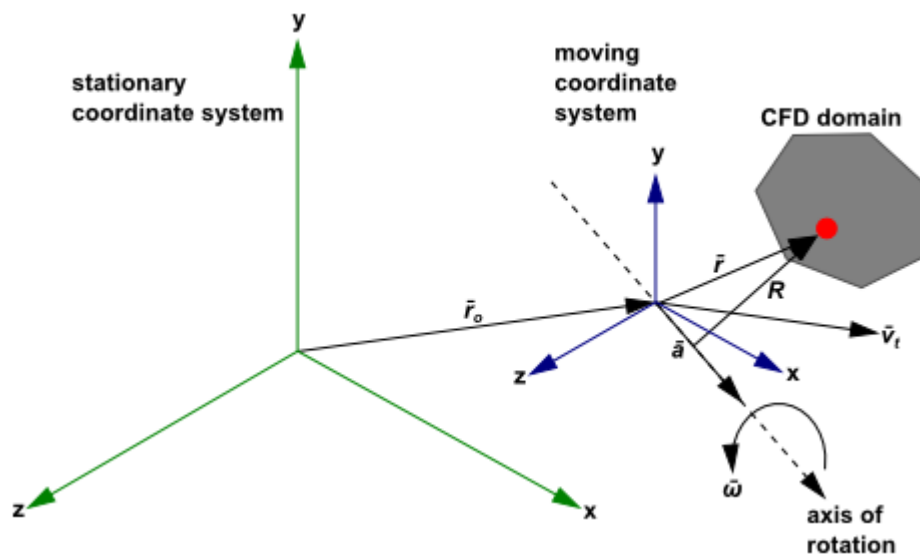

Figure 3.1: Stationary and Moving coordinate system[27]

The fluid velocities can be transformed from the stationary frame to the moving frame using the following relation [27]:

$$\vec{v_r} = \vec{v} - \vec{u_r} \quad \text{(3.9)}$$

where,

$$\vec{u_r} = \vec{v_t} + \vec{w} \times \vec{r} \quad \text{(3.10)}$$

$\vec{v_r}$ is the relative velocity (the velocity viewed from the moving frame), $\vec{v}$ is the absolute velocity (the velocity viewed from the stationary frame), $\vec{u_r}$ is the velocity of the moving frame relative to the inertial reference frame and $\vec{v_t}$ is the translational frame velocity.

Using a formulation in reference to the absolute velocity, the governing equations of fluid flow for a steadily moving frame can be written as follows [27]:

Conservation of mass,

$$\frac{\partial \rho}{\partial t} + \nabla \cdot \rho \vec{v_r} = 0 \quad \text{(3.11)}$$

Conservation of momentum,

$$\frac{\partial}{\partial t} \rho \vec{v} + \nabla \cdot (\rho \vec{v_r} \vec{v}) + \rho [\vec{\omega} \times (\vec{v} - \vec{v_t})] = -\nabla p + \nabla \cdot \overline{\overline{\tau}} + \vec{F} \quad \text{(3.12)}$$

Conservation of energy,

$$\frac{\partial}{\partial t} \rho i + \nabla \cdot (\rho \vec{v_r} H + p \vec{u_r}) = \nabla \cdot (k \nabla T + \overline{\overline{\tau}} \cdot \vec{v}) + S_h \quad \text{(3.13)}$$

In this formulation, the Coriolis and centripetal accelerations can be simplified into a single term ($[\vec{w} \times (\vec{v} - \vec{v_t})]$) [27].

3.1.3   Turbulent Flow Modelling

Being the aim of this manuscript to analyze the flow characteristics around a blade from the fan of the CFM56-3, it becomes necessary, to give information on the turbulence flow and also the turbulence model that we can use to solve this flow.

By definition, "*Turbulent fluid motion is an irregular condition of flow in which the various quantities show a random variation with time and space coordinates, so that statistically distinct average values can be discerned*" [29]. It is a complex process, mainly because it is three dimensional,unsteady and consists of many scales. It can have a significant effect on the characteristics of the flow. Turbulence occurs when the inertia forces in fluid become significant compared to viscous forces, and is characterized by a high Reynolds Number. In a computational point of view, this flow, that can have high frequencies with low amplitudes, become quite difficult to simulate and certainly increases, greatly, the simulation time.

Because of this random characteristics, the statistical approaches are used to express mean and fluctuating parts, Chen, C.J, and Jaw, S.Y. [30] concludes that from an engineering point of view, what we would like to know is the mean effect of turbulence quantities, and not so much the instantaneous fluctuation quantities. Under this circumstances, the instantaneous

Navier-Stokes equations can be transformed to use an average times approach, that decreases the necessary computation time. The problem that arises from this transformation, is that in our system of equations their will be some additional terms, known as the Reynolds Stress $\overline{u_i u_j}$, that will make the number of unknowns bigger than the available equations, so the system is unsolvable. To solve this problem a set of equations can be added based on empirical information in order to solve the new variables. This empirical relationships are known as turbulence models. Turbulence models have been specifically developed to account for the effects of turbulence without recourse to a prohibitively fine mesh and direct numerical simulation.

As we said before, the original Navier-Stokes equations can be modified by the introduction of averaged and fluctuating quantities to produce the Reynolds Averaged Navier-Stokes (RANS) equations. Turbulence models based on the RANS equations are known as Statistical Turbulence Models due to statistical averaging procedures employed to obtain the equations. Simulation of the RANS equations greatly reduces the computational effort compared to a direct Numerical Simulation [26].

3.1.3.1 Reynolds Averaged Navier-Stokes

In Reynolds averaging, the solution variables in the instantaneous Navier-Stokes equations are decomposed into the mean (time-averaged) and fluctuating components. For the velocity components [26]:

$$u_i = \bar{u}_i + u_i' \quad (3.14)$$

where $\bar{u}_i$ and u_i' are the mean and fluctuating velocity components.
We use the same approach for pressure and other scalar quantities [26]:

$$\phi = \bar{\phi} + \phi' \quad (3.15)$$

where ϕ denotes a scalar such as pressure or energy.
The averaged component is given by:

$$\overline{\phi} = \frac{1}{\triangle t} \int_t^{t+\triangle t} \phi_i dt \quad (3.16)$$

where $\triangle t$ is a time scale that is large relative to the turbulence fluctuations, but small relative to the time scale to which the equations are solved.
Substituting the averaged quantities into the original transport equations results in the Reynolds Averaged equations below [26]:

$$\frac{\partial \rho}{\partial t} + \frac{\partial}{\partial x_i}(\rho u_i) = 0 \quad (3.17)$$

$$\frac{\partial}{\partial t}(\rho u_i) + \frac{\partial}{\partial x_j}(\rho u_i u_j) = -\frac{\partial p}{\partial x_i} + \frac{\partial}{\partial x_j}\left[\mu\left(\frac{\partial u_i}{\partial x_j} + \frac{\partial u_j}{\partial x_i} - \frac{2}{3}\delta_{ij}\frac{\partial u_l}{\partial x_l}\right)\right] + \frac{\partial}{\partial x_j}\left(-\rho\overline{u_i' u_j'}\right) \quad (3.18)$$

Equations 3.17 and 3.18 are called RANS equations.They have the same general form as the instantaneous Navier-Stokes equations, with the velocities and other solution variables now representing time-averaged values. Additional terms now appear, that represent the effects of turbulence. These Reynolds stresses, $-\rho\overline{u_i'u_j'}$, represent the effects of the turbulence. [26]

The Reynolds-averaged approach to turbulence modeling requires that the Reynolds stresses in 3.18 are appropriately modeled. A common method employs the Boussinesq hypothesis to relate the Reynolds stresses to the mean velocity gradients [26]:

$$-\rho\overline{u_i'u_j'} = \mu_t\left(\frac{\partial u_i}{\partial x_j} + \frac{\partial u_j}{\partial x_i}\right) - \left(\rho k + \mu_t\frac{\partial u_k}{\partial x_k}\right)\delta_{ij} \quad (3.19)$$

The Boussinesq hypothesis is used in the Spalart-Allmaras model, the k-ε models, and the k-ω models. The advantage of this approach is the relatively low computational cost associated with the computation of the turbulent viscosity, μ_t. In the case of the Spalart-Allmaras model, only one additional transport equation (representing turbulent viscosity) is solved. In the case of the k-ε and k-ωmodels, two additional transport equations one for the turbulence kinetic energy, k, and either the turbulence dissipation rate, ε, or the specific dissipation rate, ω, are solved, and $\mu_t$is computed as a function of k and εor k and ω. [26]

For compressible flows exists another averaging process called Favre averaging. The Favre averaging is sometimes used in compressible flow to separate turbulent fluctuations from the mean-flow. In most cases it is not necessary to use Favre averaging though, since turbulent fluctuations most often do not lead to any significant fluctuations in density. In that case the more simple Reynolds averaging, which we demonstrate previously can be used. Only in highly compressible flows and hypersonic flows is it necessary to perform the more complex Favre averaging.

3.1.4 k-ω SST Model

There are several turbulence models available in ANSYS CFX at our disposal, and one of the challenges that we face in this simulation is the selection process of the most adequate turbulence model regarding the specificity of our case. Bradshaw [30] considers that the turbulence modelling is closer to an art than a science. So, since we understand that in this case there is no right or wrong answer, we need to base our choice in previous studies, and through the perfect understanding of the characteristics of our problem as well as the turbulence models. It is very important that the user is perfectly aware of the turbulence model capabilities and limitations, so it's important to keep in mind that the best choice is a turbulence model that is closer to the real situation and uses less computational resources. In our case, after the study of the majority of the turbulence models and a literature research trying to find similar analysis or indications about which should be the more precise with less computational complexity. In, Simões, M. et al [33] the aim is to compare and validate three different turbulence models applied to CFD simulation of turbulent flow inside a rotor of an axial flow compressor of which flow field was obtained experimentally.

Three turbulence models were used , $k - \varepsilon$,$k - \omega$ and SST. It was concluded that the SST turbulence model was validated for this problem for presenting the most accurate results among the three models evaluated, when comparing them to the experimental data of the compressor performance. Besides, all the differences between our case and the case analyzed in this

work, we can learn based in this project that the SST turbulence model has some advantages comparing to others in this cases. Based, not only in this information, we decide to proceed using **SST model** in our simulation. Although, in the Reynolds Stress Transport Model one of its advantages when compared to the previous models is the ability to simulate the additional anisotropy of the Reynolds stresses due to the Coriolis force in the rotating frame of reference, which we are using, but this model is very complex and has a very high computational cost.

The shear-stress transport (SST) - model was developed by Menter [34] to effectively blend the robust and accurate formulation of the $k-\omega$ model in the near-wall region with the free-stream independence of the $k-\varepsilon$ model in the far field. To achieve this, the $k-\varepsilon$ model is converted into a $k-\omega$ formulation. The SST $k-\omega$ model is similar to the standard $k-\omega$ model, but includes some refinements. First, the standard $k-\omega$ model and the transformed $k-\varepsilon$ model are both multiplied by a blending function and both models are added together. The blending function is designed to be one in the near-wall region, which activates the standard $k-\omega$ model, and zero away from the surface, which activates the transformed $k-\varepsilon$ model. The SST model incorporates a damped cross-diffusion derivative term in the ω equation. The definition of the turbulent viscosity is modified to account for the transport of the turbulent shear stress. Lastly, the modeling constants are different.

These features make the SST $k-\omega$ model more accurate and reliable for a wider class of flows (for example, adverse pressure gradient flows, airfoils, transonic shock waves) than the standard $k-\omega$ model. [34]

The Transport equations for this model, SST, can be written as follows:

$$\frac{\partial}{\partial t}(\rho k) + \frac{\partial}{\partial x_i}(\rho k u_i) = \frac{\partial}{\partial x_j}\left(\Gamma_k \frac{\partial k}{\partial x_j}\right) + G_k - Y_k \quad (3.20)$$

$$\frac{\partial}{\partial t}(\rho \omega) + \frac{\partial}{\partial x_i}(\rho \omega u_i) = \frac{\partial}{\partial x_j}\left(\Gamma_\omega \frac{\partial \omega}{\partial x_j}\right) + G_\omega - Y_\omega + D_\omega \quad (3.21)$$

In these equations, G_k represents the generation of turbulence kinetic energy due to mean velocity gradients and G_ω represents the dissipation of ω. Γ_k and Γ_ω represent the effective diffusivity of k and ω, respectively, Y_k and Y_ω represent the dissipation of k and ω due to turbulence. D_ω represents the cross-diffusion term.

The effective diffusivities for the SST $k-\omega$ model are given by [34]:

$$\Gamma_k = \mu + \frac{\mu_t}{\sigma_k} \quad (3.22)$$

$$\Gamma_\omega = \mu + \frac{\mu_t}{\sigma_\omega} \quad (3.23)$$

where σ_k and σ_ω are the turbulent Prandtl numbers for k and ω, respectively. The turbulent viscosity, μ_t, is computed as follows [34]:

$$\mu_t = \frac{\rho k}{\omega} \frac{1}{max \left[\frac{1}{\alpha^*}, \frac{SF_2}{a_1\omega} \right]} \quad (3.24)$$

Where S is the strain rate magnitude and α^* damps the turbulent viscosity causing a low-Reynolds number correction.

σ_k and σ_ω can be defined as follows,

$$\sigma_k = \frac{1}{\frac{F_1}{\sigma_{k,1}} + \frac{(1-F_1)}{\sigma_{k,2}}} \quad (3.25)$$

$$\sigma_\omega = \frac{1}{\frac{F_1}{\sigma_{\omega,1}} + \frac{(1-F_1)}{\sigma_{w,2}}} \quad (3.26)$$

All functions and constants missing in this description can be consulted in the ANSYS theory documentation for the solvers, (Fluent® and CFX) in references [28] [27] [26].

3.1.5   Near Wall Turbulence

When discussing turbulent flows we need to keep present that this flows are greatly affected by the presence of walls, in a case like this investigation (confined) this gains special importance. Obviously the mean velocity field is affected through the no-slip condition that has to be satisfied at the surface (wall). In the other hand the turbulence is also changed by the presence of the wall. In a region close to the wall, viscous damping reduces the tangential velocity fluctuations, while kinematic blocking reduces the normal fluctuations. Toward the outer area of the near-wall region, the turbulence is rapidly augmented by the production of turbulence kinetic energy due to the large gradients in the mean velocity [26].

The modeling of the near-wall region has a meaningful effect on the accuracy of the numerical solutions, specially because walls are the main source of mean vorticity and turbulence. In this near-wall region is the area where the solution variables have the largest gradients, and the momentum and other scalar transports occur most vigorously. So, an accurate representation of the flow in this region will determine the success of the predictions of the turbulent flow. Based in several experiments it is possible to divide the near-wall region in three layers. The first and innermost layer is called viscous sublayer and in this region the flow is almost laminar, and the molecular viscosity dominates in the momentum and heat or mass transfer. The third and more outer layer, called the fully-turbulent layer or log-law region, specially because in this region the turbulence dominates any other effect. Finally, there is a interim region between this two, called blending region where the effects of molecular viscosity and turbulence are equally important.[26] These regions are illustrated in figure 3.2.
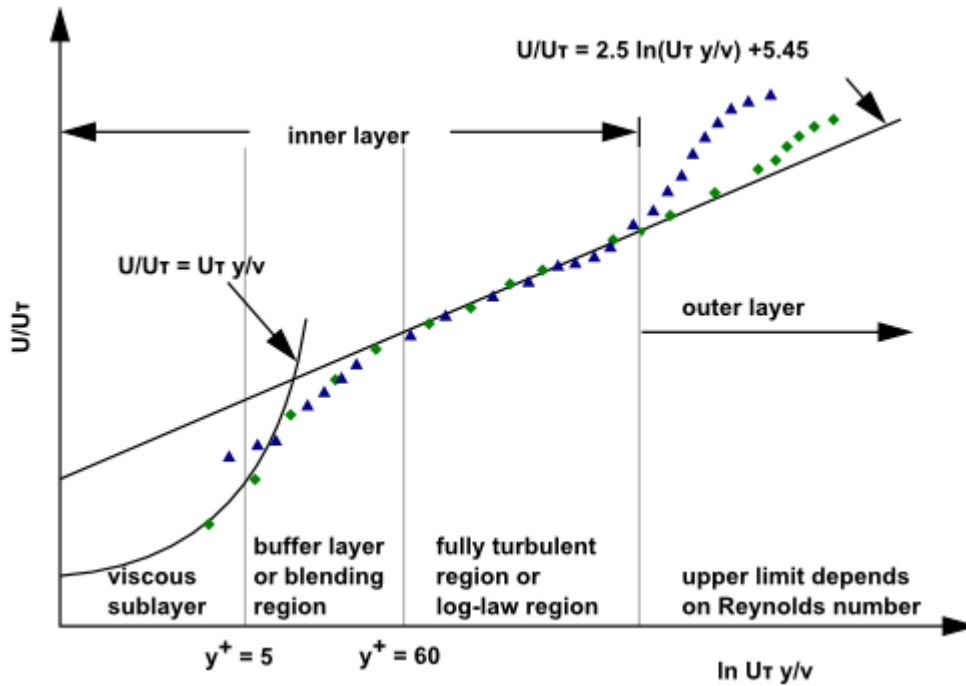
Figure 3.2: Subdivisions of the Near-Wall Region[26]

In figure3.2 it is possible to see the value of y^+ used to subdivide the regions. This value can be computed as follows [41]:

$$y^+ = \frac{\rho u_t y}{\mu} \quad (3.27)$$

where u_t is the friction velocity and y is the distance to the wall.

The y^+ is a non dimensional measurement of distance from a wall. It is used to describe the height of the first grid element next to a wall in a CFD simulation [28]. We use y^+ because experimental observation has confirmed that flows of all scales (big or small, fast or slow) tend to demonstrate very similar flow patterns as the flow approaches a wall. So y^+ **is really used to identify where in the boundary layer profile our first calculation point resides**. We can then utilize this y^+ number to determine the applicability of near wall turbulence modeling we intend to use, and these should be applicable regardless of internal or external flow conditions. So if we have a $y^+ \simeq 1$, we do not need any wall models and instead one are resolving the flow all the way to the wall (typically with 10-15 cells within the boundary layer thickness). If we intend to use a coarser mesh and utilize wall functions to capture the near wall velocity profile, we may aim for a y^+ between 30 and 300. Whilst this range is often quoted as a general rule of thumb for both external and internal flows, it is very important to consider that the appropriate range of y^+ will vary according to Reynolds number.

Chapter 4

Numerical Model

In this chapter will be presented the process used to implement our simulation in ANSYS® software, the simulation is performed to modulate the flow around the fan of the engine CFM56-3. In chapter 1, it was enunciated, generally, the phases of the CFD resolution process, the following sections in this chapter intended to give a detailed description from almost all this phases. This will start with a comparison of the general characteristics, between two ANSYS softwares. After, the geometry construction process will be presented with some details about the control volume that will be used in the simulation, following is the discretization subsection to discuss the mesh construction process and the topology used in this process. Finishing, it will be two subsections dedicated to the case set up, starting with the boundary conditions applied to these simulations, after a subsection dedicated to the simulation process starting with a brief description about the iterations calculations and to conclude the convergence criteria used to assess when the iterative process should be stopped.

4.1   CFD Codes

This section will describe a decision making process that we where faced during the course of this project in order to decide which CFD Software shall be the most adequate, taking into account the specifics of this work. The initial software used to create the geometry, CATIA V5, was selected based on better familiarization with this software and the large amount of information available about it, which save time to do a more elaborated decision on the mesh and solver software, that will be used.
The decision was made between two CFD codes from the same company, ANSYS FLUENT® and ANSYS CFX®

FLUENT is a cell centered finite volume, segregated/coupled, implicit/explicit, density/Pressure based solution technique. In cell centered schemes the flow variables are stored at the centers of the mesh elements.
CFX is cell-vertex finite volume, coupled implicit, pressure based solution technique (solves for pressure and velocity at the same time). Pressure and velocity are co-located, so p-v decoupling is dealt with using a Rhie-Chow approach [35]. In vertex based schemes the flow variables are stored at the vertices of the mesh elements.
Both codes are about the same in accuracy, but hard to compare on an unstructured mesh, since CFX is a Cell-Vertex and Fluent is Cell Centered. CFX assembles control volumes around the element vertices, resulting in polyhedral control volumes and hence there are fewer nodes than cells with a tetrahedral mesh. While this results in fewer control volumes, there are far more integration points so the resolution of gradients is more accurate per control volume. Comparing FLUENT and CFX solutions, it is possible to find that the FLUENT solution is slightly more accurate for the same mesh, but much more costly to run (since you are solving 5 times the number of equations), so is affordable to run a finer mesh in CFX.

In order to understand the general characteristics of the two CFD codes that we are analyzing, the table 4.1 was created.

Table 4.1: CFX vs FLUENT

CFX	FLUENT
CFX is cell-vertex finite volume. To implement boundary condition better and to avoid corner singularity better.	Fluent is a cell-centered code.
Robustness for steady problems is better in CFX	It takes a little tuning to get Fluent to converge.
ANSYS CFX software has focused on a solution strategy using a coupled algebraic multi-grid techniques that delivers fast and reliable convergence that is completely scalable with mesh size.	ANSYS Fluent offers robust solvers for any application: a fully segregated pressure based solver, a coupled pressure based solver with pseudo-transient option, an implicit and an explicit density based solver
CFX has an easy to use CFX command language to do simple things. Otherwise CFX Command Language is not well documented.	Fluent User-defined Function are very well documented, archived and very flexible.

From the information that was gather previously and some statistical data as well as some unofficial opinions from experienced users, is possible to state that both flow solvers tend to provide similar results, assuming that a good quality mesh was created with the appropriated number of nodes and the y^+ values are adequated, but the general conclusions that we can extract from all this informations are as follows:

1. Regarding the turbulence models it is possible to use the same turbulence models in both solvers.

2. Regarding the calculation time to obtain a solution it is possible to conclude that CFX takes less time to converge when dealing with the same problem. In some cases this difference is quite significant, based on unofficial data when FLUENT took 72 hours CFX took approximately 18 hours (1.5 million nodes with 4GB Ram memory).

3. In CFX a scaling feature is available, this feature in CFX allows iteration time to remain unchanged when increasing the number of mesh nodes.

4. In terms of memory management CFX can run, generally, 50% more mesh nodes than FLUENT for the same computer capacity.

Finally, it is possible to state that FLUENT has slightly better accuracy in most cases and a much wider applicability (almost all cases are possible to simulate with good accuracy), CFX has many limitations in terms of applicability, although the main reason for the selection of this solver in this simulation, was the experience in rotating machinery which ensures that ANSYS CFX software provides all the models and infrastructure for accurate, robust and efficient modeling of all types of pumps, fans, compressors, gas and hydraulic turbines. Within ANSYS CFX, tailored pre- and post-processing tools complement a full suite of interface models to capture the interactions between the rotating and stationary components present in turbomachinery. [36]

4.2   Geometry

In order to modulate the flow around the fan blades of the CFM56-3 it was decided that the computational control volume will be composed by 3 parts, the bellmouth intake (inlet domain), the fan and the outlet domain as can be seen in figure 4.1.
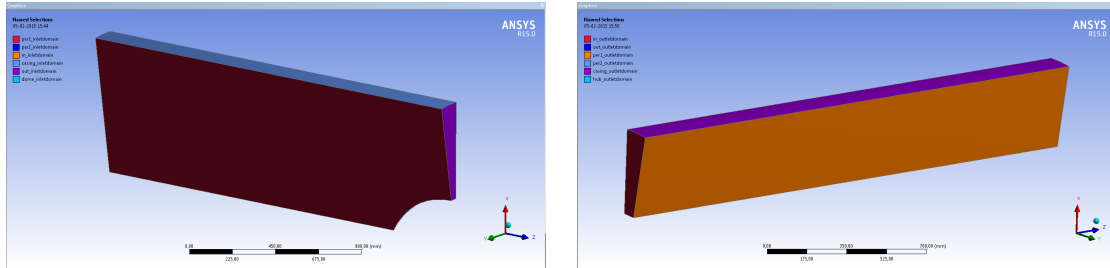

Figure 4.1: Inlet (left) and Outlet (right) domain

All domains where created attempting to reproduce the real conditions inside the test bench, since was intended to simulate the engine fan (38 blades, 360°) which can be simplified by only 9,47° (1 blade), once it was used the periodicity concept available in CFD softwares. Therefore, the control volume starts with the inlet domain, that represents the engine bellmouth installed in the engine prior to each assay, this domain has the exact same dimensions of the real model. The second domain, the blade, was obtained through a reverse engineering process, by using a real blade, that was removed from an CFM56-3 (version) during a maintenance process at TAP. The blade was sent to an outsourcing company that was responsible for the digitization process and has delivered a 3D file containing the blade geometry. After, some surface treatment was necessary in order to have this geometry ready to be used. To understand the changes in the flow characteristics three different blade chord were created:

- **Small chord (5.607 in - 142,418 mm)**

- **Medium Chord (5,764 in - 146,138 mm) and**

- **Large chord (5,900 in - 149,860 mm),**

this dimensions were selected based on a previous work conducted at TAP. The last domain, Outlet, was produced with the same length as the inlet domain and this decision was mainly based in a few points which were considered to be the most realistic solution and are described hereinafter. First of all, in this type of analysis it is necessary to manage the upstream and downstream distance from the blade in order to have a fully developed flow downstream of the blade, and avoid the blade static pressure field interference in the inlet flow. According to Dixon and Hall [37] the upstream distance should be somewhere between 50% to 100 % of the blade chord from the leading edge, however, this is not relevant because we have a inlet domain starting long before when compared to this dimensions. For the Outlet domain according to Berbente et al. [16] the downstream distance should be, at least, equal to the blade row pitch, although was decided to create the outlet domain with the same length as the inlet, mainly because, as we have seen before, the Pressure sensor PT17 is located in the secondary flow, so with this conditions it is possible to compare and validate the outlet flow variables with the information provided by this sensor.

Concluding, the control volume can be defined from the engine bellmouth all the way to the exit of the outlet domain, with the blade located in the middle of the control volume, regarding

the upper and lower limits, the volume is bounded below by the axis of rotation all the way to the engine *abradable*.

4.3 Discretization

Analytical solutions to the Navier-Stokes equations exist for the simplest of flows under ideal conditions but to obtain solutions for real flows a numerical approach must be adopted whereby the equations are replaced by algebraic approximations that can be solved by a numerical method. CFX uses an element based finite volume method, which first involves discretize the spatial domain using a mesh, this mesh is used to construct finite volumes, which are used to conserve relevant quantities such as mass, momentum and energy. The control volume are divided in three domains, whereby three meshes were created using, *ICEM CFD* for the inlet and outlet domains and *Turbo Mesh* for the blade domain.

In the Inlet domain, an unstructured mesh was applied with 2947 Nodes and 15678 Elements, and a progressive mesh refinement was implemented towards the blade domain (Figure 4.2). For the Putlet domain was chosen a structured mesh composed by 85731 Elements and 80000 Nodes, as we can see in figure 4.2, the mesh is significantly refined closer to the blade and the elements density decreases towards the domain exit (outlet). The Blade domain is clearly the space where more elements are needed in order to solve all the physical phenomenons presented, therefore a structured mesh was implemented with a maximum of 1139412 Elements and 1180178 Nodes, the mesh is progressively more refined towards the blade surfaces in order to solve the boundary layer formed in this region (Figure 4.4).
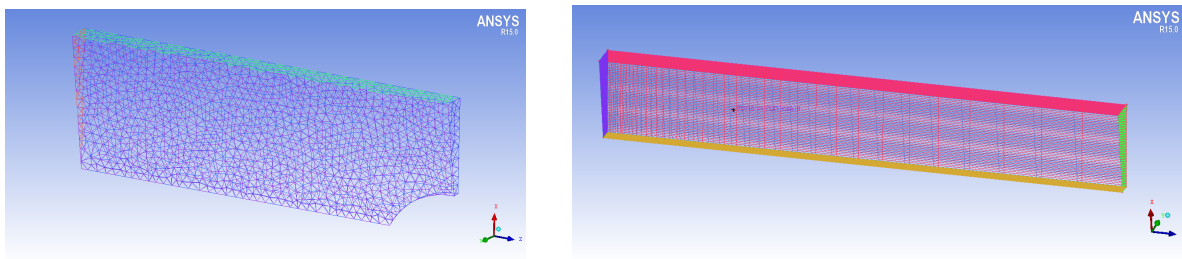

Figure 4.2: Inlet mesh (left) and Outlet mesh (right)

When meshing a blade structure it is necessary to chose the mesh topology, which represents the form that the mesh will assume around the blade. There are several different topologys such as H/J/C/L grid, as we can see in annex A.2 [27]. Alternatively, it is possible to use the option *ATM Optimized,* which was the option used in the meshing process as showed in figure 4.3, this feature enables the user to create high-quality meshes with less effort, not needing any control point adjustment. The *ATM Optimized* method automatically computes a default mesh, based on the blade characteristics using all other known topologys and sets the base mesh dimension. However, it is possible to adjust any necessary settings, like the overall mesh size or the boundary layer resolution near the wall, if needed.

As it was previously highlighted the mesh creation is a critical process in order to ensure convergence and accuracy specially for turbulent flow.

As we have seen before y^+ is a non dimensional measurement of distance from a wall. It is used to describe the height of the first mesh/grid element next to a wall in a CFD simulation, which allow us to assess the applicability of the near wall modeling selected to use. For boundary layers in adverse pressure gradients, to correctly solve the boundary layer flow it is imperative
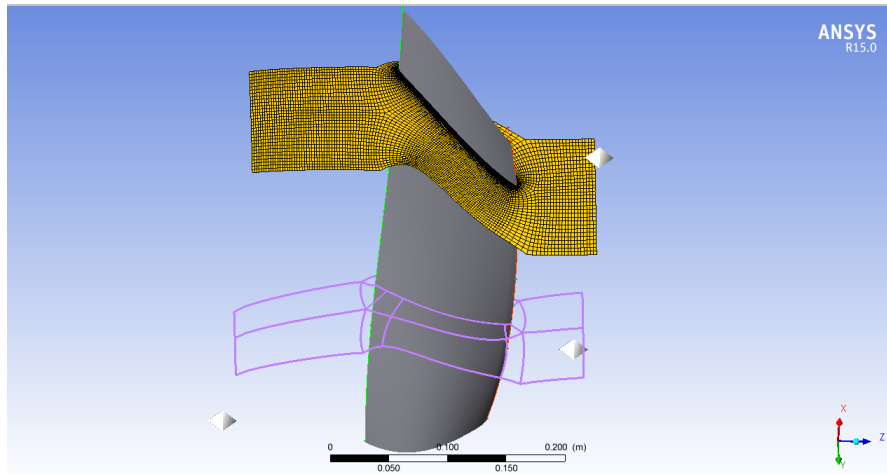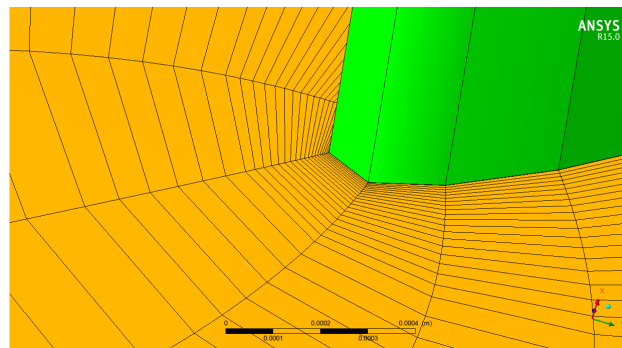
Figure 4.3: Mesh Topology

Figure 4.4: Leading edge mesh detail

to have a y^+ less than or equal to 1, meaning we are resolving the boundary layer flow all the way to the laminar sub-layer. For this reason the SST model is ideal, since the use of the $k - \omega$ formulation for the boundary layer region means we can resolve to the viscous sub-layer and no extra wall functions are introduced. In the free-stream (outside the boundary layer), the SST model switches to a $k - \varepsilon$ formulation which is better suited to free shear flows.

Altought, the modern implementation of turbulence models in ANSYS are y^+ insensitive. This ensures that regardless of where the first grid height lies, it will be modeling the boundary layer profile comparatively.

In this simulation, using a SST $k - \omega$ model, a refined mesh near the wall is used (Figure 4.4) in order to solve the sub-layer where the molecular viscosity is more prominent. To guarantee that the mesh is correctly refined it is important to look for a y^+ around 1 or less, and 10 to 15 cells within the boundary layer.

After the mesh construction process finalization it is necessary to evaluate the mesh quality. The three mesh domains that compose our control volume were analyzed with the mesh analysis toll available in the software. The mesh quality analysis is a process that analysis several parameters such as: *Maximum Face angle, Minimum Face Angle, Connectivity number, Element Volume Ratio, Minimum Volume* and *Edge Length Ratio*.

The *Maximum Face Angle* variable is the angle between the two edges of the face that touch the node and is calculated for each face, the largest angle from all faces is returned as the result of this variable. The *Minimum Face Angle* is the smallest face angle for all faces that touch the node. *Connectivity number* is the number of elements that touch a node, the result

41

for this variable is the maximum connectivity number on any element, this variable is one of the least important in a mesh analysis. *Element Volume Ratio* is defined as the ratio of the maximum volume of an element that touches a node, to the minimum volume of an element that touches a node. *Minimum Volume* is used to ensure that no negative volumes are created within the domain, this variable is the most important in a mesh analysis and its value must be fixed before the mesh would be usable. *Edge Length Ratio* represents the ratio of the longest edge of a face divided by the shortest edge of the face, the largest ratio is returned as result. This value can be considered to be a measure of aspect ratio [36].

All domains were analyzed, but the most important to be considered are the blade domain where the number of nodes is larger and the flow solution is more important. Based on this analysis the meshes were considered acceptable to be used, with all parameters within limits except for the *Element Volume Ratio* value which returns a 0,0478 % *bad solution,* which is not a relevant value for the mesh total performance, based on this, the mesh was accepted with this slight deviation from the optimum.

4.4 Boundary Conditions

The CFD solution convergence and accuracy is, also, highly dependent on the boundary conditions and initial values that are set for the simulations. In order to set a proper set of boundary conditions and initial values it is necessary to perfectly understand the real physical process that is undergoing, this will allow the creation of a solvable and close to reality simulation.

The following combinations of boundary conditions are all valid configurations commonly used in ANSYS CFX. They are listed from the most robust option to the least robust [36]:

- Most Robust: Velocity/mass flow at an inlet and static pressure at an outlet. The inlet total pressure is an implicit result of the prediction.

- Robust: Total pressure at an inlet and velocity/mass flow at an outlet. The static pressure at the outlet and the velocity at the inlet are part of the solution.

- Sensitive to Initial Guess: Total pressure at an inlet and static pressure at an outlet. The system mass flow is part of the solution.

- Very Unreliable: Static pressure at an inlet and static pressure at an outlet. This combination is not recommended, as the inlet total pressure level and the mass flow are both an implicit result of the prediction (the boundary condition combination is a very weak constraint on the system).

- Not Possible: Total pressure cannot be specified at an outlet. The total pressure boundary condition is unconditionally unstable when the fluid flows out of the domain where the total pressure is specified.

In this simulations, based on the information that was obtained from the test bench, it was used a robust combination with a Total Pressure Inlet and mass flow in the outlet, as it is described below.

- **Inlet**

In the inlet a boundary condition of *Total Pressure* was selected, when this condition is selected it is necessary to specify, the flow regime (subsonic), the total pressure value (101325 Pa)

and the flow direction (axial component). It was also necessary to specify the turbulence (Intensity=5%) and a value of static temperature (288 K).

- **Outlet**

For the Outlet a boundary condition of *Mass Flow Rate* was chosen, in this boundary condition it is only necessary to specify the mass flow rate, since all the other variables will be obtain from the simulation iterations.

- **Blade Domain**

The blade domain was defined as a rotating domain and the blade being a solid surface, the *No-Slip Wall* was imposed, this is a very common type of wall boundary condition, the fluid immediately next to the wall assumes the velocity of the wall.

- **Rotational Periodic Interface**

The lateral boundaries of the control volume were defined as periodic interfaces in order to represent the periodic characteristics that is presented in the flow around adjacent blades.The interface model defines the way the solver models flow physics across the interface, so the periodic condition ensures that the flow out of one side of the interface automatically appears on the other side (Figure 4.5) . In this case, the two sides of the periodic interface can be mapped by a single rotational transformation about an axis. For our simulation the Z axis was chosen for the rotational transformation.
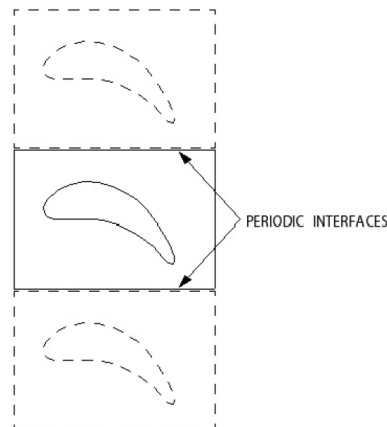

Figure 4.5: Example of Periodic Interfaces [36]

- **Walls**

For our simulation in inviscid flow, the walls were set with a condition of *Free Slip Wall,* with this condition the shear stress at the wall is zero, and the velocity of the fluid near the wall is not retarded.

4.5   Simulation

The software ANSYS CFX uses an element-based finite volume method, which first involves discretizing the spatial domain, that was discussed previously.
Regarding the equations resolution process, CFX uses a *Pressure-Based* solver with this process the mass conservation (continuity) of the velocity field is achieved by solving a pressure, or a
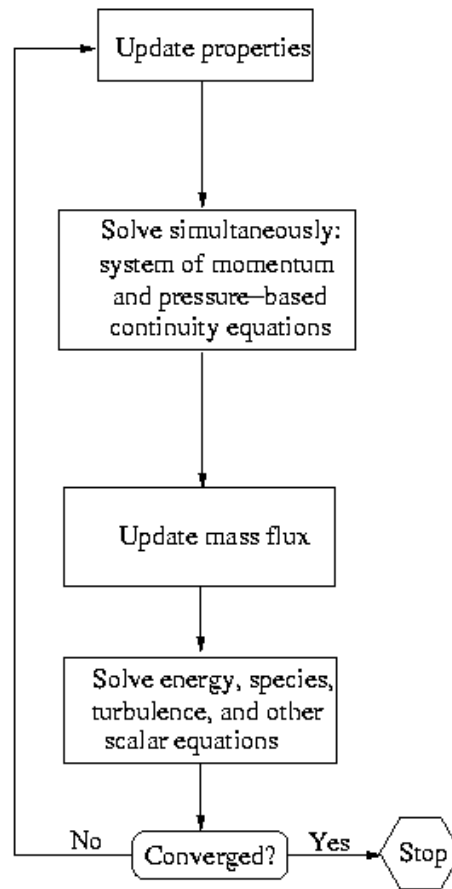
Pressure—Based Coupled Algorithm

Figure 4.6: Pressure-Based Coupled Algorithm [26]

pressure correlation, equation. The pressure equation is derived from the continuity and the momentum equations in such a way that the velocity field, corrected by the pressure, satisfies the continuity. The Pressure-Based solver is very versatile, being able to work from low speed incompressible flows to high speed compressible flows. [26]

The Pressure-Based solver uses a coupled approach to solve the flow equations, which solves the hydrodynamic equations as a single system. This approach uses a fully implicit discretization of the equations at any given time step. Using the coupled approach, offers some advantages over the non-coupled approach, this scheme obtains a robust and efficient single phase implementation for steady-state flows, with superior performance compared to the segregated solution schemes [28]. The coupled algorithm solves the momentum and pressure-based continuity equations together, as can be seen in figure 4.6

Since the momentum and continuity equations are solved in a coupled manner, the rate of solution convergence improves when compared to the segregated algorithm, however, the memory requirement increases about 2 times when compared to a segregated algorithm since the discrete system of all momentum and pressure-based continuity equations needs to be stored in the memory when solving for the velocity and pressure fields.[26]

The flow chart in figure 4.7 illustrates the general field of solution used in the CFX-Solver.
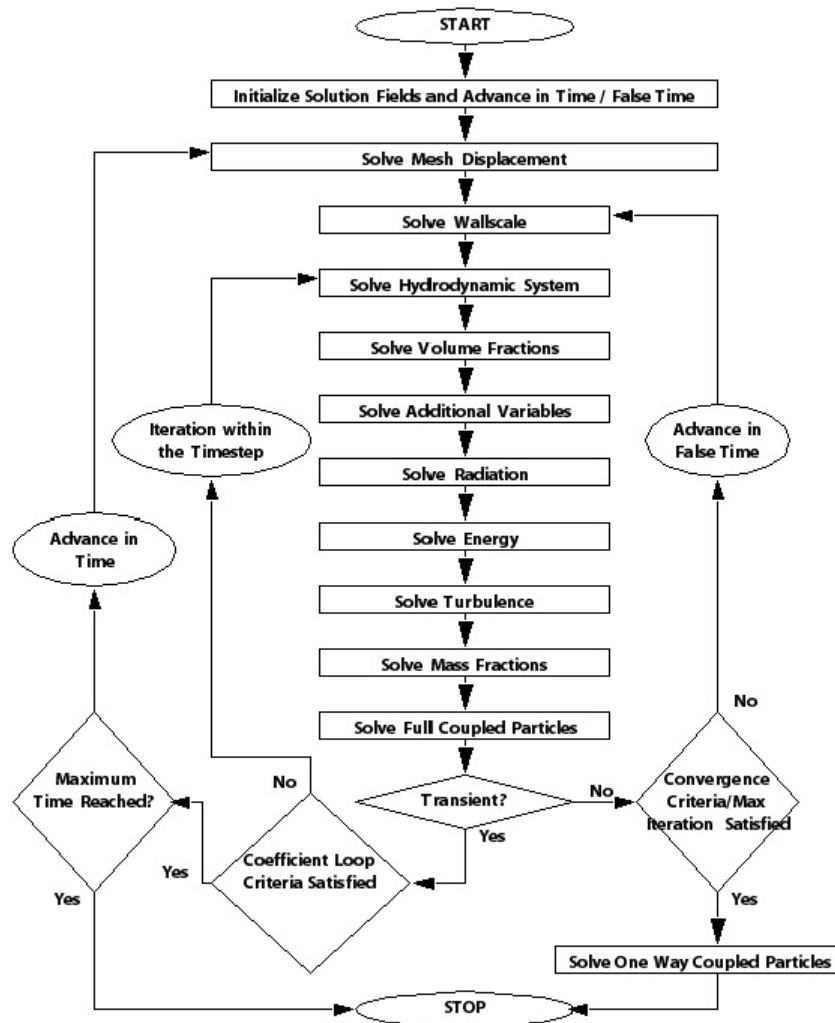
Figure 4.7: CFX Solver [28]

In this work three different blade chords have been created (Small, Medium, Large) and those three blades were tested in two different operational conditions (changing mass flown,speed), making a total of **six different simulations**. The table 4.2 was created to summarize the differences between these.

Table 4.2: Simulations

	Case 1 [3 Simulations]	Case 2 [3 simulations]
N1 [rpm]	4933	4817
Inlet Total Pressure [Pa]	101325	101325
Outlet Mass Flow [Kg/s]	8,36	8,04
Blade Chord	Small;Medium;Large	Small;Medium;Large

To conclude this analysis, it is necessary to assess the validity of the numerical solution obtained, as have been seen before, in CFD the results can be evaluated by several parameters that will define how accurate or valid a solution is.

Basing this analysis in [38] and CFX Documentation, a numerical solution can generally be found convergent if two important properties of **consistency** and **stability** are satisfied. Convergence can be defined as *"the solution of the system of algebraic equations approaching the true solution of partial differential equations having the same initial and boundary conditions as the refined grid system"*[38]. The property of consistency is important and concerns the discretiza-

tion of the partial differential equations where the approximation performed should become exact if the time step or the mesh spacing tend to zero. In other words when the truncation error, which measures the difference between the discretized equation and the exact one, will decrease as the time step or the mesh spacing are reduced, it is possible to affirm that the process shows consistency. As have been seen before, the second property that also strongly governs the numerical solution method is stability, this property concerns the growth or decay of errors that are introduced during the computation process. The numerical solution is therefore considered stable if these errors are not increased in the course of the numerical solution process.

As previously mentioned and according to Lax's Theorem [38] stability and consistency are necessary and sufficient conditions that need to be satisfied for convergence.

Commercial CFD codes usually solve interatively the system of algebraic equations, therefore, *iterative convergence* takes an important place in this process. In order to achieve this type of convergence there are three important aspects to deal with. First, all the discretized equations are considered to be converged when they reach a specific tolerance at every nodal location, second the numerical solution undergoes no change with additional iterations, and finally the overall mass, momentum , energy and scalar *balances* are obtained [38].

The concept of residuals is applied for each discretized equation of the system of transport equations, it is the most important measure of convergence as it relates directly to whether the equations have been solved. In CFX the normalized residuals are used to judge convergence. For each solution variable, the normalized residual can be defined as follows [38]:

$$[\widetilde{r}_\phi] = \frac{[r_\phi]}{a_p \Delta \phi} \quad \text{(4.1)}$$

where ϕ represents the solution variable, r_ϕ is the raw residual, a_p represents the control volume coefficient and $\Delta\phi$ is the range of the variable in the domain. Convergence will be achieved so long as the residual $\widetilde{r}_\phi$ satisfies a specified tolerance ε ($R \leq \varepsilon$) [28]. It is important to emphasize that the normalized residuals are independent of the initial guess as well as from the time step. In this project the dimensionless residuals were used as a stopping criterion in addition to a limitation to the number of iterations, therefore the convergence is assumed, for all simulations, when the **residuals decrease to** 10^{-6} **or the limit of 1000 iterations** are reached. Although, it is important to notice that the residuals decreasing to 10^{-6} means a very strong convergence and in some cases this result can not be achieved, but a value of 10^{-5} represents a good enough convergence for almost all processes.

Can be said that residuals are not a direct measure of solution accuracy, but are a measure of the numerical imbalance of the partial differential equations. The percentage of imbalance will measure the conservation in a domain or from a particular equation [36]. Small values in the imbalances indicates that the conservation has essentially been achieved. The percentage of global imbalance can be computed as follows [36]:

$$\% imbalance = \frac{Doamain\, Imbalance}{Maximum\, Over\, All\, Domains} \quad \text{(4.2)}$$

The previous analysis about convergence primarily concerns the solution behavior, since the discretized forms of the transport equations governing the flow are always solved numerically

on a finite grid and the turbulence solved through approximate theories, the final solution is always an approximation. Regarding this, another important consideration will be the solution *accuracy* [38]. The solution accuracy is dependent on various errors, to manage the solution accuracy the user should understand and try to mitigate those errors. There are five main factors that influence the solution accuracy, being those, the *Discretization error, Round-off error, Iteration or convergence error, Physical-modeling error and Human error*. A detailed explanation about this errors can be found in [38], therefore it was decided not to include all this information in this document.

It is possible to conclude that a numerical solution is dependent on several factors, regarding this the solution process must be monitored in order to ensure convergence of the solution and try to get as much accuracy as possible for the results. In this project, in order to validate the simulations results it was produced a subsection where a comparison between simulation results and real results from the test bench is done.

Chapter 5

Results

This chapter presents the key results obtained in this work, where we intended to create the most accurate simulation of the flow around the CFM56-3's fan, using three different blade chord and trying to analyze the effect that this change will have in flow properties downstream from the fan. In order to accomplish this goal, six simulations were performed (Table 4.2), using all the parameters referred on the previous chapters, that can be consulted in a summarized report, as it is possible to see an example in annex A.4.

Has is understandable the six performed simulations deliver us a very significant amount of results, so in this chapter will be presented the main results to understand the relationship that is intended to study. This chapter will start with an evaluation of the numerical solution quality in terms of the convergence of the iterations regarding all variables, a quick analysis of the solution imbalances, and then will be evaluated the y^+ to guarantee that the boundary layer on the blade is correctly resolved in our simulations.

Afterwards, the main results of the simulations will be presented and discussed, some comparisons between the variables will be performed in order to better understand the flow changes imposed by a blade chord variation. As have been previously stated the results validation through the real test bench measurements, configures a very important step in this project in order to confirm our model which will allow the utilization of this results for future engine evaluation within the TAP Engine Shop, regarding this a subsection was created to realize the comparison between the simulation results and the test bench measurements. To conclude, an overview of the program that is being created, based on our results, to assist the TAP engineer's team on the engine shop during the CFM56-3 engine maintenance.

5.1 Convergence

As have been previously highlighted it is important to evaluate the iterative convergence of the solution, this convergence is considered to be achieved when all discretized transport equations reach the convergence criteria, in addition with balances in some parameters, or when the maximum number of iterations is reached.

In this simulations, **two convergence criteria were selected**, one that is satisfied when the dimensionless residuals decrease until 10^{-6}, and the second when the iterations have reached 1000 (value defined after a trail and error approach). In Figure 5.1, it is possible to analyze an example of the residuals evolution during the iterative process, these example refers to the Case 2, specifically the Large chord simulation with 4817 rpm of N1.
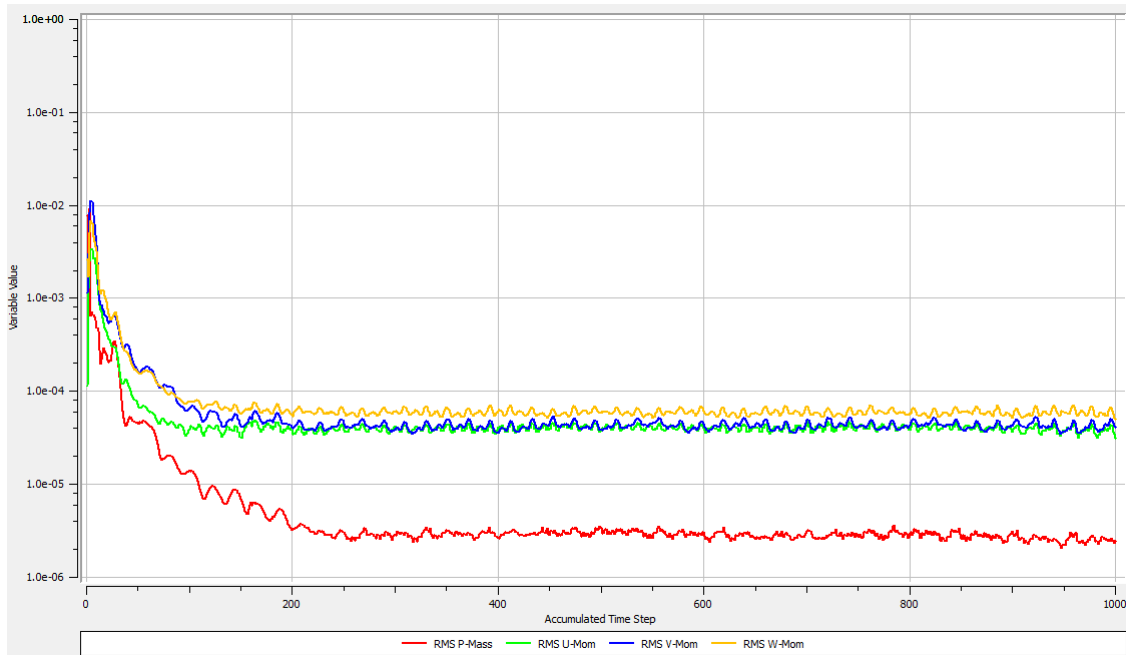
Figure 5.1: Residuals

It is possible to understand from the examination of figure 5.1 that the simulation residuals did not decrease to 10^{-6} which was defined as the convergence target, therefore the simulation stopped when the process reached 1000 iterations, this actually occurred for all simulations. The fact that the residuals do not decrease to the defined limit does not mean that our solution is not converged, the defined target (10^{-6}) means a very strong convergence that in most cases is not possible to achieve. So, residual values close to 10^{-5} is also a very good convergence and the results are not very far from this reference, also, as can be seen in the graph, approximately from iteration 400 on until 1000, the residuals values stop decreasing and for the next 600 iterations the values remain almost unchanged in terms of medium value, which indicates that the solution will remain in this values regardless of how many iterations we run.

```
+----------------------------------------------------------------------+
|                      Normalised Imbalance Summary                    |
+----------------------------------------------------------------------+
|        Equation        |      Maximum Flow      |     Imbalance (%)     |
+----------------------------------------------------------------------+
| U-Mom-R1               |        1.1191E+05      |        -0.0002        |
| V-Mom-R1               |        1.1191E+05      |        -0.0001        |
| W-Mom-R1               |        1.1191E+05      |         0.0000        |
| P-Mass-R1              |        1.2095E+02      |         0.0000        |
| U-Mom-S1               |        1.1191E+05      |         0.0000        |
| V-Mom-S1               |        1.1191E+05      |         0.0000        |
| W-Mom-S1               |        1.1191E+05      |         0.0000        |
| P-Mass-S1              |        1.2095E+02      |         0.0000        |
| U-Mom-S2               |        1.1191E+05      |        -0.0002        |
| V-Mom-S2               |        1.1191E+05      |         0.0001        |
| W-Mom-S2               |        1.1191E+05      |         0.0000        |
| P-Mass-S2              |        1.2095E+02      |         0.0000        |
+----------------------------------------------------------------------+
| H-Energy-R1            |        4.6630E+06      |         0.0000        |
| H-Energy-S1            |        4.6630E+06      |         0.0000        |
| H-Energy-S2            |        4.6630E+06      |        -0.0004        |
+----------------------------------------------------------------------+
```

Figure 5.2: Imbalances

50

After these analysis, the **imbalances**, are another important criteria that needs to be considered in order to evaluate a good solution convergence. The difference between incoming and outgoing, in terms of quantity of a certain parameter, is called the imbalance, and it should be zero or a very small value. In a converged solution, the total quantity of say mass coming into the domain equals that going out.

In figure 5.2 are represented the percentage of imbalance per equation in specific domains. As we can see the imbalances values are zero or very close to zero which indicates, also that this solution is a converged solution.

Finally, is possible to analyze, individually, a specific parameter's behavior, using the available graph of say mass flow variation during the iterative process. In figure 5.3 is represented one of these graphs and is, again, possible to notice the convergence of this parameters and the perfect agreement between the mass flow entering the domain and the exiting for the all domain.
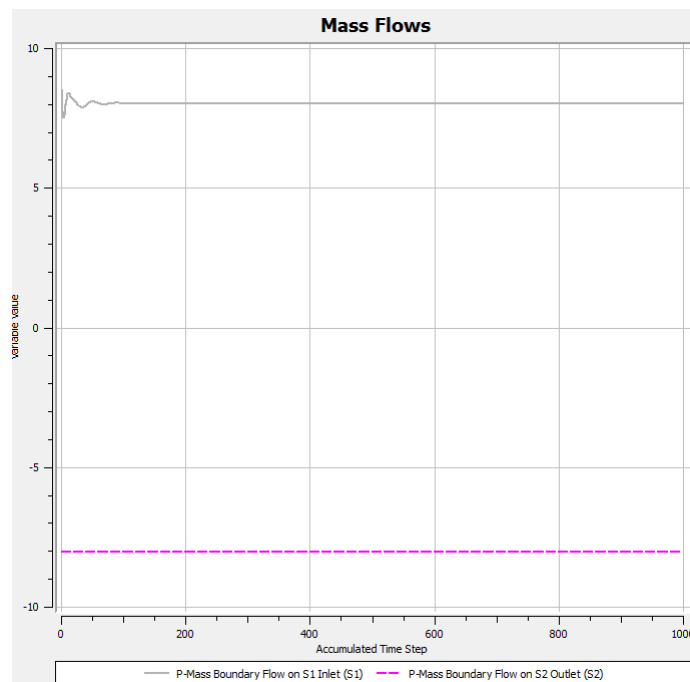
Figure 5.3: Mass Flow

5.1.1 y^+ Analysis

In this work all the simulations were made with the SST turbulence model selected and combined with the automatic wall function treatment. This automatic option allows the user of a formulation that will automatically switch from wall functions to a low-Re formulation, as the grid is refined. The automatic wall treatment avoids the deterioration of the results typically seen if low-Re models are applied on under-resolved meshes. Compared to the standard wall-function or the low-Re approach it is clearly visible that the grid dependency of the results for the automatic wall treatment is significantly reduced compared to the standard formulations. A blending function depending on y^+ is also used in this option. Nevertheless, in this work we try to build a very fine mesh, in order to achieve a distribution of y^+ smaller than 1 along the blade surface. However, y^+ values up to 5 can also be accepted since those values are within the viscous sub layer.

In order to prove that y^+ are within the referred intervals, figure 5.4 was created from our

simulations. The represented values are from the adjacent elements of the blade's upper and lower sides.
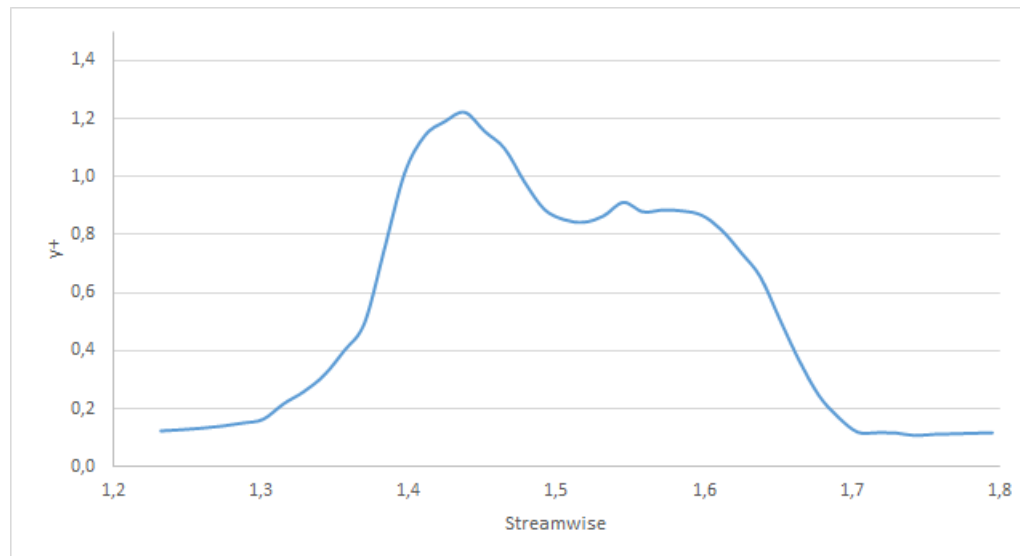
Figure 5.4: y^+ distribution along blade surface

In figure 5.4 it is possible to notice that all the values along the blade surface are well below 5, in fact the majority are between 0,2 and 1. With this results it is possible to state that, the used mesh and the chosen options were appropriated, and during the calculations, the software computes all the boundary layer close to the blades surface. In this conditions, theoretically, no wall functions will be used in the blade surface.

5.2 Fan Flow analysis

In this section the simulations results will be presented, interpreted and discussed. As described before, this work is divided in two cases, each case composed by three simulations and to each simulation corresponds a different blade chord. After the completion of the simulation process the results were transferred to CFD-post for the post processing process.

Having a total of 6 simulations we have a very wide variety of results that can be withdrawn, it was decided to closely analyze two specific properties, mach number and total pressure, these properties were considered important to learn the flow properties downstream from the fan and evaluate the fan performance. To do that it was used a meridional views that represent the blade domain and the outlet domain, then the blade views that presents only the blade domain at two different span locations, 15% and 60% of the span. It were also created a few comparative graphs that will help in understanding changes or differences between simulations It is also important to mention that all conditions applied assume that these tests were conducted under a **standard day at mean sea level**.

5.2.1 Case 1

The so called, case 1 corresponds to the conditions presented in table 4.2, these set of conditions are called, Takeoff regime and it was applied to every engine during assays in test bench. All three blade chords were simulated in Takeoff regime, using the referred turbulence model, k-ω SST, and all other settings previously discussed.

Figures below in sections 5.2.1.1, 5.2.1.2, and 5.2.1.3, displays results achieved with 3 different blade chords in takeoff regime.

5.2.1.1 Small Chord

In figure 5.5 a meridional view of the blade and outlet domain are presented, regarding mach number (left) and total pressure (right). In a general way, the small chord simulation in a stationary frame of reference, the mach number and the total pressure increases when the flow passes the fan blades. It is possible to confirm that the mach number increases but not uniformly, the biggest raise happens close to the blade hub, where the mach number will be higher, and decreases towards the blade tip. At the blade tip, can actually be noticed a decrease in the mach number comparing with value upstream from the blade. With regard to total pressure the tendency is approximately the same, since the total pressure increases specially close to the blade hub and is also decreasing towards the blade tip.
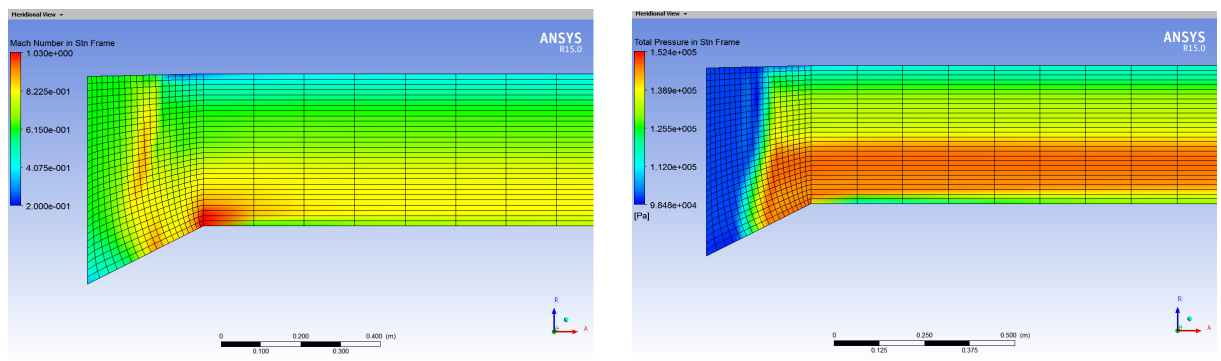
Figure 5.5: Mach number & Total Pressure Meridional view - Small chord

In order to better visualize the flow changes along the span it was decided to analyze two locations, at 15% and 60 % of the span, in figure 5.6 are presented these blade views corresponding to the mach number. As have been noticed, at 15% the mach number increases more, to approximately 0.80, when compared to approximately 0.65 at 60%. In this figure it is also possible to notice in the leading edge the stagnation point where the flow speed is zero.
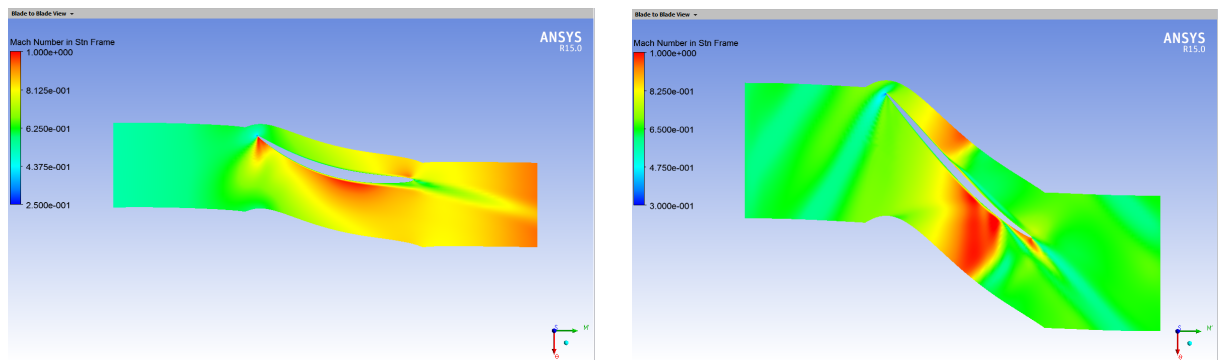
Figure 5.6: Mach number 15% span (Left) 60% span (Right)

Figure 5.7 presents the, blade views, for the total pressure variation in the blade domain, as have been said before, the total pressure increment close to the blade hub is higher, so at 15%, the total pressure increased to approximately 150.000 Pa. At 60% of the span, total pressure increases, but as previously said, to an inferior value when compared to the blade hub. The stagnation point on the blade leading edge, is the point with maximum pressure.
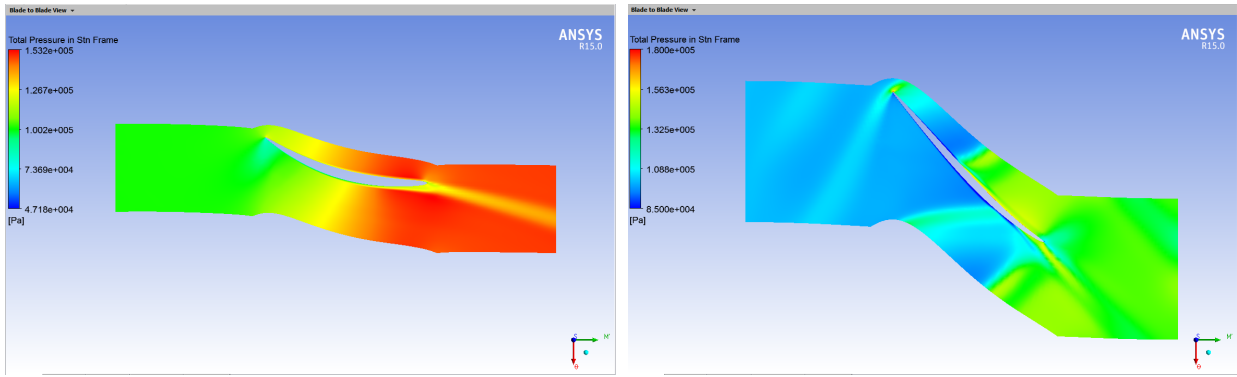
Figure 5.7: Total Pressure 15% span (Left) 60% span (Right)

5.2.1.2 Medium Chord

In this sub-subsection, the following figures, present the results for the simulation in takeoff regime with the medium blade chord. Starting with the two meridional views, in figure 5.8, is possible to notice that the flow mach number and total pressure in a stationary reference frame, increases when passing the blade. Once again, the increment in the mach number and the total pressure are greater close to the blade hub and decreases towards the tip.
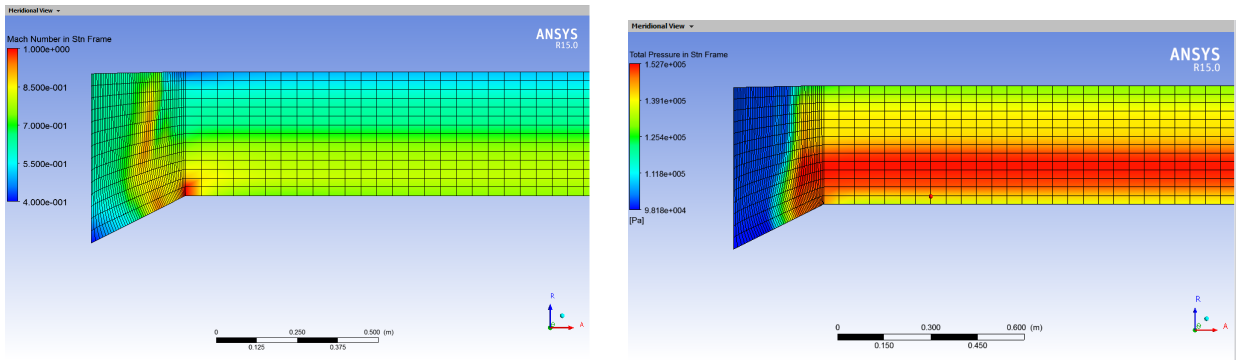
Figure 5.8: Mach number & Total Pressure Meridional view - Medium chord

In figure 5.9 the mach number results are showed in two blade views. As previously said, this results verify the tendency that shows a higher mach number at 15% of the blade span than at 60%. The specific values will be discussed in more detail later in this text, however at 15% the value is approximately 0.83 and at 60% is 0,68.
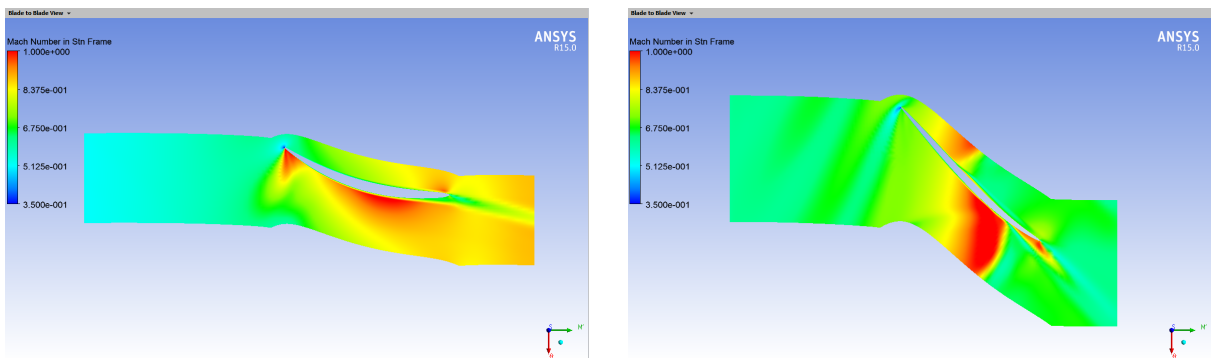
Figure 5.9: Mach number 15% span (Left) 60% span (Right)

To complete the results relative to medium chord in takeoff regime, figure 5.10 shows the total

54

pressure distribution in two blade views. As in previous cases the total pressure increases when the flow passes through the fan blade, the increment is higher at 15% of blade span than at 60%.
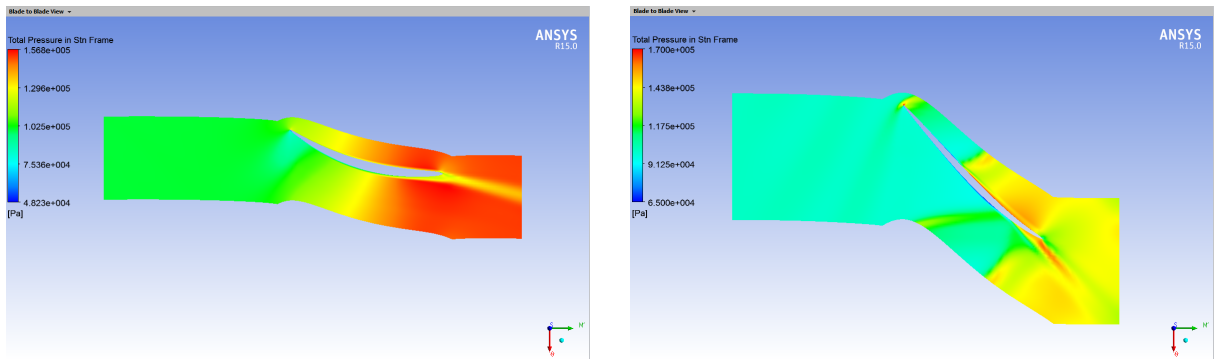
Figure 5.10: Total Pressure 15% span (Left) 60% span (Right)

5.2.1.3   Large Chord

The following sub-subsection shows the results for the large chord simulation in takeoff regime, the meridional views displayed in figure 5.11 for mach number and total pressure in a stationary reference frame, present similar tendencies when compared to the previous cases. The fan blade increases the flow mach number and total pressure specially on the vicinity of the blade hub.
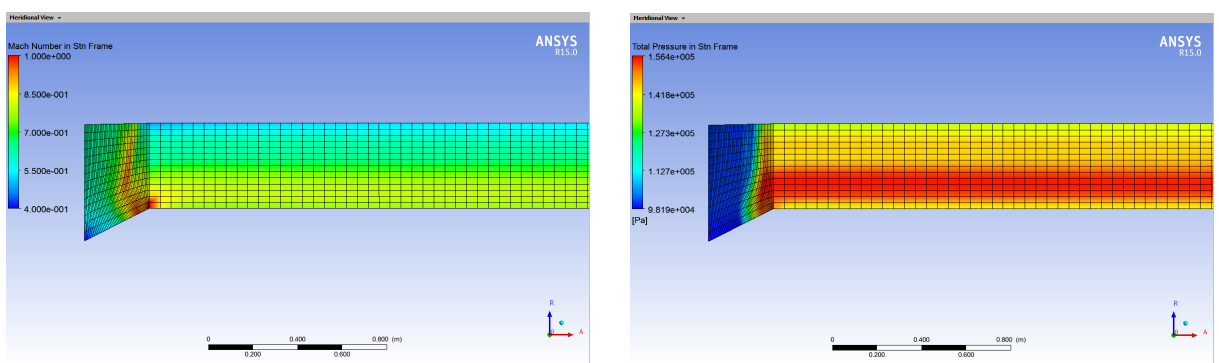
Figure 5.11: Mach number & Total Pressure Meridional view

Figure 5.12 display, once again, two blade views from the mach number distribution at two different span locations. This results shows the same overall tendencies as the other simulations with smaller blade chords, this means that the mach number is higher at 15% of the blade span and at 60% the mach number increment applied by the fan blade is smaller.
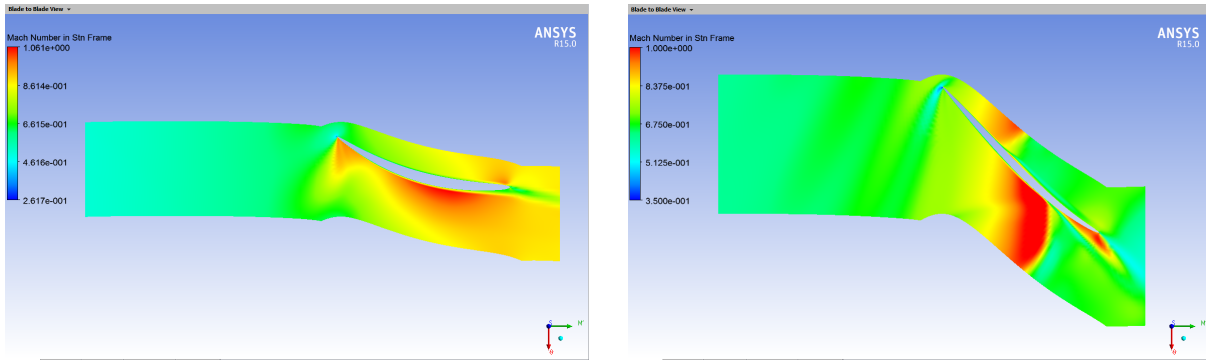
Figure 5.12: Mach number 15% span (Left) 60% span (Right)

Following, figure 5.13 has the same characteristics as the previous figure, but in this case the representation of the total pressure is displayed. At 15%, the total pressure increases to approximately 155.000 Pa in the other hand at 60% the increment is smaller and the total pressure is, approximately, 147.000 Pa.
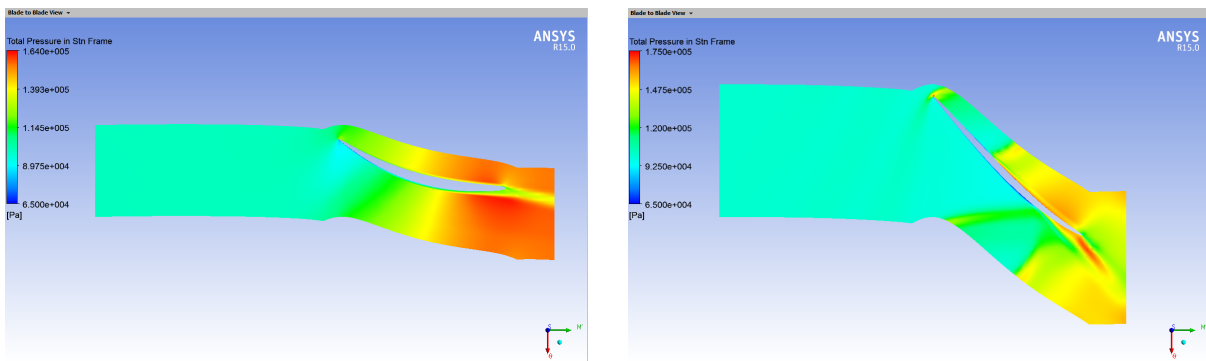

Figure 5.13: Total Pressure 15% span (Left) 60% span (Right)

5.2.1.4   Comparison of results

In the previous sub-subsections have been shown some flow properties when passing the fan blade and the resulting changes. In order to better evaluate the real differences between the three simulations performed for three blade chords, the following graphs were created (see figures 5.14, 5.15, 5.16, 5.17). These graphs show the variation in mach number and total pressure, from hub to tip and from inlet to outlet for the three blade chords. Results used to create both these graphs were obtained from CFD-post, but it is important to understand the exact location from where these results are extracted. The *hub to shroud* graph represents the outlet section of the blade domain, which means the results are parallel to the blade span but in the blade domain exit. The *inlet to outlet* graph represents the horizontal middle section of all the blade domain and outlet domain.

Figure 5.14 represents the mach number variation from hub to shroud for the three blade chords analyzed. It is clearly observed in this graph that, for all chords, the highest Mach numbers are detected in the blade hub. Even with small differences the large chord has a higher Mach number of, approximately, 0,97, then the medium and small chord with approximately 0,94. The mach number decreases along the span for all chords, but the large chord has always higher values. At 90 % of the blade span the large chord has Mach number of, approximately, 0,64, while the medium chord has 0,60 and the small chord 0,53. Close to the blade tip, the flow Mach number decreases very significantly for all chords, because the blade efficiency in
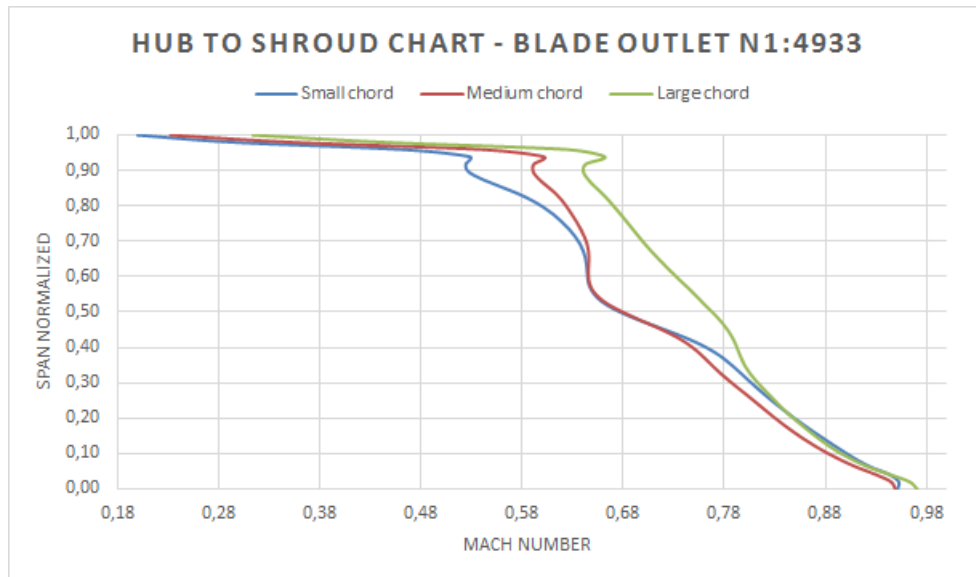
Figure 5.14: Mach number analysis - Hub to shroud

this area is very low. Analyzing the blade inlet to outlet graph, on figure,5.15, is possible to understand that this graph represents all the control volume (inlet, blade and outlet). In the inlet domain the Mach number is about 0,5 for all blade chords, when the flow approaches the blade domain the Mach number increases. In the large chord simulation the mach number reaches his maximum value of 0,87 in about 60% of the blade domain, in the medium chord simulation the maximum Mach number is 0,85 at about 55% of the blade domain and finally, the small chord simulation reaches the maximum Mach number of 0,82 at 50% of the blade domain. After this, the Mach number for all simulations decreases until, approximately, 0,68, although, the Mach number for the large chord simulation is slightly higher. Then, Mach number stabilizes and remains almost constant in about 0,68.

After a careful analysis is possible to understand that in take-off regime the Mach number is higher at the blade hub and decreases very significantly when approaching the blade tip, but the Mach number for the large chord simulation is always the highest and the Mach number for small chord is the lowest. Analyzing this property from the inlet to the outlet of the control volume, can be concluded that the large chord simulation reaches the highest Mach number value and the small chord simulation reaches the lowest mach number, but even with this decrease in the Mach number, the blade chord decreases, the point in the domain where the maximum is reached is also changing. In other words when the blade chord reduces the Mach number reduces, and also the maximum Mach number point decreases (60% to 50% of the blade domain). The general change in Mach number through the fan is from 0,5 at inlet to approximately 0,68 at outlet.

In figure 5.16 is presented an analysis of flow total pressure variation when changing the blade chord. In the figure the total pressure tendency from blade hub to tip is constant for all chords. However, the simulation performed with large chord has always higher values, starting at the blade hub in 153000 Pa reaching a maximum of 155000 Pa at 40% of blade span. The small chord simulation starts at 147000 Pa and has always the lowest values when compared with other simulations. Once again, when approaching the blade tip (95% of the span) the total pressure decreases very significantly.

Regarding the graph that give the variation of the flow total pressure from the blade inlet to
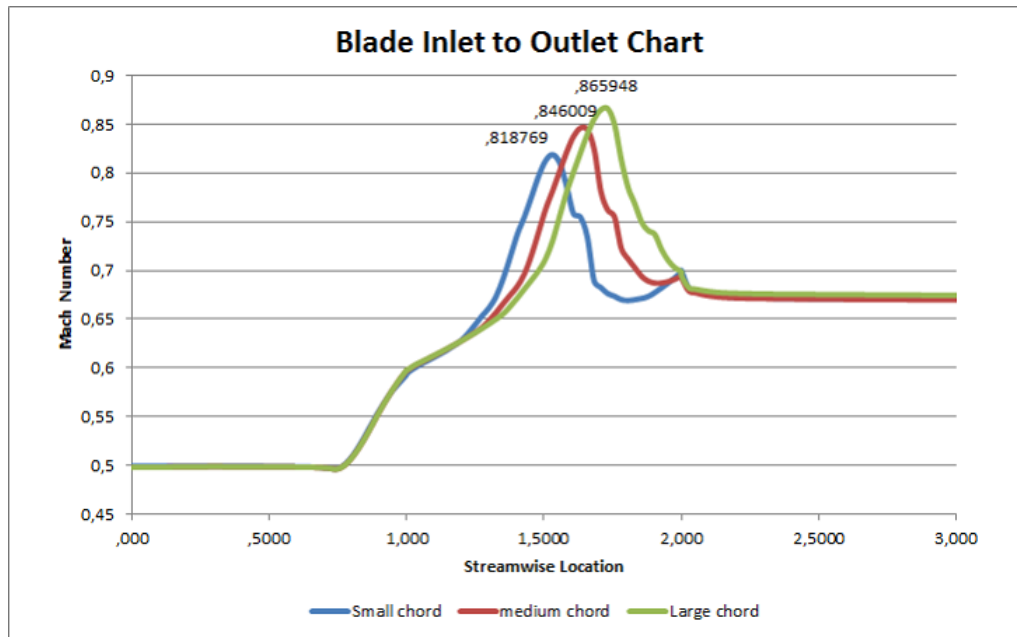
Figure 5.15: Mach number analysis - Inlet to Outlet

the outlet domain for the three blade chords (see figure 5.17), it is possible to see that the tendency is the same for all blade chords, the flow enters the blade domain at 100000 Pa and raises, for the large chord the maximum is 148000 Pa which is the highest, for the medium chord is 144829 Pa and for the small chord 136531 Pa is the maximum total pressure which is the lowest for all three. After passing the blade, in the outlet domain the total pressure remains almost constant for all blade chords, but at different values. For the large chord the flow total pressure in the outlet domain is 146000 Pa, for the medium chord is 143000 Pa, finally in the smallest chord is 135000 Pa.

After analyzing this information, can be concluded that from "hub to shroud" the flow total pressure is always higher in the large chord simulation and the lowest values are obtained in the small chord simulation, and is also observable that the highest values, for all simulations, happen at approximately 40% of the blade span. In the inlet to outlet analysis can be concluded that, also in this case the larger chord corresponds to the highest total pressure, and the pressure at the outlet domain is also the highest, in the other hand the smallest chord corresponds to the lowest total pressure. Based on this information can be concluded that in the large chord case the fan pressure ratio is 1,46 for the medium chord the FPR is 1,43, finally for the small chord is 1,35. The engine manufacturer indicates a FPR of 1,5 in the engine specifications. The large chord simulation is the one closest to this feature.

Finally, it is also important to notice that the difference between outlet total pressure of the large chord simulation and the medium chord simulation is 3000 Pa and the difference between the medium and the small chord simulation is 8000 Pa. However the blade chord is reduced by the same amount (3,72 mm), can be concluded that the effect of a blade chord reduction in a certain amount will vary depending in which interval that chord is.
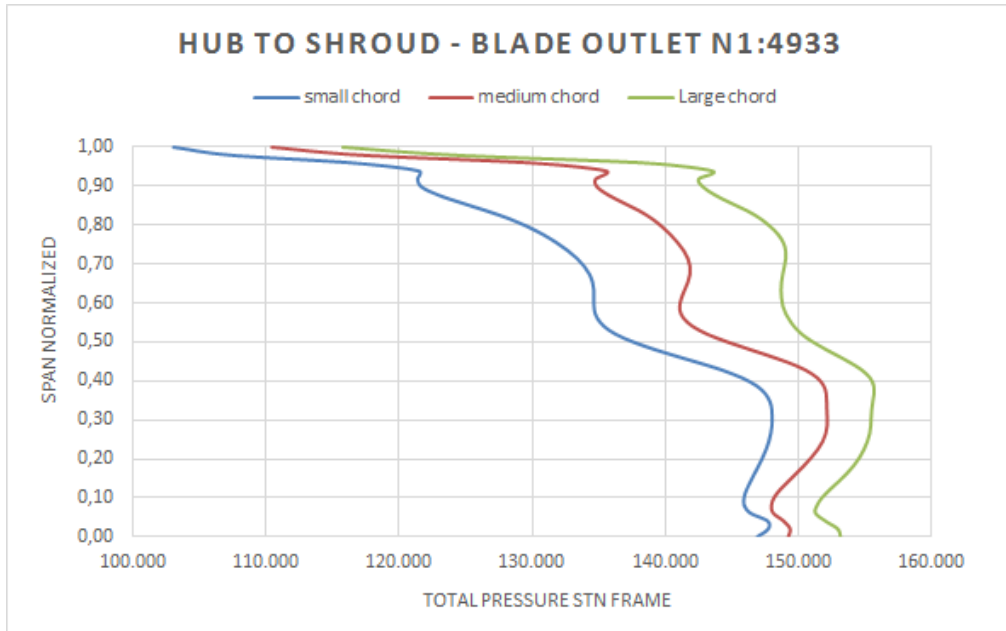
58

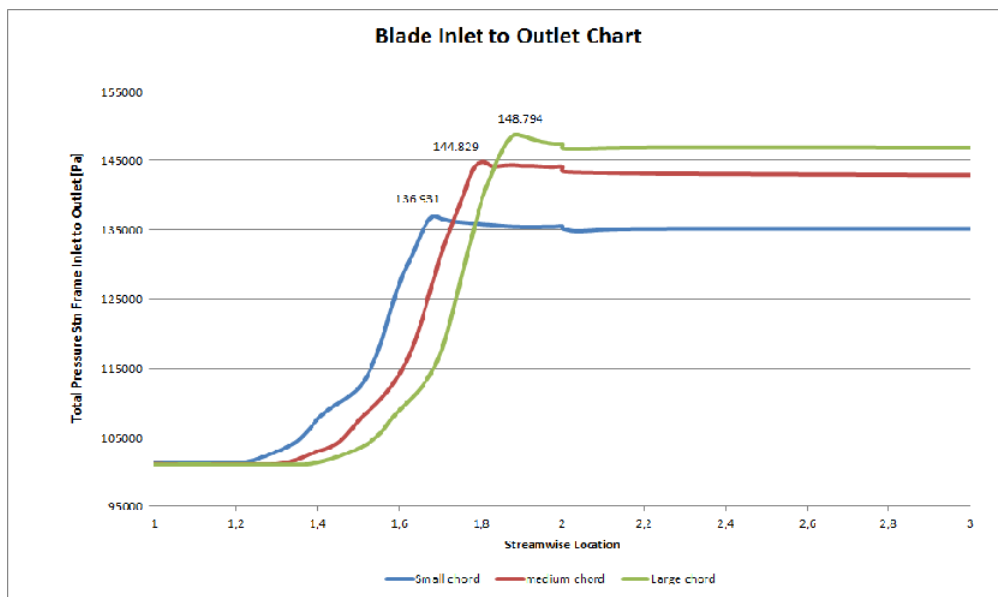Figure 5.16: Total Pressure analysis - Hub to shroud

Figure 5.17: Total Pressure analysis - Inlet to Outlet

5.2.2   Case 2

The following section presents the results for case 2 that corresponds to the conditions referred in table 4.2, these set of conditions are similar to the parameters used in real test bench tests and this regime is called Maximum Continuous Power. All others settings that were used in these simulations are similar to the ones used for case 1.

5.2.2.1   Small Chord

Figure 5.18 presents a meridional view of the blade and outlet domains. The results presented here are in the same conditions as the ones presented in case 1. The Mach number increases

when passing the fan blade, like the previous simulations the highest value is close to the blade hub. Regarding the total pressure meridional view (figure 5.18 right) the area with the highest total pressure is around 65% of the blade span, showing a value of approximately 155000 Pa. The area close to the blade hub, in this case, has a significantly lower total pressure, that will increase towards the point of Maximum Total Pressure.
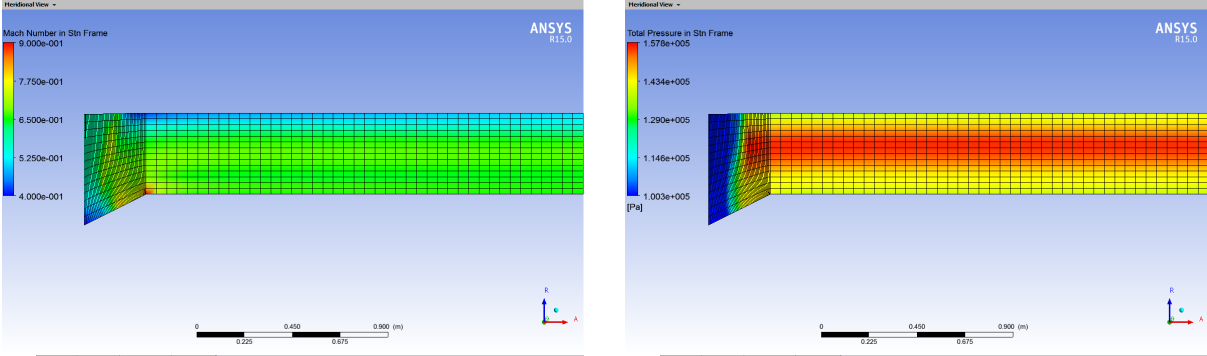

Figure 5.18: Mach number & Total Pressure Meridional view

As previously shown, the blade views (15% and 60%) are presented in figure 5.19 for flow Mach number through the blade domain for the small chord simulation. At 15% of the blade span the Mach number is higher than at 60%. These results will be analyzed in detail in the comparison of results section.
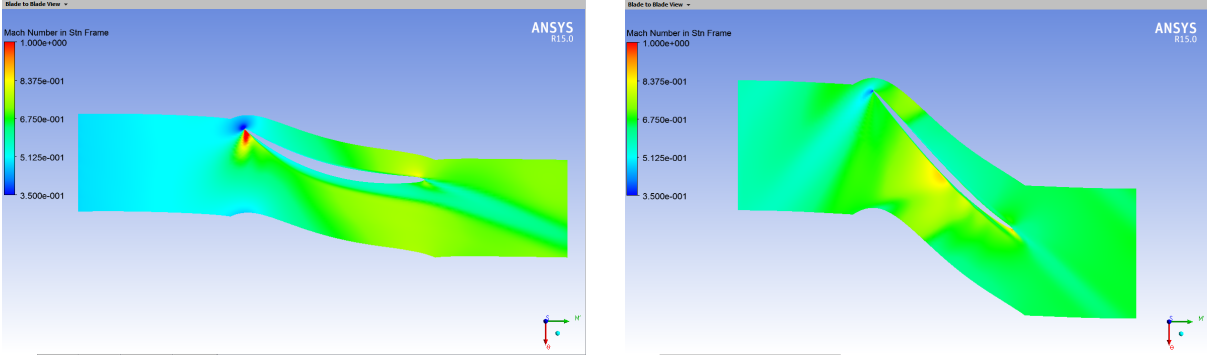
Figure 5.19: Mach number 15% span (Left) 60% span (Right)

Figure 5.20 presents the blade views, for the total pressure change over the blade domain. Analyzing this two figures is possible to confirm the results observed in the meridional view. The blade view at 60% of the blade span has an outlet total pressure of about 155000 Pa, which will be very close to the highest value. Closer to the blade hub at 15% of the span, the flow total pressure will be lower, about 145000 Pa.
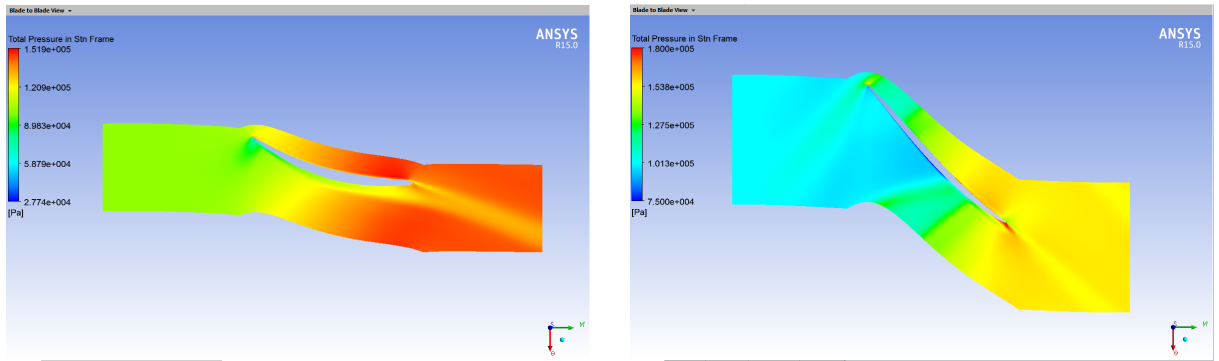
Figure 5.20: Total Pressure 15% span (Left) 60% span (Right)

5.2.2.2 Medium Chord

The following sub-subsection presents the results for the simulation in Maximum Continuous Power with the medium chord. In figure 5.21 the two meridional views of Mach number and Total Pressure are presented. Once again, the results show the same tendency as the small chord simulation, the Mach number decreases from the maximum value at blade hub, towards the blade tip. Close to the blade tip, the blade efficiency decreases and is possible to notice a significant and quick Mach number decrease. The flow total pressure, once again, has is maximum value at circa 60%.
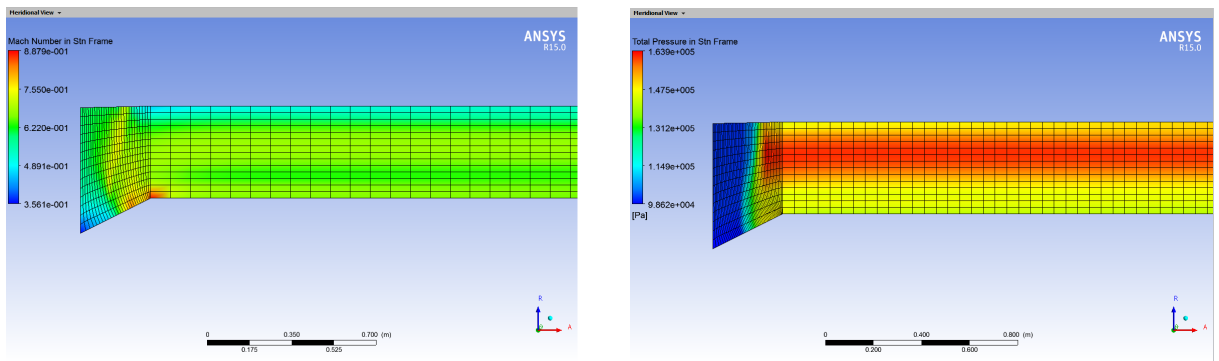
Figure 5.21: Mach number & Total Pressure Meridional view

Figure 5.23 presents two blade views, showing the Mach number variation along the blade domain. At 15% the outlet flow has a bigger Mach number increment when compared to the 60% increment. In order to confirm this, is possible to indicate that at 15% blade span, the Mach number is around 0,82 and at 60% is 0,65.
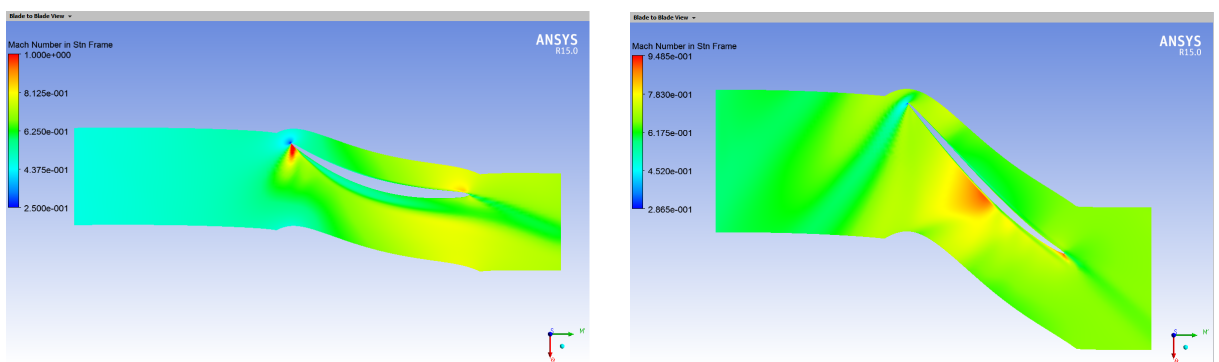

Figure 5.22: Mach number 15% span (Left) 60% span (Right)

To finish the results analysis of the medium chord simulation it is necessary to discuss figure 5.23 where, once again, the flow total pressure variation is represented in two blade views. As have been said before, the maximum total pressure is at 60% (157000 Pa) which means that the Fan Pressure Ratio in this blade region is approximately 1,5.
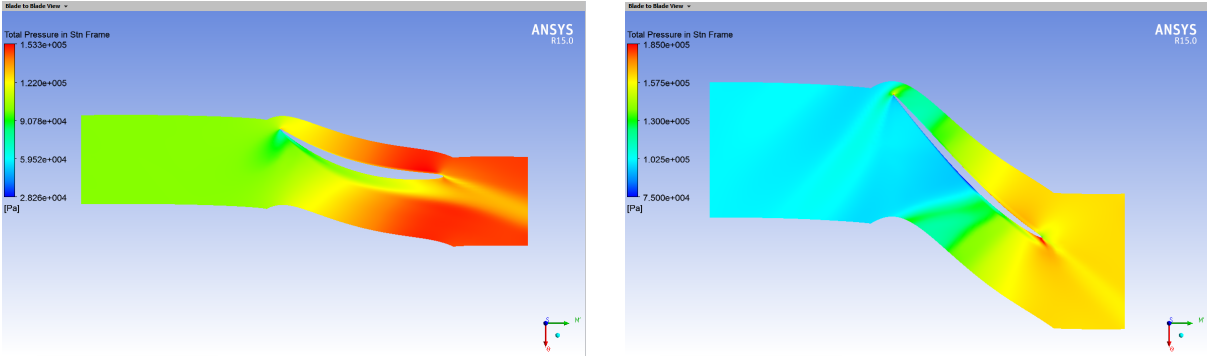

Figure 5.23: Total Pressure 15% span (Left) 60% span (Right)

5.2.2.3   Large Chord

Finally the following sub-subsection presents the results obtained for the large chord simulation. The first figure, 5.24, once more confirm the tendency obtained in previous results, the Mach number has the biggest value close to the blade hub and decreases until blade tip, but in general, the flow , when passing the blade increases the Mach number from 0,5 to 0,65 approximately. Regarding the total pressure, the highest value appears in a region close to 70% of the blade span. In this case, the region close to blade hub is the one lowest total pressure.
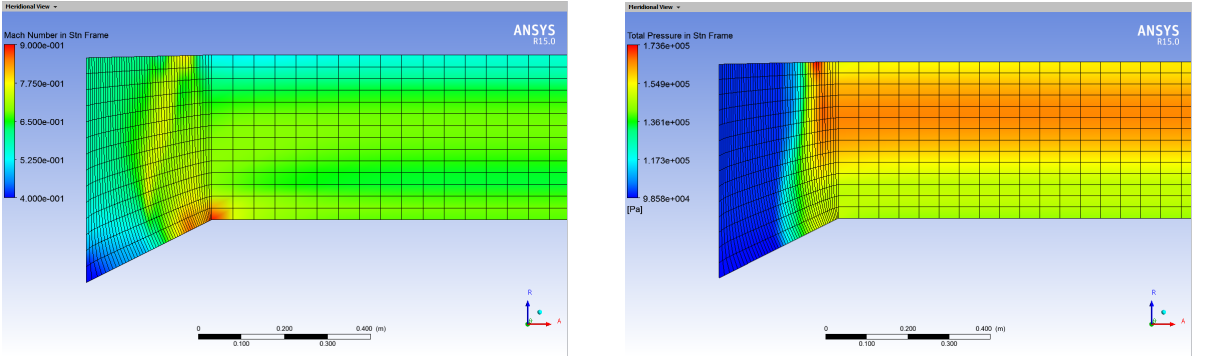

Figure 5.24: Mach number & Total Pressure Meridional view

Figure 5.25 showing two blade views, just helps to confirm the conclusions written previously. At 15% of the blade span, the Mach number increases from 0,47 to 0,80 and at 60% the outlet Mach number is lowest, approximately 0,68.
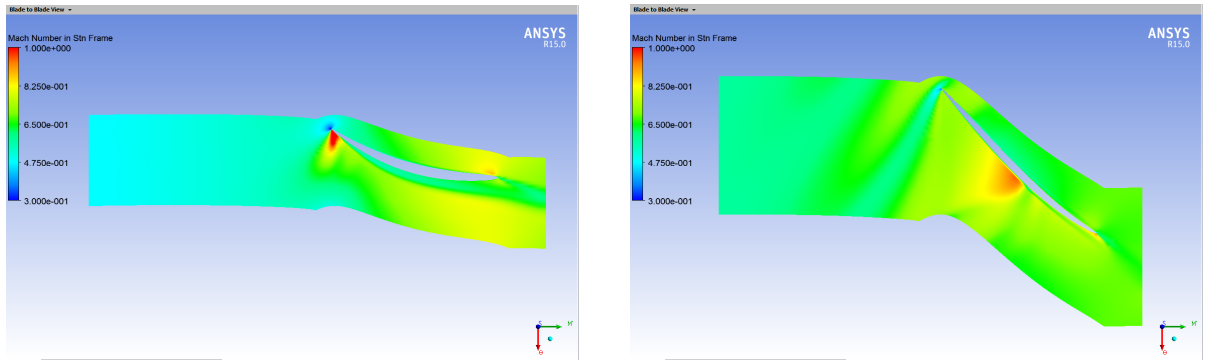
Figure 5.25: Mach number 15% span (Left) 60% span (Right)

As have been said for the anterior findings, the total pressure variation along the blade domain in figure 5.26, is higher at 60% of the blade span, with a value of circa 167000 Pa, on the other hand, at 15% the total pressure presents the lowest value. Overall, it is possible to say that in average the total pressure in this simulation increases from 100000 Pa at inlet to 160000 Pa at outlet.
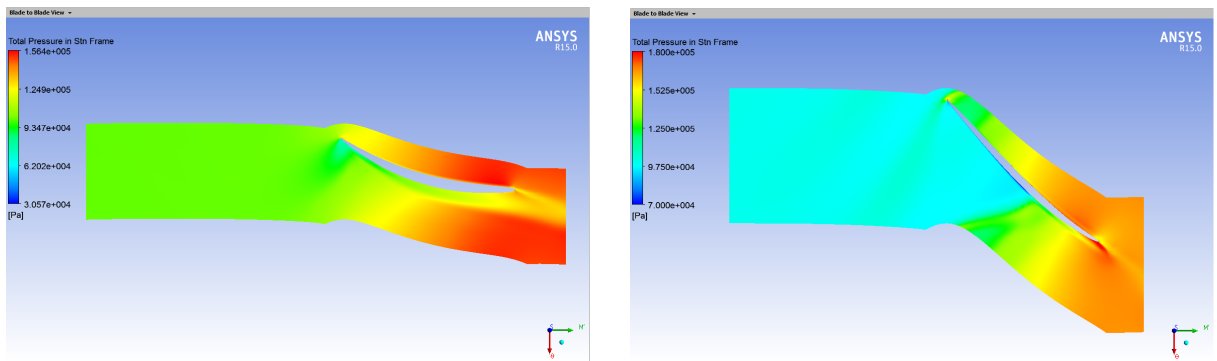

Figure 5.26: Total Pressure 15% span (Left) 60% span (Right)

5.2.2.4 Comparison of results

In this sub-subsection, as have been done for case 1, some graphs were created in order to evaluate how the blade chord change, influencing the flow properties often the fan. All information described in case 1, regarding the locations and the process of extract are still valid in this analysis, since the results were obtained according to the same standard.

First, in figure 5.27 which represents the Mach number variation along the span distance for all three chords. It is possible to observe that for all simulations the tendency is the same. The trend in all simulations is to have the highest Mach number at the hub, and then decreases rapidly until 20% of the span, after the reduction is much smoother until 95%, and at blade tip the reduction in the Mach number is very significantly. Even having the same trend in all simulation, the simulation with a large chord has always higher Mach number values, and at the other hand is the small chord simulation that presents the lowest values, all the way to blade tip.

Analyzing now the Mach number profile from the inlet to outlet, for all simulations, which are represented in figure 5.28, it is possible to observe that this graph represents the three domains (inlet, blade and outlet). During the inlet domain the Mach number remains almost constant for all simulations, when the flow approaches the fan blade, the Mach number increases. Once
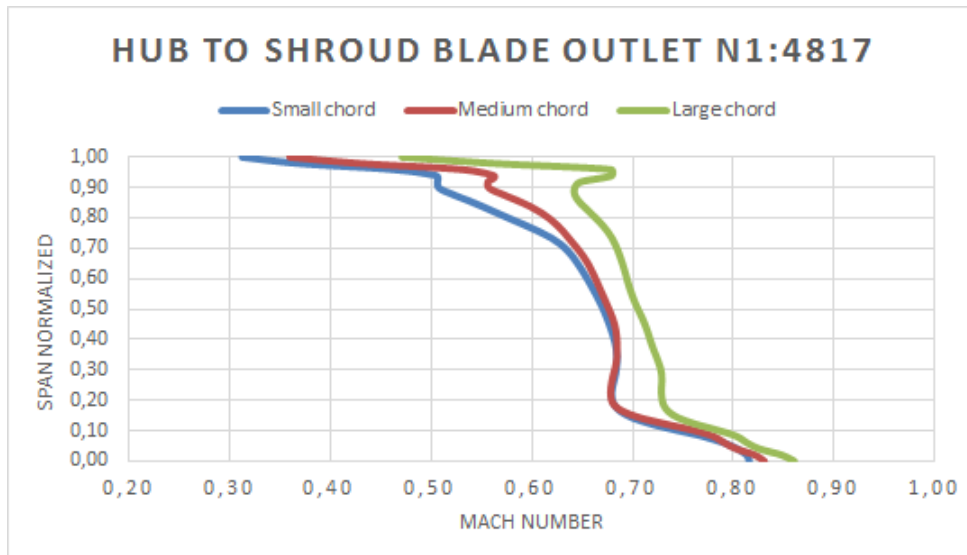
Figure 5.27: Mach number analysis - Hub to shroud

again the simulation with the large chord has the highest Mach number at about 70% of the blade domain with a value of 0,73, the medium chord has 0,72 at 60% and the lowest value is achieved with the small chord, 0,70 at 50% of the blade domain. After this, the Mach number decreases for all simulations, but when the flow enters in the outlet domain remains almost constant in all simulations.

However there are differences between simulations, for the large chord the Mach number at the outlet is circa 0,64, for medium chord is 0,63 and finally for the small chord simulation is, approximately, 0,62.

After this analysis is possible to conclude that regarding the mach number variation for all the simulations with different blade chords, the Mach number decreases from the blade hub to the tip, and in that profile the large chord presents always the highest values. Thus, increasing the blade chord will increase the Mach number. Comparing the inlet flow to the outlet flow, is possible to conclude that when the blade chord increases the Mach number if the outlet flow increases. Globally, the fan blade increases the flow Mach number in almost 0,18.

This analysis will end with the discussion regarding the flow total pressure in these simulation of the case 2 starting with figure 5.29 it is possible to see that in all simulations the trends in the Mach number along the span are equal. However, once again, the highest values of flow total pressure are achieved by the larger chord and the lowest values by the smaller chord. Nevertheless, the maximum value of total pressure happens at, approximately, 65% of the span. At this location the value in the large chord simulation is 167000 Pa, for the medium chord the value is 162000 Pa, and finally for the small chord is 156000 Pa. Once again, close to the blade tip strong and significant changes in total pressure occur.

In figure 5.30, it is possible to examine the flow total pressure change from the blade domain until the exit of the outlet domain, for all simulations. The total pressure at the inlet is constant, at about 100000 Pa. When passing the fan blade, the larger chord simulation increases to a maximum of 161000 Pa and after decreases to a constant value of 156000 Pa throughout the outlet domain. The medium chord increases to a maximum of 155768 Pa and then decreases and stabilizes at 153000 Pa, approximately, throughout the outlet domain.

Finally, the small chord increases to a maximum of 150100 Pa and then remains constant throughout the outlet domain at, approximately, 148000 Pa. Having all this information it is
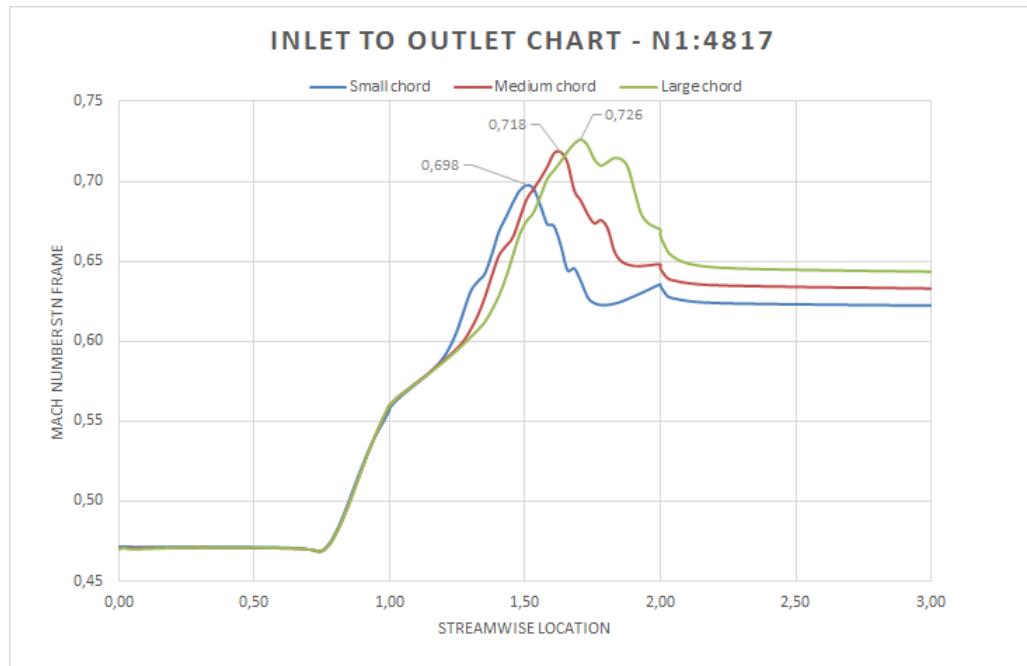
Figure 5.28: Mach number analysis - Inlet to Outlet

possible to understand some aspects about the total pressure variation throughout the flow blade for the three blade chords.

For both analysis (figure 5.29 and figure 5.30) the general conclusion that is understandable, is that when the blade chord increases the flow total pressure also increases, thus the outlet flow will have a higher total pressure. Another important aspect is the fact that in the total pressure profile along the span the points with highest total pressure are close to 70% of the blade span. When comparing this with the values achieved in case 1 is possible to say that with a lower fan rotation, the point of maximum pressure will travel outwards.
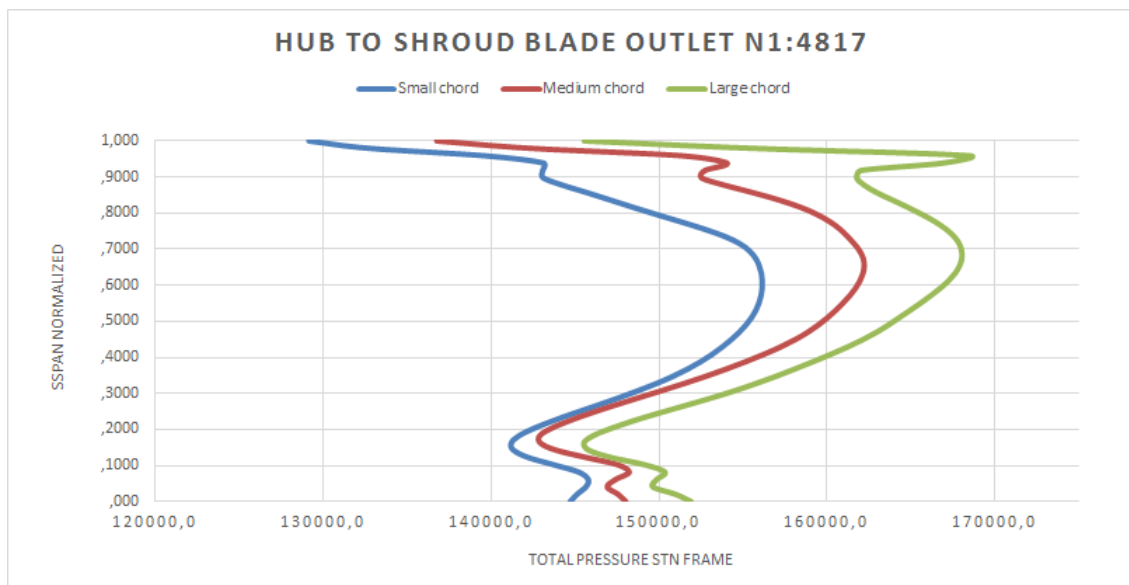

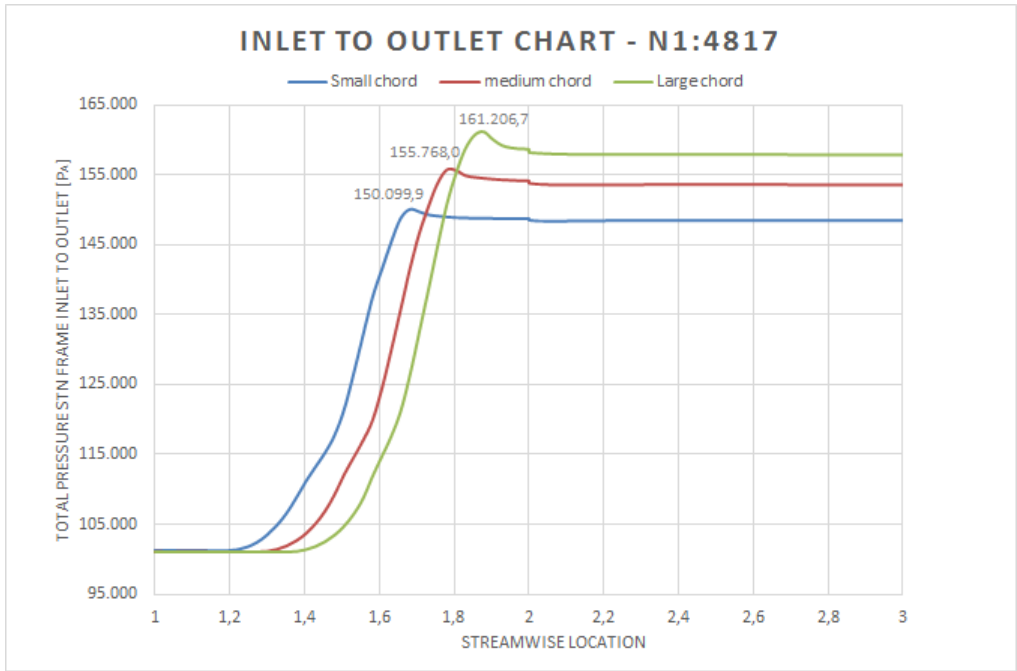Figure 5.29: Total Pressure analysis - Hub to shroud

Figure 5.30: Total Pressure analysis - Inlet to Outlet

5.3   Results Validation

The validation of results in CFD is a process of comparison between numerical results and experimental results, this is a very important process since it permits to evaluate the quality of the numerical solution and also assess the associated errors. In this work, validation is even more important since, as have been said, TAP-ME has a test bench and some databases of results that can be used to evaluate the simulations.

First, is important to mention that some information from TAP-ME databases are classified and can not be presented in this work, however, the data that is used throughout this work and especially in this section is considered necessary to validate the numerical results. It is also important to mention that the Reynolds number was not mentioned before, because the variation of this parameter is not relevant for the scope of this work. However, the Reynolds number of these simulations are around $2,05 \times 10^7$ considering standard day conditions and a speed of 240 m/s in the fan.

In order to compare the simulations results, some tests from the database were chosen, and the simulations were performed in those conditions. The test bench, for each test, delivers files with a large variety of readings. In this work, two of those readings were selected to validate the numerical results, as can be seen in table 5.31.

Figure 5.31: Test bench data

	PT2 [Pa]	T2 [℃]	$\dot{m}$	PT17 [Pa]	TS17 [℃]
TO	100180,64	14,95	316,38	164960,16	68
MC	99973,98	15,05	306,76	162773,73	68

The presented data for these two tests are from the test bench database, except for the TS17 which was obtained statistically. Having this information it is possible to compare TS17, real values, with the simulations.

The take-off readings presented in table 5.31 can be compared to the results of case 1 and Maximum Continuous (MC) to case 2. The numerical results that will be compared to the real test bench data are the results for large chord, because is the closest value when comparing to the engine actual blades. In case 1, the total pressure at the blade domain inlet is very close to 102000 Pa and the value achieved in the test bench is 100180,64 Pa, so there is good agreement. The mass flow in these simulations were imposed at the exit of the outlet domain, but after the simulation results achieved, is possible to see that the mass flow at the inlet has converged to the same value.

In regard to the total pressure after the fan, in the take-off regime, the test bench results indicates a value of 164960,16 Pa. In the numerical results, considering the area of highest total pressure the value at the fan exit is close to 162000 Pa, which shows a good agreement between this properties.

Finally, for the T.O. regime, the numerical solutions indicate an average temperature of 66 ℃, which shows a good agreement with the temperature calculated, based on test bench results (68 ℃). Continuing this analysis for case 2 results in M.C. regime, it is possible to start saying that the inlet total pressure in test bench (99973,98 Pa) is in good agreement with numerical results (101000 Pa). As in case 1, it is very important to validate the flow total pressure after the fan. The test bench sensor PT17 indicates, in this regime, a total pressure of 162773,73 Pa, comparing this value to the numerical result achieved from the simulations, which is 160000

Pa, it is possible to conclude that a good agreement, between experimental and real results, exists.

Finally, for this case, it is also possible to confirm a good agreement in the temperature at the blade outlet. The simulations results indicate a value of 65 ℃ and the test bench results give an indication of 68 ℃. Generally, with this process it is possible to conclude that the numerical results achieved in this work can be considered valid, since those results are in complete agreement with the real ones. However, it is necessary to understand that this comparative process has some limitations, specially linked to the way of acquiring the data in the test bench. (see Chapter 2).

5.4 Conclusions

The flow passing through the fan blades of a CFM56-3 was investigated in this work, using the commercial software CFX for this purpose. The main goal for this investigation was to evaluate the flow around the fan blades and search for a relationship between flow changes and a variation in the blade chord. All six simulations were performed using ANSYS CFX, with a $k - \omega$ SST turbulence model and automatic wall treatment. The simulations were concluded successfully and the results transferred to the post processing programme. From all the available variables it was decided to work with the flow total pressure and the Mach number. In order to better visualize the changes in the flow properties, figures of horizontal and vertical profiles were created and also graphs to compare the different blade chords.

First of all, it was concluded that the achieved solutions are converged and have a good level of quality, using for that several parameters as the residuals or the solution imbalances. For case 1, in take-off regime, after a careful analysis of the Mach number variation in all three blades, it was concluded that along the blade span, the Mach number increases when the blade chord increases, achieving the maximum value close to the blade hub.
In an axial approach these simulations permitted to understand that with a larger blade, higher mach numbers will happen at the outlet domain and higher the maximum value achieved in the domain. For a larger chord the maximum Mach number will happen closer to the exit of the blade domain. Having the same type of information for the flow total pressure, was concluded that along the blade span, the larger chord has always higher pressure values and for all simulations the maximum value happens at 40% of the blade span. Analyzing the flow total pressure variation, for the inlet to the outlet, permits to attain the same conclusion, because the larger chord creates the biggest pressure increment to 146000 Pa, which represents a FPR of 1,45 that is very close to the one indicated by the manufacturers. The difference between the larger and the smaller chord is 12000 Pa. The overall tendency in case 1 was the increase in all flow properties with the blade chord increase. In case 2, the same three blade chords were simulated with the maximum continuous regime implemented.

Analyzing the Mach number, the same tendency was found, because the larger chord has the highest Mach number values, and the maximum values appear closer to the hub. Also, in the axial direction the increment, in the Mach number through the fan blades is higher for the large chord, increasing the Mach number in 0,03 more than the smaller chord. Analyzing the total pressure in case 2, it was concluded that the total pressure increases as the blade chord increases, and the maximum values for all simulations happen at about 70% of the span. The difference between the small chord and the large chord is about 12000 Pa. This conclusions can be extrapolated for the inlet to outlet analysis were the total pressure raise is higher for the large chord and the difference between the smallest and largest chord is about 10000 Pa.
After an analysis of these results and a validation using data from the actual test performed in the test bench, it was concluded that the results are valid and very close to the real values, thus all conclusions extracted from this work are valid.

The conclusions in both cases are very similar, although, in case 2 the maximum values of total pressure happen in the secondary flow and in case 1 it occur close to the blade hub in the primary flow. Regarding the differences between the blade chords it is not possible to conclude if in take-off regime the blade changes have a bigger or smaller influence when compared to the maximum continuous regime.

Since the beginning of this study was expected that a larger blade chord correspond to a flow with higher pressure and higher mach number. This investigation was very important to understand this variations and will be an important tool for the engineering team, and with the necessary development can bring very significant financial savings for the company.

This was a very challenging project, which over several months required a lot of commitment. The project objectives were achieved successfully, and has began a path that allowed the development of many complementary works based on this information. As such, it began to already being developed a project to develop an Excel calculation sheet that will enable the compilation of this data and its use in engine maintenance processes. This calculation sheet will be an available tool for the engineering department to assess performance that will want to achieve and how the alteration of the blade chord will be able to contribute for that.
However, there are other works that can be suggested, it is also very important perform a study that analysis the primary and secondary flows separately, in order to evaluate in which the blade changes has more impact. It will also be interesting to build a LPC model and evaluate its performance together, and thus be able to validate with more information from the test bench.
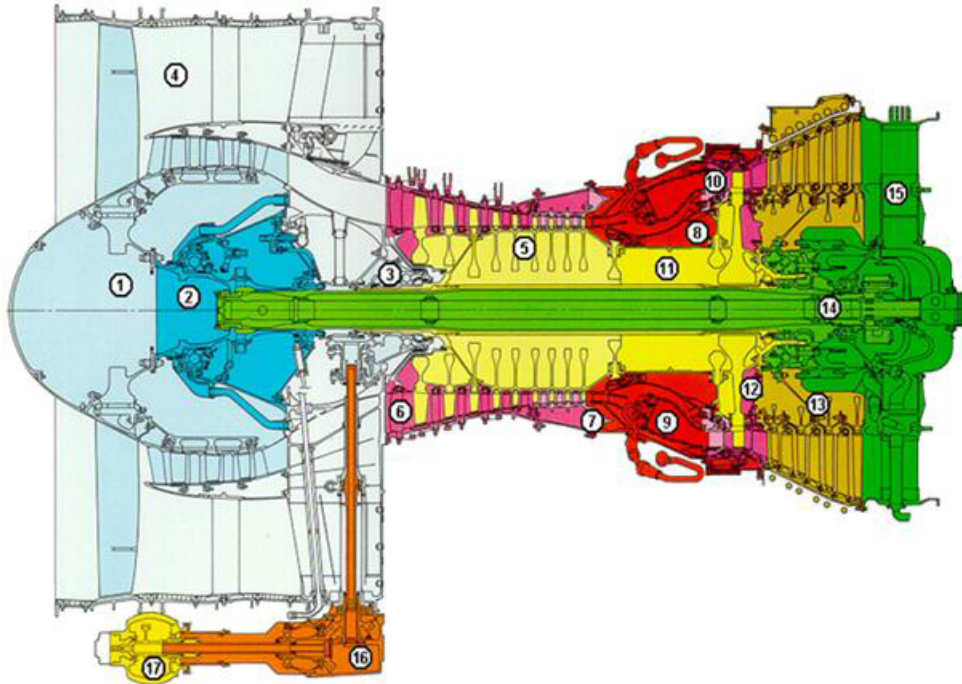
Appendix A

Annexes

A.1 Cfm56-3

Figure A.1: Modules and components of the CFM56-3 [25]
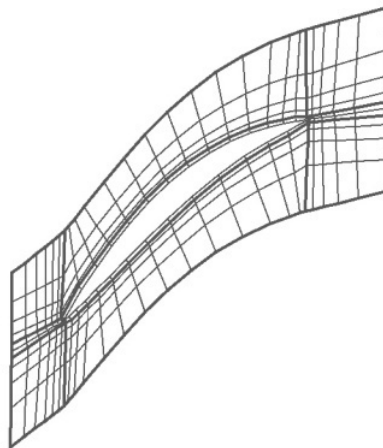
A.2 Topologys

Figure A.2: Type H Grid [26]
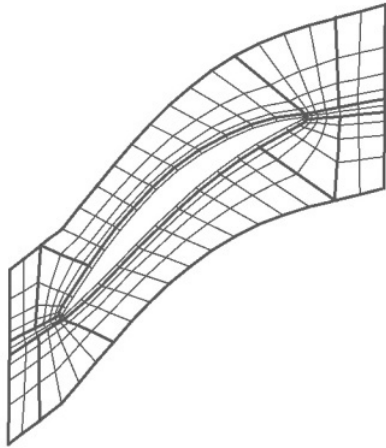
Figure A.3: Type J Grid [26]
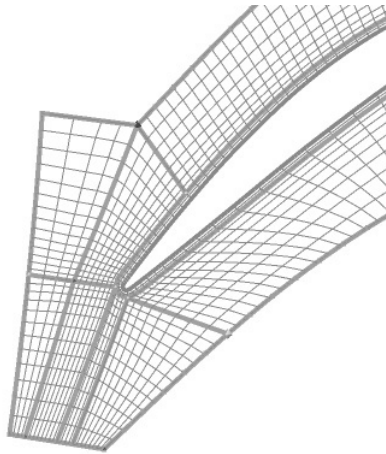

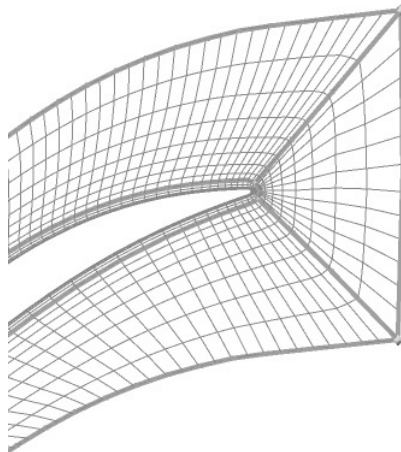Figure A.4: Type L Grid [26]

Figure A.5: Type C Grid [26]

A.3 Tip Clearance

Figure A.6: Fan Blades

A.4   CFX report

2. Mesh Report

Table 2. Mesh Information for meduim chord

Domain	Nodes	Elements
R2	1173116	1132628
S1	2947	11703
S2	80000	74529
All Domains	1256063	1218860

3. Physics Report

Table 3. Domain Physics for meduim chord

Domain - R2	
Type	Fluid
Location	Passage
Materials	
Air Ideal Gas	
Fluid Definition	Material Library
Morphology	Continuous Fluid
Settings	
Buoyancy Model	Non Buoyant
Domain Motion	Rotating
Alternate Rotation Model	On
Angular Velocity	-4.8170e+03 [rev min^-1]
Axis Definition	Coordinate Axis
Rotation Axis	Coord 0.3
Reference Pressure	0.0000e+00 [atm]
Heat Transfer Model	Total Energy
Turbulence Model	SST
Turbulent Wall Functions	Automatic
High Speed Model	Off

Figure A.7: CFX Report sample

Bibliography

[1]   - Richter, Hanz. *Advanced Control of Turbofan Engines*. New York, NY: Springer, 2012.

[2]   - Rolls-Royce. *The jet engine*. Rolls Royce technical publications 5th edition (1996).

[3]   - F. Bleier. *Fan Handbook: Selection*, Application, and Design. McGraw-Hill, 1998

[4]   – TAP company Manuals.

[5]   – TAP Quality Reports

[6]   - Aircraft commerce – Aircraft Owner's and Operator's guide

[7]   - US Patent Application Publication. Pub No: US2013/0161297 A1 Date: 27/06/2013

[8]   - Kang, M.; Ogaji, S.; Pilidis, P.; Kong, C. *An Approach to Maintenance Cost Estimation for Aircraft Engines*. A.S.M.E. paper, (GT2008-50564), American Society of Mechanical Engineers, New York, NY, 2008.

[9]   - Kennet, & Kennet, D. M. (Winter de 1993). *Did maintenance affect aircraft maintenance? An empirical policy analysis*. The RAND Journal of Economics, 24, 4.

[10]   - Kennet, D. M. (October/December de 1994). *A Structural Model of Aircraft Engine Maintenance*. Journal of Applied Econometrics, 9, Issue 4, 351-368.

[11]   – H.K. Versteeg e W. Malalasekera, *An introduction to Computational Fluid Dynamics: The Finite Volume Method*, Prrentice Hall, 2nd Edition, (2007).

[12]   – Maliska C.R., *Transferencia de Calor e Mecânica dos fluidos Computacional*, LTC,2ª Edição, (2004).

[13]   - Introduction to FLUENT, *Training Manual*, ANSYS Inc., Release 12.0, 1st Edition, (2009)

[14]   - Beiler, M. G., Carolus T. H. - *Computation and Measurement of the Flow in Axial Flow Fans With Skewed Blades*. Journal of Turbomachinery 121, pp. 59-66, 1999.

[15]   - B. Curnock, J. Yin, R. Hales, P. Pilidis, *High-bypass turbofan model using a fan radial-profile performance map, Aircraft Design*, Volume 4, Issues 2–3, June–September 2001, Pages 115-126, ISSN 1369-8869.

[16]   - C. Berbente, I.C. Andrei, N.M. Ene, F. Frunzulica e E. Korody, *Special Topics on Map Meshing in Turbomachinery*, Periodica Polytechnica Ser. Transport Engineering, Vol. 34, No. 1-2, pp. 59-68, (2006).

[17]   - J.Masud & S.Ahmed, *Design Refinement and Performance Analysis of Two Stage Fan for Small Turbofan Engines* 45th AIAA Aerospace Sciences Meeting Jan 8-11 2007 Reno Naveda.

[18]   - Yang LI, Jie LIU, Hua OUYANG, Zhao-Hui DU, *Internal flow mechanism and experimental research of low pressure axial fan with forward-skewed blades*, Journal of Hydrodynamics, Ser. B, Volume 20, Issue 3, June 2008.

[19]   - Jingjun Zhong, Shaobing Han, Huawei Lu, Xiaoxu Kan, *Effect of tip geometry and tip clearance on aerodynamic performance of a linear compressor cascade*, Chinese Journal of Aeronautics, Volume 26, Issue 3, June 2013.

[20]   - Leye M. Amoo, *On the design and structural analysis of jet engine fan blade structures, Progress in Aerospace Sciences*, Volume 60, July 2013.

[21]   - A. Sahili, B. Zogheib and R. Barron, "*3-D Modeling of Axial Fans*," Applied Mathematics, Vol. 4 No. 4, 2013, pp. 632-651.

[22]   - Dwivedi,D., Dandotiya,D.S., "*CFD Analysis of Axial Flow Fnas with skewed Blades*", International Journal of Emerging Technology and Advanced Engineering, Volume 3, Issue 10, October 2013.

[23]   - Ahmed Fayez EL-Saied, Mohamed Hassan Gobran, Hassan Zohier Hassan, *Erosion of an Axial Transonic Fan due to Dust Ingestion*, American Journal of Aerospace Engineering. Special Issue:Hands-on Learning Technique for Multidisciplinary Engineering Education. Vol. 2, No. 1-1, 2015.

[24]   - Stefan Leschka, *Modelling of Flow in Vertical Porous Structures Solving the Reynolds-Averaged Navier-Stokes Equations (RANS) using the Volume of Fluid Method (VOF)*, diplom.de, 2002

[25]   – TAP CFM56-3 Hardware Manual

[26]   – ANSYS FLUENT, *Theory Guide*, ANSYS inc., Release 12.0

[27]   - ANSYS FLUENT, *User's Guide*, ANSYS inc., Release 14.5

[28]   – ANSYS CFX, *Solver Theory Guide*, ANSYS inc., Release 12.1

[29]   - Hinze, J.O., "*Turbulence*", McGraw-Hill, 1975.

[30]   - Jaw, S.Y., Chen, C.J., "*Present Status of Second Order Closure Turbulence Models*", Journal of Engineering Mechanics, May 1998, pp 485-501.

[30]   – P. Bradshaw, *Turbulence Modeling with Application to Turbomachinery*, Progress in Aerospace Sciences, Vol.32, pp. 575-624, (1996)

[31]   - D.C. Wilcox, *Turbulence Modeling for CFD*, DCW Industries, 1st Edition, (1994).

[32]   Karthik Duraisamy,Department of Aerospace Engineering,University of Glasgow

[33]   - Simoes, Marcelo R., et al. "*Validation of turbulence models for simulation of axial flow compressor.*" 20th International Congress of Mechanical Engineering. 2009.

[34]   - 28 F. R. Menter. "*Two-Equation Eddy-Viscosity Turbulence Models for Engineering Applications*". AIAA Journal. 32(8). 1598–1605. August 1994.

[35]   - C.M.Rhie and W.L.Chow, *A numerical study of Turbulent Flow Past an Isolated Airfoil with the Trailing Edge Separation.* Aiaa Journal, 1982: p. 82- 0998

[36]   - ANSYS CFX, *Solver Modeling Guide*,ANSYS inc.,

[37]   S Larry Dixon, Cesare Hall, *Fluid Mechanics and Thermodynamics of Turbomachinery*, Butterworth-Heinemann, 2013

[38]   - Jiyuan Tu, Guan Heng Yeoh, and Chaoqun Liu. 2007. *Computational Fluid Dynamics: A Practical Approach*. Butterworth-Heinemann, Newton, MA, USA.